Fossil Record 29 (1) 2026, 373–410 | DOI 10.3897/fr.29.192018

PENSOFT

MUSEUM FÜR NATURKUNDE BERLIN

Deciduous dentition and ontogenetic development of the skull and teeth of *Chilotherium* (Mammalia, Perissodactyla, Rhinocerotidae) from the Late Miocene of Eurasia

Panagiotis Kampouridis[1,2], Luca Pandolfi[3], Christina Kyriakouli[1,2], Nikolai Spassov[4], Madelaine Böhme[1,2]

1 *Department of Geoscience, Eberhard Karls University of Tübingen, Hölderlinstraße. 12, 72074, Tübingen, Germany*
2 *Senckenberg Centre for Human Evolution and Palaeoenvironment (HEP Tübingen), Hölderlinstraße. 12, 72074, Tübingen, Germany*
3 *Università di Pisa, Dipartimento di Scienze della Terra, via S. Maria 53-56126, Pisa, Italy*
4 *National Museum of Natural History at the Bulgarian Academy of Sciences, Sofia, Bulgaria*

https://zoobank.org/33C26AAA-328C-4047-A52C-340260017491

Corresponding author: Panagiotis Kampouridis (pkampouridis94@gmail.com)

Academic editor: Florian Witzmann ♦ **Received** 18 March 2026 ♦ **Accepted** 19 May 2026 ♦ **Published** 4 June 2026

Abstract

The hornless rhinoceros genus *Chilotherium* is characterised by high taxonomic complexity, with more than 30 species having been included in the genus at some point. This frequently prevents the identification of incomplete material, which has historically limited understanding of the genus's diversity and evolution. Although recent work has enhanced the comprehension of the systematics of hornless rhinoceroses, the ontogeny of the cranium and deciduous dentition of chilotheres is still poorly known. Herein, juvenile skulls and mandibles at different ontogenetic stages are investigated, along with the deciduous teeth of four Late Miocene chilothere species: *Chilotherium persiae* from Maragheh (Iran), *Chilotherium habereri* from Kutschwan (China), *Chilotherium schlosseri* from Samos (Greece), and *Chilotherium anderssoni* from Daijiagou (China). The results show that several dental characters in the deciduous premolars are informative for species discrimination. The eruption sequence of the deciduous teeth is broadly uniform within the genus. Only the relative eruption of D1 and D4 varies, with *C. schlosseri* showing delayed D1 eruption. Lastly, enamel hypoplasia is also documented in the deciduous teeth. Although d/D2 and d/D3 exhibit hypoplasias only sporadically, d/D4 consistently bears prominent hypoplasias associated with the individual's birth. The position of the latter hypoplasia is consistent across chilotheres, occurring in the middle of the tooth crown, except in *C. schlosseri*, where it is located at the base of the crown.

Key Words

Milk teeth, morphology, Neogene, pathology, rhinoceros, taxonomy

Introduction

Mammals are generally characterised by highly specialised dentition that reflects ecological adaptations (Ungar 2010). A major modification in the evolutionary history of mammals was diphyodonty: the existence of only two generations in dental replacement, initially the deciduous or milk teeth and then the permanent teeth (e.g. Jäger et al. 2019; Cabreira et al. 2022). Despite their potential systematic value (e.g. Fernández et al. 2021; Gomes Rodrigues et al. 2021; Kampouridis et al. 2023a), deciduous teeth are rarely studied in detail or used in phylogenetic and taxonomic analyses.

The significance of the deciduous dentition for the reconstruction of phylogenetic relationships was recently highlighted for Hippopotamoidea (Gomes Rodrigues et al. 2021). Although many studies have addressed the phylogenetic relationships of rhinoceroses, in the past, most did not include any characters related to the deciduous teeth (e.g. Heissig 1981; Fortelius and Heissig 1989; Cerdeño 1995).

Antoine (2002) incorporated nearly 20 characters specifically related to deciduous dentition into his newly compiled comprehensive character matrix, which set the framework for subsequent rhinocerotid phylogenetic analyses. However, chilotheres are underrepresented in most phylogenetic analyses, with only a few including any chilothere taxa (e.g. Deng 2006a; Pandolfi 2016; Lu et al. 2023). The morphology of the deciduous dentition in chilotheres is also almost unknown for most taxa, as it is usually not explicitly described. A first step to resolving this is describing the morphology of the milk teeth of chilotheres and their variability.

The hornless rhinoceros genus *Chilotherium* Ringström, 1924, was autochthonous to Eurasia and lived only during the Late Miocene (e.g. Deng and Downs 2002; Deng 2006b; Kampouridis et al. 2022b). Its biogeographical distribution ranged from eastern China to the Balkan Peninsula in the west (e.g. Deng 2006b; Geraads and Spassov 2009; Spassov et al. 2018). The genus was initially described by Ringström (1924), who revised several hornless rhinoceroses, most of which had been attributed to the genus *Aceratherium* Kaup, 1832, until then. The most characteristic features that connected these species were the depression in their frontals, widely separated parietal crests, a wide mandibular symphysis with large tusk-like lower second incisors, and short limb bones (Ringström 1924). While the permanent dentition of chilotheres is well known and presents many diagnostic features differentiating the group from other rhinoceroses (e.g. Geraads and Spassov 2009; Kampouridis et al. 2023b; Țibuleac et al. 2023), little is known about the deciduous dentition of these animals.

The aim of the present study is to describe juvenile crania, mandibles, and teeth of the hornless rhinoceros *Chilotherium*. This allowed a better understanding of their tooth morphology, including potential variability, dental eruption, and skull development, to shed light on aspects of their systematics and ecology.

Abbreviations

AMNH, American Museum of Natural History, New York (USA); **AMPG**, Palaeontological and Geological Museum of the University of Athens (Greece); **BSPG**, Bayerische Staatssammlung für Paläontologie und Geologie (Germany); **GMM**, Geomuseum of the University of Münster (Germany); **GPIH**, Geologisch-Paläontologisches Institut der Universität Hamburg (Germany); **GPIT**, Geologisch-Paläontologisches Institut der Universität Tübingen (Germany); **MLU**, Martin-Luther Universität Halle-Wittenberg (Germany); **MNHN**, Muséum national d'Histoire naturelle, Paris (France); **NHMUK**, Natural History Museum, London (UK); **NHMW**, Naturhistorisches Museum in Wien (Austria); **PMU**, Museum of Evolution (Palaeontological Museum), Uppsala (Sweden); **SMF**, Senckenberg Museum in Frankfurt (Germany); **SMNS**, Staatliches Museum für Naturkunde Stuttgart (Germany); and **SNSB**, Staatliche Naturwissenschaftliche Sammlungen Bayerns (Germany).

Fossil sites

Samos

The island of Samos (Fig. 1) has been known to yield Late Miocene vertebrate fossils since the 19th century, with the first excavations taking place in the 1880s, led by C. I. Forsyth Major (Koufos 2009). Since then, numerous palaeontologists and fossil hunters have visited the island to collect fossils (Koufos 2009). This led to several impressive collections of Samos material in major natural history museums throughout the world, including the AMNH, the NHMW, and the SMNS. Most recently, the Aristotle University of Thessaloniki, led by Professor George Koufos, excavated on Samos Island, bringing to light a rich collection of mammalian remains (e.g. Kostopoulos et al. 2009; Koufos 2009). The material was studied in detail, providing crucial information about the biostratigraphical context and the fauna itself (e.g. Kostopoulos et al. 2003, 2009; Koufos et al. 2009, 2011). The rhinoceros material from Samos has been assigned to several different taxa over the years (for an overview, see Giaourtsakis 2022). Today, it is generally accepted that two large tandem-horned rhinoceroses are present, *Ceratotherium neumayri* (Osborn, 1900) and *Dihoplus pikermiensis* (Toula, 1906), along with two smaller, hornless rhinocerotids belonging to the chilotheres. The taxonomy of chilotheres has experienced many difficulties in the past, with the variously suggested presence of five species – *Chilotherium schlosseri* (Weber, 1905), *Eochilotherium samium* (Weber, 1905), *Chilotherium wegneri* (Andree, 1921), *Chilotherium angustifrons* (Andree, 1921), and *Chilotherium kowalevskii* (Pavlow, 1913) – depending on the authors (Weber 1905; Krokos 1917; Andree 1921; Giaourtsakis 2003, 2009, 2022; Athanassiou et al. 2014). Recently, it was suggested that *C. wegneri* and *C. angustifrons* represent junior synonyms of *C. schlosseri* (e.g. Giaourtsakis 2022; Kampouridis et al. 2023b). The identification of *C. kowalevskii* in Samos stems from the erroneous synonymisation of this species with *C. angustifrons* (see Kampouridis et al. 2022b). Therefore, *C. schlosseri* and *E. samium* are the two valid chilothere species present in Samos (Kampouridis et al. 2022b, 2023b, 2025; Giaourtsakis 2022; Svorligkou et al. 2025).

Maragheh

The locality of Maragheh is situated in northwestern Iran (Fig. 1). The Late Miocene fauna has been well known since the late 19th century (Rodler 1885; Pohlig 1886; Mecquenem 1908b; Mirzaie Ataabadi et al. 2013, 2016). Several fossil sites have been excavated over more than 100 years; recent studies have suggested the existence of three distinct fossiliferous levels and were able to associate the historical fossil sites with them (Campbell et al. 1980; Bernor 1986). Material from this locality is scattered throughout many collections, such

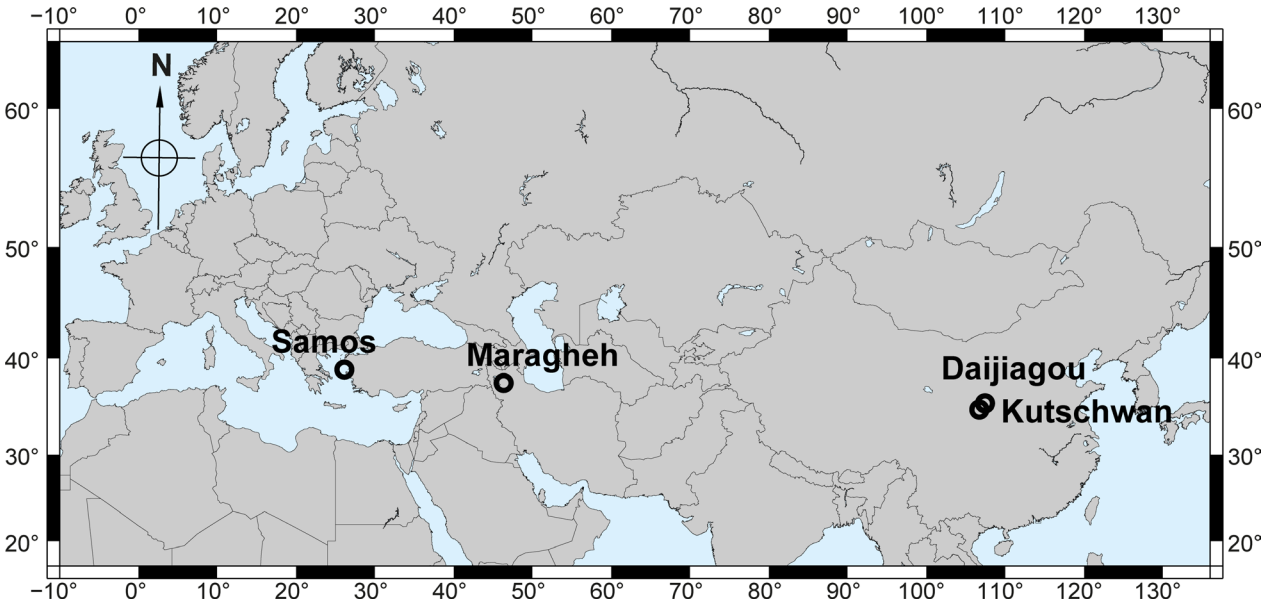

Figure 1. Geographical map. Fossil localities from which the material studied herein comes (Samos in Greece, Maragheh in Iran, Daijiagou, and Kutschwan in China) are shown. The map was generated using Generic Mapping Tools 6 (GMT6) (Wessel et al. 2019).

as the NHMW, MLU, MNHN, NHMUK, and SNSB-BSPG. The rhinoceros assemblage in Maragheh is quite rich and includes the large single-horned *Iranotherium morgani* (Mecquenem, 1908a), the large tandem-horned *Ceratotherium neumayri*, and two small hornless rhinoceroses, *Chilotherium persiae* (Pohlig, 1885) and *Persiatherium rodleri* Pandolfi, 2016 (e.g. Pohlig 1885; Mecquenem 1924; Pandolfi 2016; Kampouridis et al. 2025). Notably, Maragheh represents the type locality for all these rhinocerotid species. *Chilotherium persiae* is the most common and most characteristic representative of the family in the Maragheh fauna, and several juvenile dental elements have been found and studied in the context of the present study. These fossils were excavated at different fossil sites in the area around Maragheh that correspond to different stratigraphical sections, although exact information about the site is often not provided on the collection labels (e.g. Pohlig 1886; Mecquenem 1908b; Kampouridis et al. 2024).

Daijiagou

The fossil site of Daijiagou (also spelled Taijiagou and Taichiakou or called Lok. 30) is found close to the Yellow River (Huang He), situated in the county of Baode in Shanxi Province, China (Fig. 1). This fossil site was discovered and excavated in the context of the Sino-Swedish expedition led by J. G. Andersson in the late 1910s and early 1920s, which created the Lagrelius Collection at the University of Uppsala. The excavation of this locality, which is referred to as "Lok. 30" in several publications, and many other localities in China between 1921 and 1923 was undertaken by O. Zdansky and later by other palaeontologists such as B. Bohlin, who also studied part of the excavated material (e.g. Zdansky 1924, 1925a, 1925b, 1927a, 1927b; Bohlin 1926, 1935). The Late Miocene faunal assemblages were mainly composed of horses, bovids, and rhinoceroses (Ringström 1923, 1924, 1927; Sefve 1927; Bohlin 1935). Based on this material, Ringström (1924) erected the genus *Chilotherium* and its type species, *Chilotherium anderssoni* Ringström, 1924. However, several other rhinoceroses, including further chilotheres, were erected by T. Ringström based on material from these excavations (Ringström 1923, 1924). The locality of Daijiagou represented only a small portion of the overall excavated material during the Sino-Swedish expedition; nonetheless, in addition to a large sample of *C. anderssoni* specimens, the elasmotheriine *Sinotherium lagrelii* Ringström, 1923, was also erected based on a left M3, and additional material was described later (Ringström 1923, 1924). The stratigraphy of these classical Upper Miocene localities in the Baode area was recently re-evaluated and the age of many localities was refined, dating Daijiagou to approximately 5.7 Ma (Kaakinen et al. 2013).

Kutschwan

The locality of Kutschwan is of Late Miocene age and was discovered by the German geographer Albert Tafel in Shanxi during his trip to China in 1905 (Killgus 1923). No information about the exact location of the fossil site is known, but the material was collected from horizontal red clay deposits close to the Yellow River (Huang He) in Shanxi Province, China (Fig. 1; Killgus 1923). The material excavated by Tafel included a large collection of mammalian remains, with many cranial and postcranial elements. The whole collection was initially prepared at the SMNS (Germany), then given to the GPIT (Germany), and is still housed there today. Hugo Killgus studied the whole collection for his Ph.D. dissertation (Killgus 1922) and recognised a quite rich mammalian fauna, based

on this limited material, including two rhinoceroses, *Chilotherium habereri* and *Parelasmotherium schansiense* Killgus, 1923, a hipparionine, *Schansitherium tafeli* Killgus, 1923, four bovids, and a hyaenid (Killgus 1923). More recently, Kampouridis et al. (2022a) re-examined the holotype of *Parelasmotherium schansiense* using micro-computed tomography to reveal unknown features important for the taxonomy and phylogeny of this taxon, and Kampouridis et al. (2025) studied the postcranial material of *C. habereri* from Kutschwan in an overview of the postcranial anatomy of the genus.

Material and methods

Material

The material investigated herein includes four species of *Chilotherium* from different Upper Miocene localities across Eurasia (Fig. 1). The first species is *C. persiae* from the Upper Miocene of Maragheh (Iran). Most of the material is housed at the MNHN and NHMW, and additional cranial, mandibular, and dental material is housed at the MLU and NHMUK. The second species is *C. habereri* from the Upper Miocene of Kutschwan (China). The material includes several partial skulls, mandibles, and isolated deciduous teeth housed in the GPIT. The third species is *C. schlosseri* from the Upper Miocene of Samos (Greece), with material of this species spread throughout different institutions, such as the AMPG, GMM, NHMW, SMF, and SMNS. The last species is *C. anderssoni* from the Upper Miocene site of Daijiagou (also referred to as "Lok. 30") in Shanxi, China. The material includes four partial skulls from the historical fossiliferous site that are housed in the collections of the AMNH and SMF. These specimens, along with other chilothere material described by Ringström (1924), were collected during the Sino-Swedish expedition led by J. G. Andersson (Mateer and Lucas 1985) and were later donated by the PMU to the SMF between 1927 and 1929 (according to the catalogues of the SMF) and to the AMNH.

Anatomical nomenclature

The anatomical nomenclature of the skull and dentition (Fig. 2) follows Guérin (1980), Peter (2002), and Antoine (2002). The ontogenetic age of the specimens was determined for more detailed comparisons between the species and the assessment of potential intraspecific ontogenetic changes in skull morphology. The ages were determined based on the wear stages of the teeth as described by Hillman-Smith et al. (1986) for the extant *Ceratotherium simum* and further elaborated for fossil rhinocerotid species by Hullot and Antoine (2020). The data concerning the wear stages of the teeth and the suggested age classes can be found in Suppl. material 1: table S1.

Enamel hypoplasia

Enamel hypoplasia is a defect in tooth development, leading to the underdevelopment of enamel in part of a tooth, and represents a unique marker of high levels of stress in an individual (e.g. Goodman and Rose 1990; Guatelli-Steinberg 2001; Hullot et al. 2021; Hullot and Antoine 2022). Herein, enamel hypoplasia was studied in the deciduous teeth of four *Chilotherium* species. For this purpose, hypoplasia in the deciduous premolars, upper and lower second (d/D2), third (d/D3), and fourth (d/D4) premolars was investigated. In total, 152 teeth were studied. If hypoplasia appeared on the same tooth position on both sides, it was counted as a single occurrence. Teeth with damaged enamel or those that had not fully erupted were excluded from this study. Additionally, in cases where teeth from Kutschwan and Samos had not fully erupted, the respective specimens were CT-scanned, as proposed by Hullot and Antoine (2022), to investigate the occurrence of potential hypoplasia.

µCT-scanning

To study the cranial and dental morphology in detail, micro-computed tomography (µCT) scans were acquired for some specimens with a Nikon XT H 320 µCT scanner operated by the 3D Imaging Lab Senckenberg Centre for Human Evolution and Palaeoenvironment and the Eberhard Karls University Tübingen, Germany. An X-ray tube containing a multi-metal reflection target with a maximum acceleration voltage of 225 kV was used. Specimen GPIT/MA/04842 (partial skull of *C. habereri*) was scanned at 215 kV and 210 µA with a voxel size of 0.05999687 mm, using a copper filter of 1.0 mm thickness. Specimen GPIT/MA/04818 (mandible of *C. habereri*) was scanned at 165 kV and 200 µA with a voxel size of 0.03678904 mm, using a copper filter of 0.25 mm thickness. Specimen GPIT/MA/04820 (mandible of *C. habereri*) was scanned at 190 kV and 130 µA with a voxel size of 0.04216668 mm, using a copper filter of 0.25 mm thickness. Specimen GPIT/MA/04849 (mandible of *C. habereri*) was scanned at 200 kV and 160 µA with a voxel size of 0.03750121 mm, using a copper filter of 0.5 mm thickness. Specimen GPIT/MA/04817 (isolated D4 of *C. habereri*) was scanned at 175 kV and 180 µA with a voxel size of 0.03139582 mm, using a copper filter of 0.1 mm thickness. Specimen SMNS 47913 (partial skull of *C. schlosseri*) was scanned at 200 kV and 205 µA with a voxel size of 0.06508365 mm, using a copper filter of 0.1 mm thickness. Specimen SMNS 47914 (partial skull of *C. schlosseri*) was scanned at 225 kV and 215 µA with a voxel size of 0.05487692 mm, using a copper filter of 2.5 mm thickness. Images were processed using VG Studio Max. The results are virtual orthoslices of the actual teeth, used for the detailed comparison of the hypoplasia observed in the deciduous teeth. The scans are available on MorphoSource (https://www.morphosource.org/) under the Project ID 000840545.

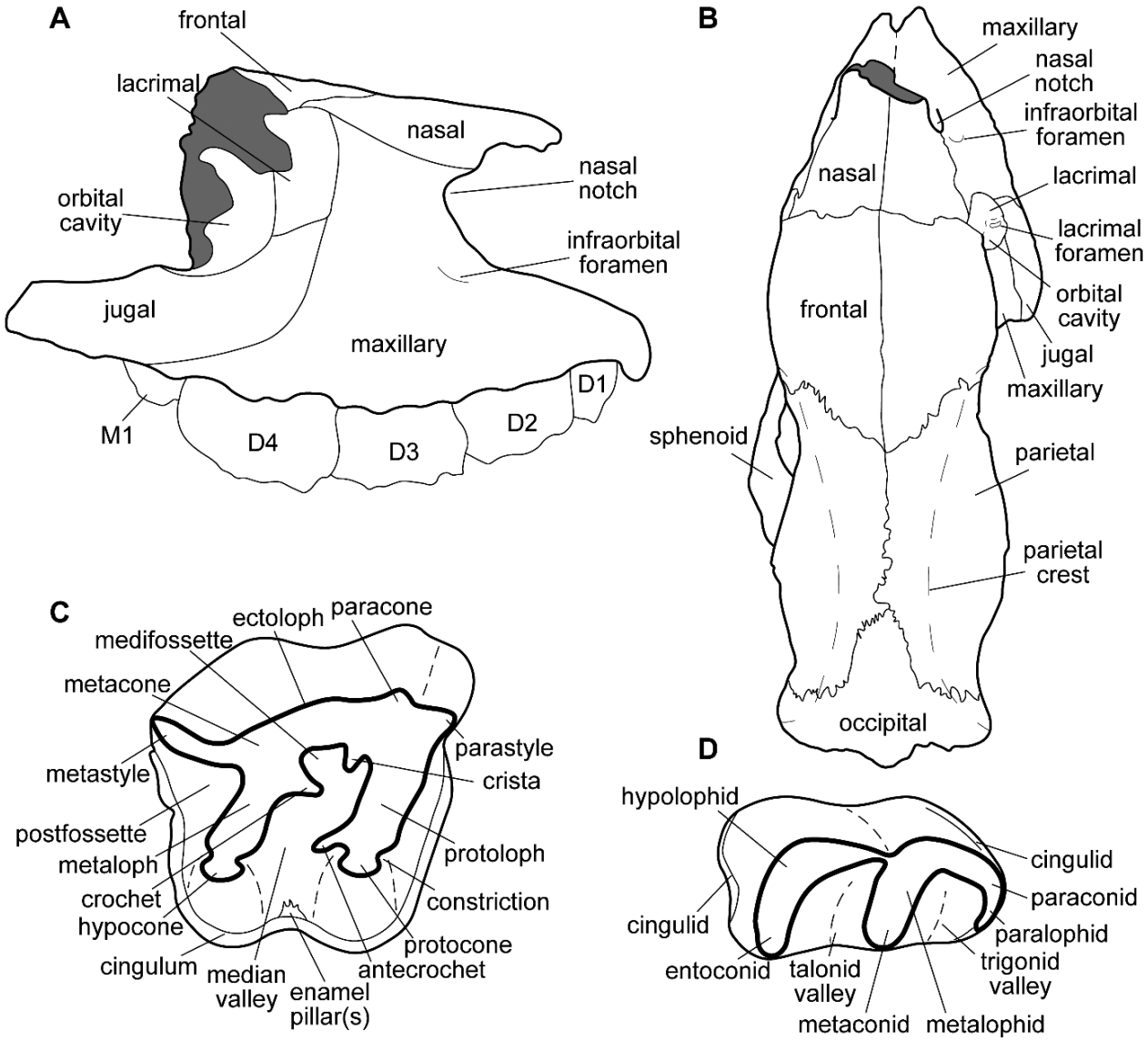

Figure 2. Anatomical nomenclature used in this study. **A.** Juvenile skull (MNHN.F.MAR3053) of *Chilotherium persiae* (Pohlig, 1885) from the Upper Miocene of Maragheh in Iran in lateral view; **B.** Juvenile skull (SMF M 3592) of *Chilotherium anderssoni* Ringström, 1924, from the Upper Miocene of Daijiagou in China in dorsal view; **C.** Upper molar; and **D.** Lower molar in occlusal view showing the anatomical nomenclature used in this study. Not to scale.

Systematic palaeontology

Class Mammalia Linnaeus, 1758
Order Perissodactyla Owen, 1848
Family Rhinocerotidae Gray, 1821
Subfamily Aceratheriinae Dollo, 1885
Subtribe Chilotheriina Qiu et al., 1987 (*sensu* Kampouridis et al. 2023b)

Genus *Chilotherium* Ringström, 1924

Type species. *Chilotherium anderssoni* Ringström, 1924 from Daijiagou in Shanxi (China).

Included species. *Chilotherium persiae* (Pohlig, 1885), *Chilotherium habereri* (Schlosser, 1903), *Chilotherium schlosseri* (Weber, 1905), *Chilotherium kowalevskii* (Pavlow, 1913), '*Chilotherium*' *wimani* Ringström, 1924, *Chilotherium sarmaticum* Korotkevich, 1958, *Chilotherium xijangensis* (Ji et al., 1980), *Chilotherium orlovi* Bayshashov, 1982, '*Chilotherium*' *primigenium* Deng, 2006a, *Chilotherium licenti* Sun et al., 2018.

Occurrence. Upper Miocene deposits of Eurasia.

***Chilotherium persiae* (Pohlig, 1885)**
Figs 3–5

Type material. Pohlig (1885) originally erected this species based on a collection of four adult and one juvenile skull from Maragheh, but he did not mention where exactly these specimens are housed (Pohlig 1884a, 1884b, 1885, 1886); therefore, the type material was never properly defined. He mentioned that the material he collected himself in Maragheh (Iran) was sent to Halle (Germany)

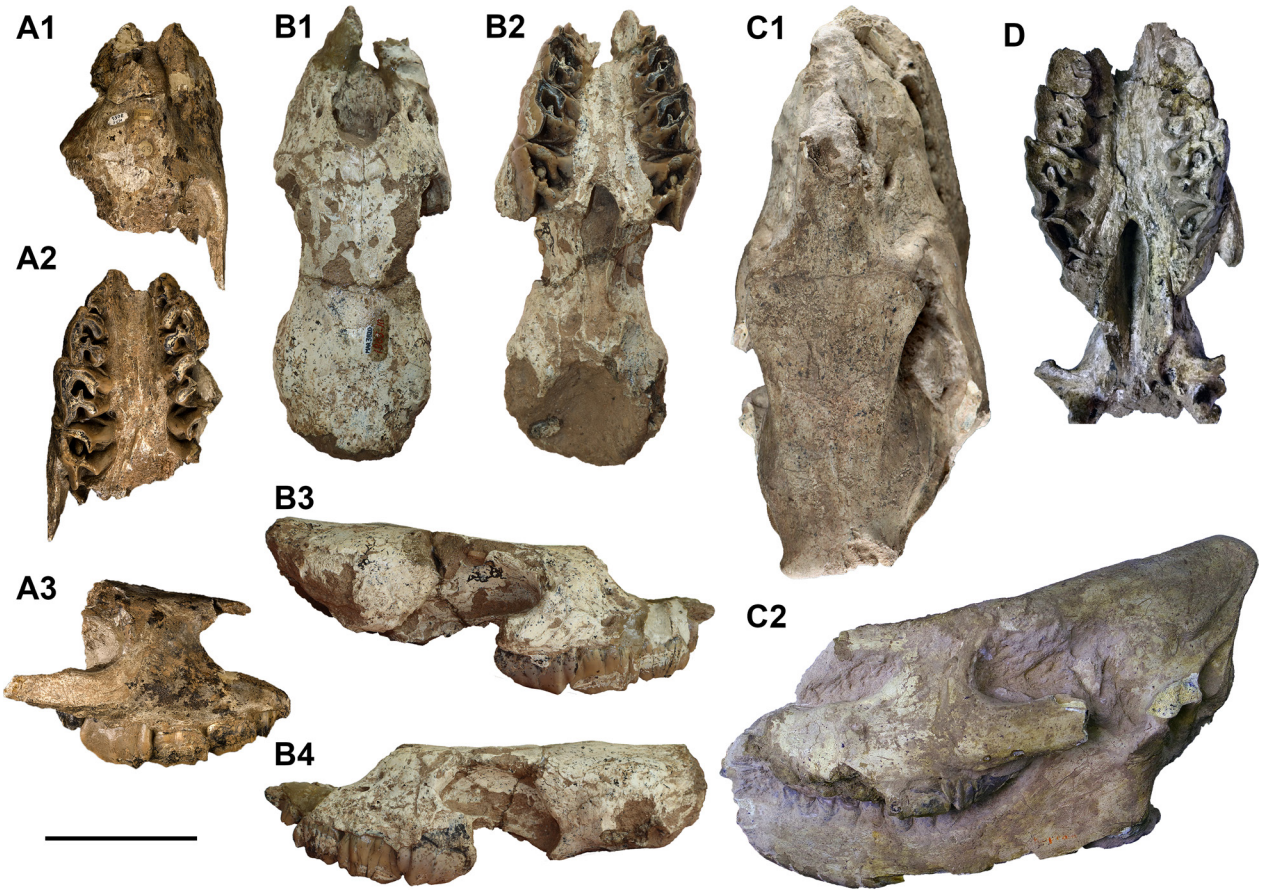

Figure 3. Juvenile skulls of *Chilotherium persiae* (Pohlig, 1885) from the Upper Miocene of Maragheh (Iran). MNHN.F.MAR3053 (**A**), MNHN.F.MAR3820 (**B**), MLU.GeoS.8030 (**C**), and NHMW-GEO-2020/0014/0093 (**D**) are juvenile skulls in dorsal (**A1**, **B1**, and **C1**), ventral (**A2**, **B2**, and **D**), and lateral (**A3**, **B3–4**, and **C2**) views. Scale bar: 10 cm.

(Pohlig 1886) and is now housed in the palaeontological collection of the MLU. However, Pohlig (1885, 1886) did not specify whether he collected the specimens he referred to as "*Rhinoceros persiae*" himself or saw them in another collection, such as the NHMW. Therefore, until further information becomes available, the type material cannot be determined with certainty, as already discussed by Kampouridis et al. (2025).

Type locality. Upper Miocene deposits of Maragheh (Iran); exact locality unknown

Material. An almost complete juvenile skull preserving D1–D4 with its associated mandible, preserving d2–d4 (MLU.GeoS.8030); a partial juvenile skull preserving part of the nasals and the frontals, and the maxillae, with D1–D4 (MNHN.F.MAR3053); a partial juvenile skull preserving the left D1–D4 and right D3–D4 (MNHN.F.MAR3078–3079); a partial juvenile skull preserving D2–D4 and M1, and its associated mandible, preserving the right d2–d4 and the left d3 (NHMW-GEO-2020/0014/0093); a partial juvenile skull preserving D2–D4 (MLU.GeoS.8028); a right maxilla preserving D1–D4 (MLU.GeoS.8029); a left juvenile maxilla preserving D2–D4 and M1 (NHMW-GEO-2020/0014/0034); a right maxilla preserving D1–D4 (NHMW-GEO-2020/0014/0030); a partial left maxilla preserving D1–D4 (MLU.GeoS.8025); a partial subadult skull preserving, on both sides, P2, P3, D4, M1, and M2, in addition to the left D1 (NHMW-GEO-2020/0014/0099); a partial juvenile skull preserving D1–D4 on both sides (NHMW-GEO-2020/0014/0006); a left partial maxilla preserving D2–D3 (NHMUK M 2006); eight isolated D4s (MLU.GeoS.8027, MLU.GeoS.8031, NHMW-GEO-2020/0014/0032, NHMW-GEO-2020/0014/0070, NHMW-GEO-2020/0014/0081, NHMW-GEO-2020/0014/0056, and NHMW-GEO-2020/0014/0067); a partial juvenile mandible preserving the left d2–d4 and the right d1–d4, with erupting m1 (MNHN.F.MAR3859); a partial juvenile mandible preserving d2–d4 and erupting m1 on both sides (NHMUK M 3916); a partial mandible preserving d2–d4 on both sides (NHMW-GEO-2020/0014/0033); a partial mandible preserving d2–d3 on both sides (MLU.GeoS.8034); a partial mandible preserving d3–d4 and m1 on both sides, in addition to the left d2 (NHMW-GEO-2020/0014/0100); a partial juvenile mandible preserving the right d2–d3 and m1, and the right d1 (MNHN.F.MAR3889); a left hemimandible preserving d4 and erupting m1 (MLU.GeoS.8031); a left hemimandible preserving d2–d4 (NHMUK M 3917); and a partial mandible preserving i2 and d1–d4 on both sides, in addition to the right i1 (NHMW-GEO-2020/0014/0037).

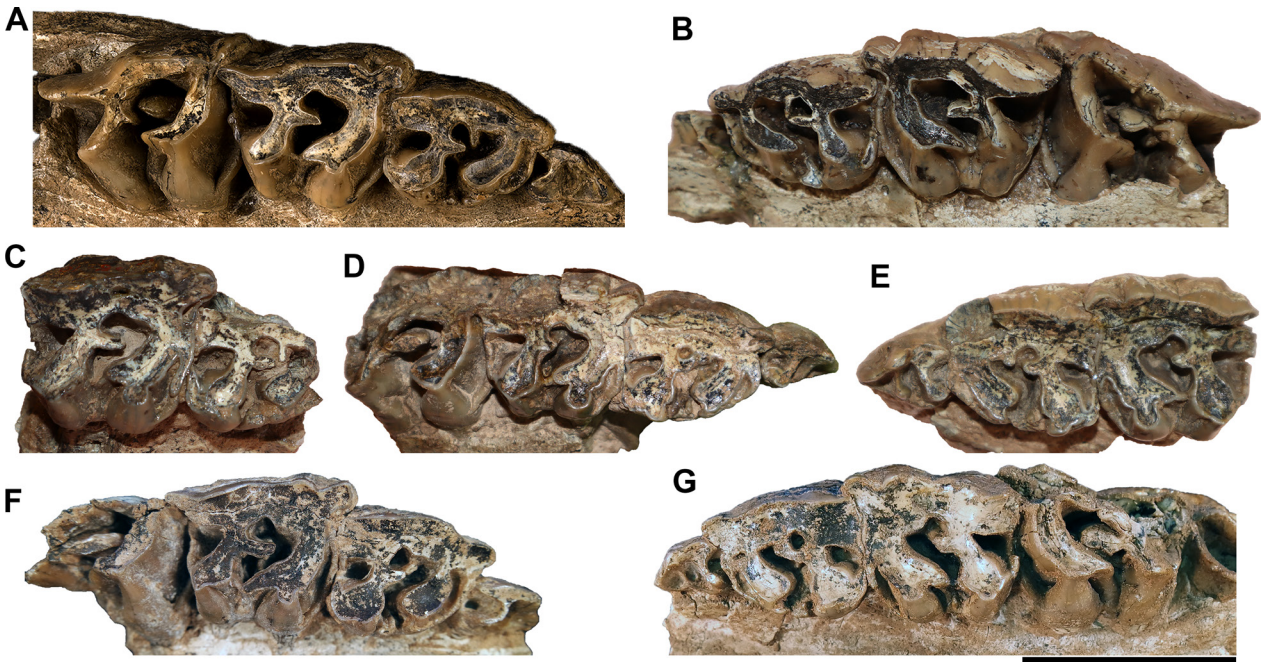

Figure 4. Upper deciduous dentition of *Chilotherium persiae* (Pohlig, 1885) from the Upper Miocene of Maragheh (Iran). **A.** MNHN.F.MAR3053 (right D1-D4); **B.** MNHN.F.MAR3820 (left D1-D4); **C.** MNHN.F.MAR3840 (right D2-D3); **D.** MNHN.F.MAR3841 (right D1-D4); **E.** MNHN.F.MAR3841 (left D1-D3); **F.** NHMW-GEO-2020/0014/0030 (right D1-D4); and **G.** NHMW-GEO-2020/0014/0006 (left D1-D4) in occlusal view. Scale bar: 5 cm.

Description. One almost complete and several partial juvenile skulls of *C. persiae* from the Upper Miocene of Maragheh (Iran) were studied (Fig. 3). The premaxillary bones are absent in all specimens. The nasals are thin, lack any pneumatisation, and share a long, central, prominent suture. In dorsal view, the suture between the nasals and the frontals is an almost straight mediolateral line. In lateral view, the suture between the nasals and the maxillary is relatively straight, starting from the nasal notch and ending at the lacrimal. The nasal notch is situated above the anterior portion of D3. In lateral view, the nasal and lacrimal also share a short suture, separating the maxillary from the frontal. The maxillary exhibits several infraorbital foramina on each side; their exact number cannot be assessed due to the state of preservation of the specimens. The maxillary is partially broken in most specimens, but the few preserved ones feature long, posteriorly projecting pockets for the unerupted molars (as seen in MLU.GeoS.8030, MNHN.F.MAR3078–3079, and NHMW-GEO-2020/0014/0099). The lacrimal is relatively small; it connects ventrally to the frontal and the nasal, anteriorly to the maxillary, and ventrally to the jugal. The jugal shares a wide suture with the maxillary. Immediately behind the orbit, it exhibits a well-developed postorbital process. In ventral view, the maxillary constitutes the largest portion of the palatine. Posteriorly, the maxillary is sutured to the palatinal; the latter reaches anteriorly to the level of the posterior edge of D3. The palatine forms the largest part of the choana. Two symmetrical foramina are present at the level of the posterior portion of D4, near the maxillary-palatinal suture.

Concerning the upper dentition (Fig. 4), several specimens preserve at least some teeth, and some skulls or maxillae preserve the complete deciduous series at least on one side (MLU.GeoS.8029, MLU.GeoS.8030, MNHN.F.MAR3053, MNHN.F.MAR3079, MNHN.F.MAR3820, MNHN.F.MAR3841, NHMW-GEO-2020/0014/0006, and NHMW-GEO-2020/0014/0030). D2 to D4 are hypsodont and highly molarised. D1 has an almost continuous lingual cingulum. The most prominent enamel fold is the metaloph, which separates a comparably large postfossette. No other enamel folds are visible within the tooth. The parastyle and metastyle are relatively well developed in comparison to the generally reduced D1. In specimen MNHN.F.MAR3820, D1 is barely starting to erupt, while D4 has already erupted, though it is not yet worn.

The morphology of D2 can be observed at different wear stages between the different specimens. D2 features a protocone that is somewhat smaller than the hypocone and bears a posterior constriction, forming an antecrochet; the latter does not bend lingually in most specimens. A discontinuous lingual cingulum is present. At the entrance of the median valley, a small enamel pillar is present, but its size varies slightly among the different specimens. In MNHN.F.MAR3079, the antecrochet features a very weak connection to the enamel pillar at the entrance of the median valley. The median valley remains open until the tooth is almost completely worn (as seen in MLU.GeoS.8029). Relatively strong crochet and crista are present; when heavily worn, they can connect to close off the medifossette in some specimens. Very strong anterior and posterior cingula are present, forming a small, closed-off prefossette and a

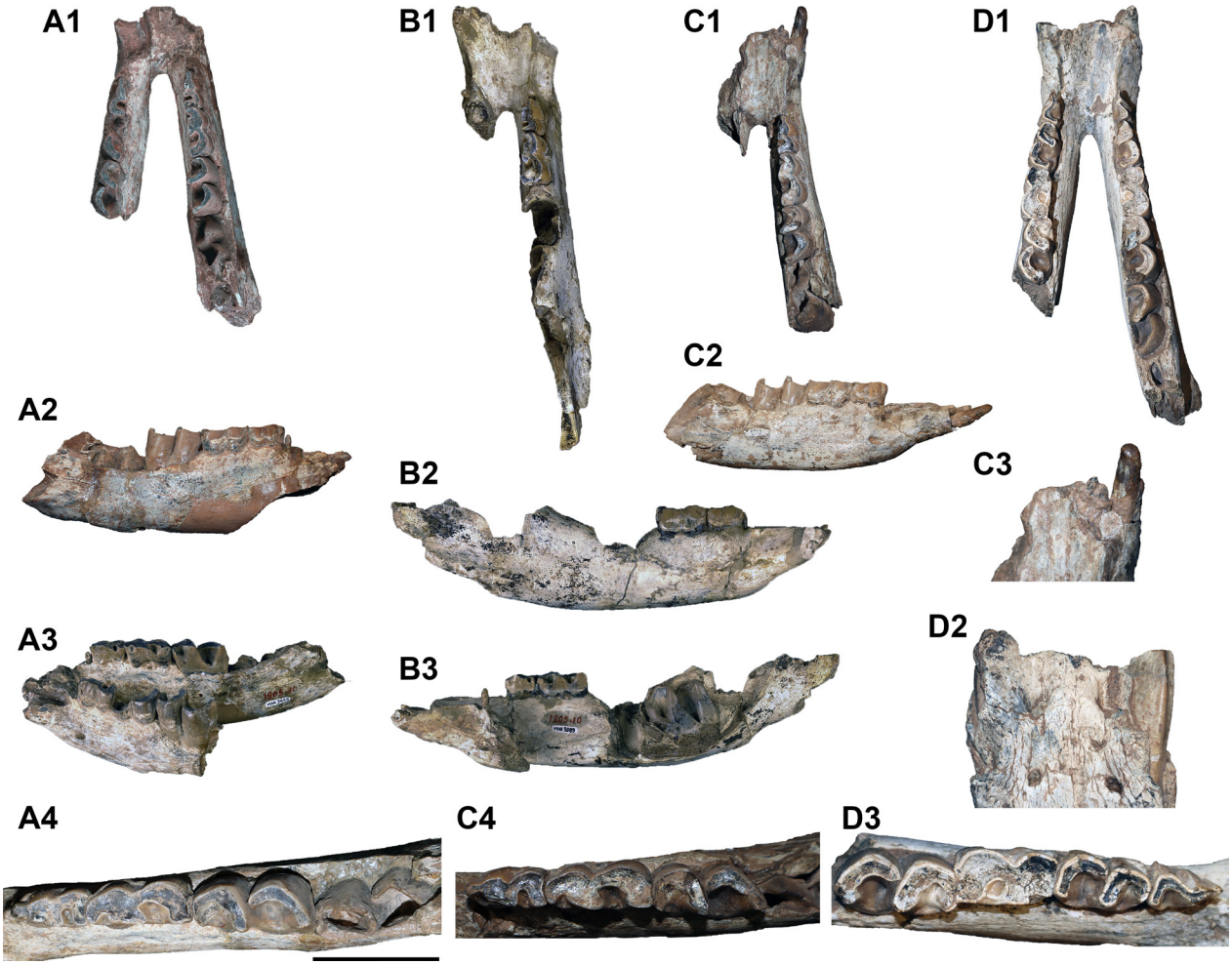

Figure 5. Juvenile mandibles of *Chilotherium persiae* (Pohlig, 1885) from the Upper Miocene of Maragheh (Iran). MNHN.F.MAR3859 (**A**), MNHN.F.MAR3889 (**B**), MNHN.F.MAR3069 (**C**), and MNHN.F.MAR (**D**) are juvenile mandibles in dorsal (**A1**, **B1**, **C1**, and **D1**), lateral (**A2–3**, **B2–3**, and **C2**), and occlusal (**A4**, **C4**, and **D4**) views. Detailed views of the anterior part of the mandibular symphysis in dorsal (**C3**) and ventral (**D2**) views are also given. Scale bar: 10 cm (**A1–3**, **B1–3**, **C1–2**, and **D1**); 5 cm (**A4**, **C3–4**, and **D2–3**).

wide postfossette. The parastyle and metastyle are wide, while the paracone and metacone folds are extremely weak and rounded.

In D3 and D4, the protocone is somewhat larger than the hypocone and bears strong anterior and posterior constrictions, forming an antecrochet that bends lingually in some specimens; the hypocone bears only an anterior constriction. The lingual cingulum is absent on both D3 and D4. At the entrance of the median valley, a small enamel pillar is present in some D3 specimens, such as MNHN.F.MAR3053, while it is absent in D4. A crochet is always present on D3 and D4. A small crista can be present on D3, as seen in NHMW-GEO-2020/0014/0093, where it fuses with the crochet and closes off the medifossette, but is absent in D4. Strong anterior and posterior cingula are present on both deciduous teeth, as well as a large postfossette. The parastyle and metastyle are well developed on both D3 and D4; the paracone fold is rather strong, while the mesostyle and metacone fold are weak. D4 is more hypsodont than D3. All D4s exhibit thin horizontal grooves on the lingual side at the base of the enamel and "ω"-shaped grooves on the buccal side in the middle of the enamel, which can be interpreted as hypoplasias (Mead 1999; Böhmer and Rössner 2018; Hullot and Antoine 2020).

Several juvenile mandibles of *C. persiae* from the Upper Miocene of Maragheh (Iran) are documented in the studied collections (Fig. 5). One specimen preserves the deciduous incisors on the right side of the symphysis (Fig. 5C3). The di1 is tiny, barely projecting from the bone, whereas di2 is much larger but still quite small, with a diameter of approximately 1 cm. Both di1 and di2 are elongated, with a round cross-section. In di1, no enamel is preserved, and in di2, the tooth crown is rounded and slightly asymmetrical. Some specimens preserve a very small, rudimentary d1, at least on one side (Fig. 5A2, A3, B3). When present, it is single-rooted and very short, and its crown has a single tip, without any distinct morphological features. The d2 is well formed; its paralophid is anteriorly oriented and bears a buccal constriction at the level of the anterior valley. The metalophid projects lingually, as does the hypolophid, and is relatively wide, with a lingual constriction. The anterior valley remains open until completely worn. The

posterior valley may form an extremely small fossettid before being completely worn down. A shallow ectolophid groove exists buccally. A relatively weak posterior cingulum is also visible. On the buccal and lingual sides, weak discontinuous cingula are present. In d3, the paralophid projects lingually, with its tip slightly curving posteriorly. A slight constriction in the metalophid can be observed. The ectolophid groove is relatively shallow but deeper than in d2. An anterior and a posterior cingulum are visible, with the anterior one extending towards the buccal side to some degree. In d4, the paralophid projects lingually and is smaller than the metalophid and hypolophid, which are similarly well developed. The trigonid and talonid are not yet connected due to wear. The ectolophid groove is deep and bears a small enamel pillar at its base. Anterior and posterior cingulids are present, and only the anterior one extends slightly to the buccal side. All d4s exhibit thin horizontal grooves in the enamel, clearly visible on the buccal side, which can be interpreted as hypoplasias (Mead 1999; Böhmer and Rössner 2018; Hullot and Antoine 2020).

Chilotherium habereri (Schlosser, 1903)

Figs 6–8

Lectotype. A set of associated P3 and P4 (SNSB-BSPG 1900 XII 622), described and illustrated by Schlosser (1903, pl. 5, fig. 18) and designated as the lectotype of the species by Kampouridis et al. (2025).

Type locality. Upper Miocene red clay deposits in Shanxi Province (China); exact locality unknown

Material. A partial juvenile skull preserving, on both sides, parts of D3, D4, and erupting M1 (GPIT/MA/04830); an almost complete juvenile skull preserving, on the right side, D2–D4 and, on the left side, D1–D4 (GPIT/MA/04843); a partial juvenile skull preserving D1–D4 on both sides (GPIT/MA/04842); a partial subadult skull preserving the heavily worn D4s on both sides (GPIT/MA/04840); a subadult maxilla preserving the heavily worn D4 (GPIT/MA/04844); an almost unworn, complete D4 (GPIT/MA/04821); a D2 (GPIT/MA/04821); a D3 (GPIT/MA/04821); an almost complete subadult mandible preserving the left d4 (GPIT/MA/04826); a partial juvenile mandible preserving, on the right side, d1–d3 and erupting d4 and, on the left side, d2–d3 and erupting d4 (GPIT/MA/04849); a partial juvenile mandible preserving d2–d3 on both sides (GPIT/MA/04820); a partial right juvenile hemimandible preserving d2–d4 (GPIT/MA/04818); and a partial left juvenile hemimandible preserving part of d2 and the unworn d3 (GPIT/MA/04821).

Remarks. The Kutschwan material housed in the GPIT was studied more than a century ago by Hugo Killgus for his PhD (Killgus 1922). He attributed the chilothere material to *Aceratherium habereri* (Killgus 1922, 1923). Soon after, Ringström (1924) erected the genus *Chilotherium* and included this species in it after he revised it. Ringström (1924) also agreed with Killgus (1922, 1923) in referring the Kutschwan chilothere to the species *Chilotherium habereri*. This identification was also supported by Kampouridis et al. (2025).

Description. Three partial juvenile skulls preserving most of the deciduous teeth (Fig. 6), along with one subadult skull and a partial subadult maxilla preserving the D4s with the permanent dentition of *C. habereri*, are present in the material from the Upper Miocene of Kutschwan (China) housed in the GPIT. The premaxillary bones are absent in all specimens. In specimen GPIT/MA/04842, the suture between the premaxillary and maxillary bones seems to start approximately above D1. In one specimen (GPIT/MA/04830), the nasals are completely broken off, while, in the other two specimens, part of the nasals is still preserved, showing that they are thin, lack any pneumatisation, and share a long, prominent suture. In dorsal view, the suture between the nasals and the frontals is an almost straight mediolateral line (Fig. 6B1, C1). The frontals are flat and seem quite porous in the younger two specimens (GPIT/MA/04843 and GPIT/MA/04842), whereas, in the somewhat older skull (GPIT/MA/04830), they are massive and bear a slight depression, resembling those of adult individuals (Fig. 6A1, B1, C1). In specimen GPIT/MA/04830, the parietal crests are very weak but widely separated, with the minimum preserved distance being 55 mm.

In lateral view, the suture between the nasals and the maxillary is relatively straight, starting from the nasal notch and ending at the lacrimal (Fig. 6A3, B4, C4). The nasal notch is situated above the middle portion of D3 in the younger specimens (GPIT/MA/04843 and GPIT/MA/04842) and above the anterior portion of D4 in the slightly more mature individual (GPIT/MA/04830). In lateral view, the nasal and lacrimal also share a short suture, separating the maxillary from the frontal. Immediately behind the orbit, at the widest part of the dorsal side of the cranium, a well-developed postorbital process is present in the frontal. From there, the frontal-parietal crests reach the nuchal crest. The maxillary exhibits several infraorbital foramina, which can vary significantly, even in the same individual, from three to up to six foramina of variable size. The intraspecific variability of this feature has also been mentioned in previous works (e.g. Ringström 1924, p. 29). Posteriorly, the maxillary features long pockets, which include the unerupted molars. The size and length of these pockets seem to depend strongly on the ontogenetic stage of the individual, as they vary in the three specimens: from more than 50 mm in the youngest individual (GPIT/MA/04842: unworn D4) to 85 mm in the slightly more mature individual (GPIT/MA/04843: slightly worn D4) to 99 mm in the oldest individual (GPIT/MA/04830: moderately worn D4). The lacrimal is relatively small, and it connects ventrally to the frontal and the nasal, anteriorly to the maxillary, and ventrally to the jugal. The jugal shares a wide suture with the maxillary. Immediately behind the orbit, the jugal exhibits a less prominent postorbital

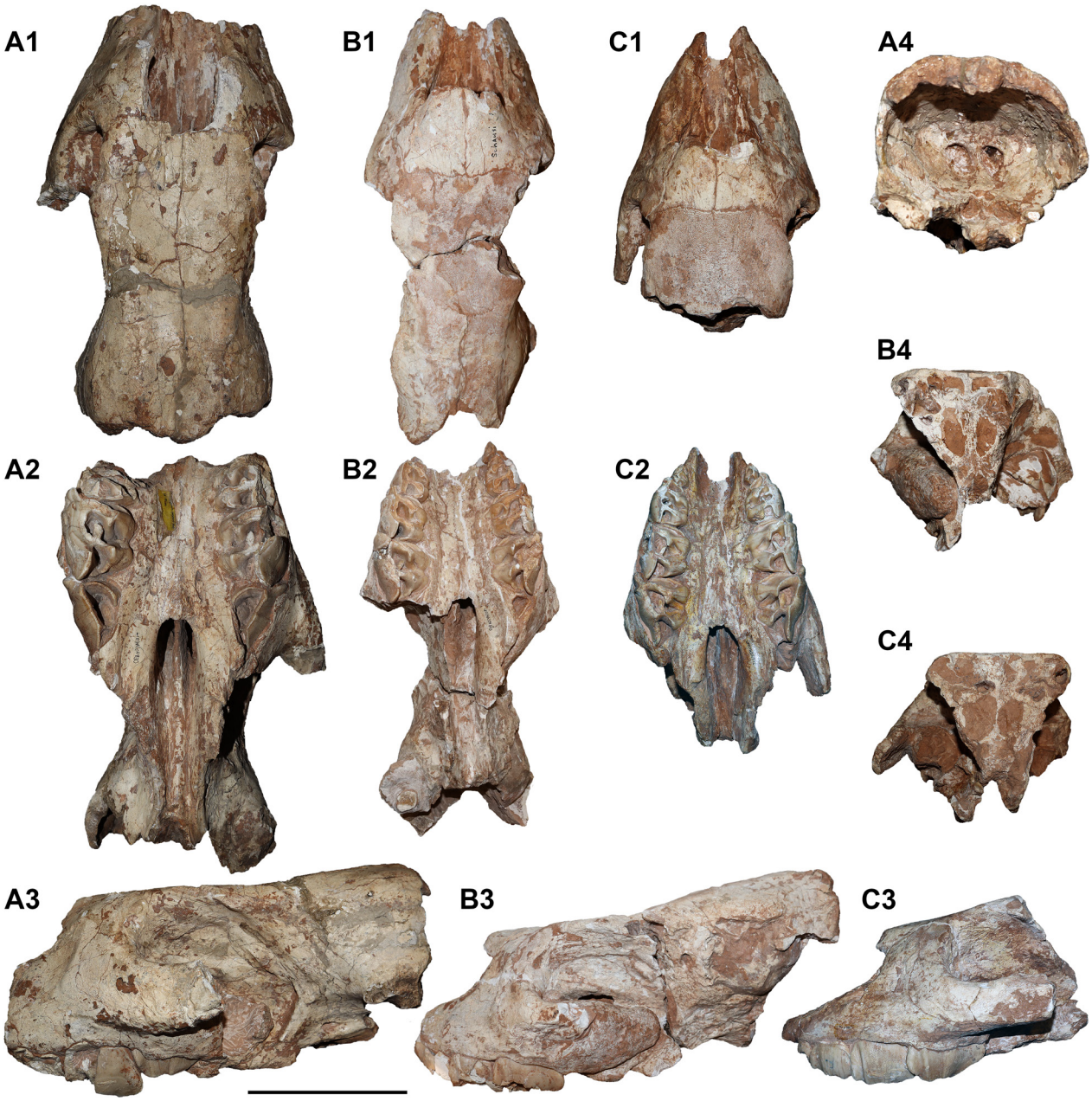

Figure 6. Juvenile skulls of *Chilotherium habereri* (Schlosser, 1903) from the Upper Miocene of Kutschwan (China). GPIT/MA/04830 (**A**), GPIT/MA/04843 (**B**), and GPIT/MA/04842 (**C**) are juvenile skulls in dorsal (**A1**, **B1**, and **C1**), ventral (**A2**, **B2**, and **C2**), lateral (**A3**, **B3**, and **C3**), and caudal (**A4**, **B4**, and **C4**) views. Scale bar: 10 cm.

process compared to the slightly more posteriorly positioned postorbital process on the frontals. The squamosal shares a suture with the jugal, starting at the postorbital process. In specimen GPIT/MA/04830, the posterior portion of the squamosal is sutured to the parietal. The zygomatic arch, along with the post-tympanic and paroccipital processes, is broken off.

In lateral view, one of the most prominent parts is the orbital cavity, which is placed very high dorsally, creating a thin dorsal orbital rim (Fig. 6A3, B4, C4). The anterior portion of the orbital cavity is formed by the frontal, lacrimal, and jugal bones. The lacrimal bone bears two small lacrimal foramina, although in specimen GPIT/MA/04843, only one lacrimal foramen is present on each side. A distinct lacrimal process is not present. The maxillary foramen is visible at the anteroventral portion of the lacrimal-maxillary suture. The sphenopalatine foramen is present at the ventral limit within the orbital cavity. The optic foramen is located posteriorly to the postorbital process, above the posterior edge of the maxillary pocket. In the more complete skull specimen GPIT/MA/04830, the sphenorbital and rotundum foramina are fused and located posteroventrally to the optic foramen, immediately behind the posterior end of the maxillary pocket. In the same specimen, a well-formed caudal alar foramen is visible on the lateral side of the sphenoid bone, immediately behind the large fused sphenorbital and rotundum foramen. Inside the orbital cavity, the sutures for the palatine and sphenoid are not distinguishable, even at this early ontogenetic stage.

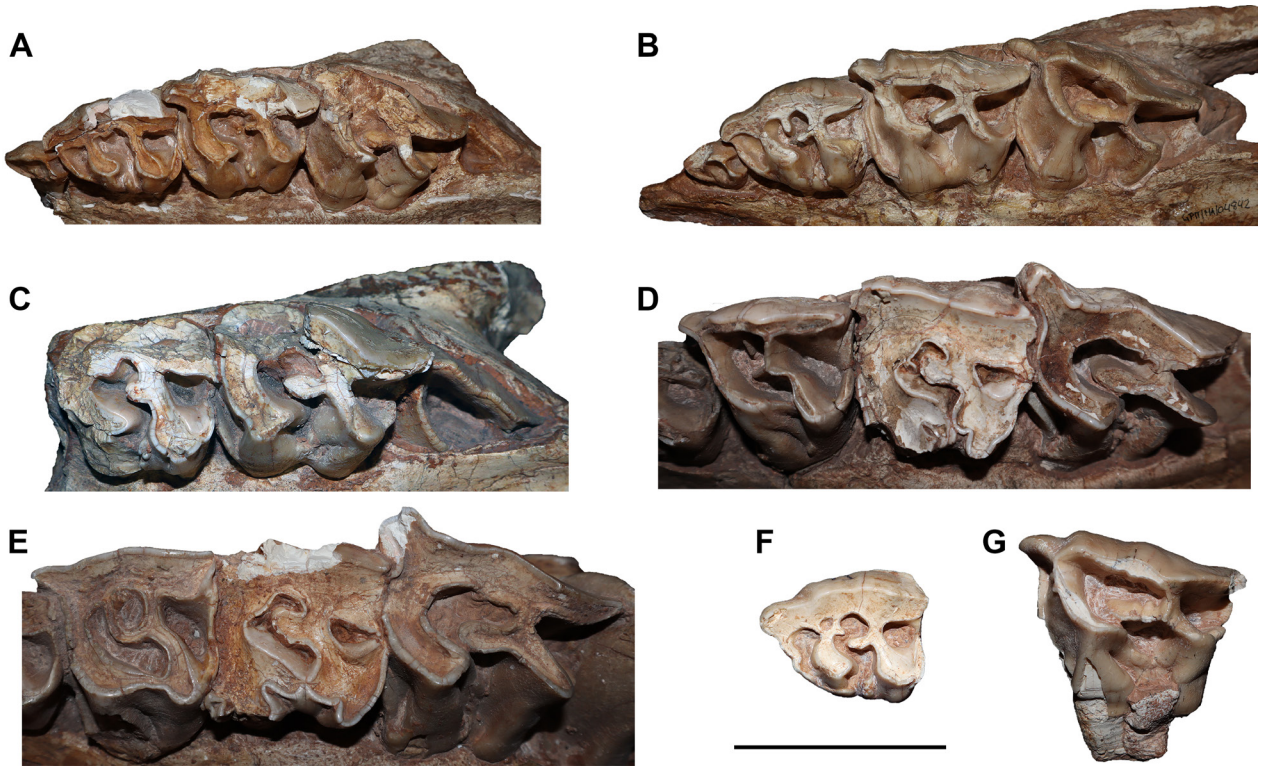

Figure 7. Upper deciduous dentition of *Chilotherium habereri* (Schlosser, 1903) from the Upper Miocene of Kutschwan (China). **A.** GPIT/MA/04843 (left D1–D4); **B.** GPIT/MA/04842 (left D1–D4); **C.** GPIT/MA/04830 (left D3–D4, erupting M1); **D.** GPIT/MA/04840 (left P3, D4, and M1); **E.** GPIT/MA/04844 (P3, D4, and M1); **F.** GPIT/MA/04821 (left D2); and **G.** GPIT/MA/04817 (left D4) in occlusal view. Scale bar: 5 cm.

In ventral view, the maxillary constitutes the largest portion of the palate. The anterior edge of the maxillary-palatine suture reaches the level of the posterior end of D3 (Fig. 6A2, B2, C2). The palatine forms the largest part of the choana. Two symmetrical foramina are present at the maxillary-palatine suture, at the level of the posterior portion of D4. In posterior view, all specimens are damaged and expose features of the endocranium. Specimens GPIT/MA/04843 and GPIT/MA/04842 are broken in the middle of the frontal bones, thus revealing several small cavities inside the skull, which are at least partially separated by thin bone layers. They represent the frontal sinuses, which have also been described for *Chilotherium* by Edinger (1937). In these specimens, there seem to be several rather small extensions of the frontal sinus. It is possible that, when complete, they were all connected, as also described by Edinger (1937) for *C. anderssoni*.

The upper dental material of *C. habereri* comprises the dentition of three partial juvenile skulls, two subadult skulls, and three isolated teeth (Fig. 7). In two partial skulls (GPIT/MA/04843 and GPIT/MA/04842), D1 is preserved and almost unworn. In specimen GPIT/MA/04842, D1 starts being worn before the eruption of D4. D2 to D4 are hypsodont and highly molarised. The morphology and dimensions of D1 are identical in both specimens. It has a single, large root and an almost continuous lingual cingulum. The most prominent enamel fold is the metaloph, which separates a comparably large postfossette. A relatively weak enamel fold in the middle of the tooth probably corresponds to the protocone. The parastyle and metastyle are relatively well developed compared to the generally reduced D1. The maximum height of the tooth crown is 18 mm.

D2 is preserved in the two younger skulls (GPIT/MA/04843 and GPIT/MA/04842). Additionally, one isolated left D2 (GPIT/MA/04821) is present in the studied collection. In all teeth, the protocone is smaller than the hypocone and bears a posterior constriction forming a short antecrochet. A small anterior constriction is present in the hypocone in GPIT/MA/04843. A slightly variable, discontinuous lingual cingulum is present in all teeth, in addition to an enamel pillar at the entrance of the median valley. The protoloph and metaloph are relatively thin. In GPIT/MA/04842 and GPIT/MA/04821, D2 bears a relatively strong crochet and crista, whereas, in GPIT/MA/04843, only a slight enamel bump is present instead of a crista. In GPIT/MA/04821, the crista connects to the protoloph, closing off a small fossette, and a secondary fold splits off from the crista. Strong anterior and posterior cingula are present, forming large pre- and postfossettes. Both cingula continue slightly onto the ectoloph. The parastyle and metastyle are very large. Weak paracone and metacone folds are present only in GPIT/MA/04821.

D3 is preserved in all three partial skulls, and an isolated lingual portion of a D3 (GPIT/MA/04821) is also present in the Kutschwan collection. In all specimens, the protocone is somewhat larger than the hypocone and

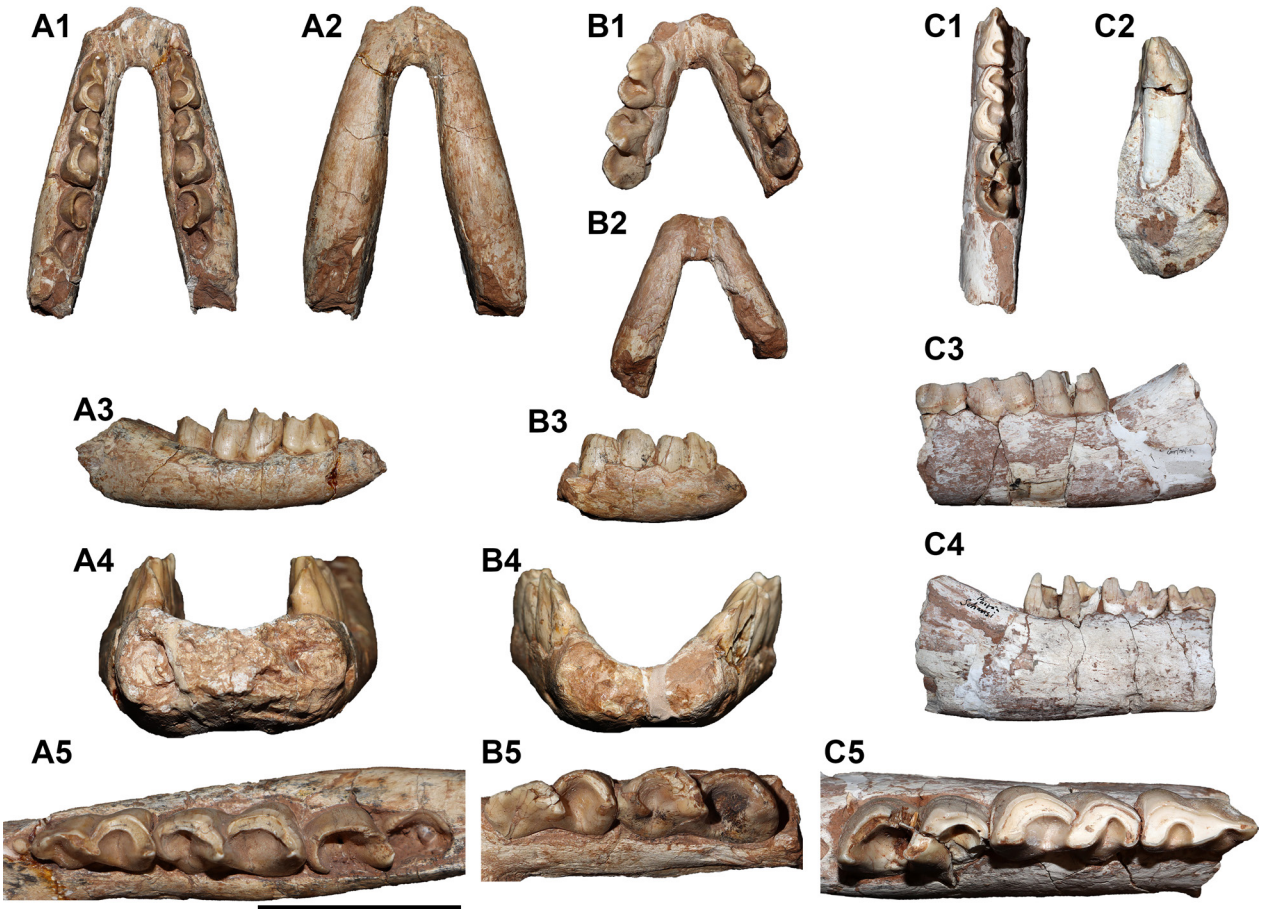

Figure 8. Juvenile mandibles of *Chilotherium habereri* (Schlosser, 1903) from the Upper Miocene of Kutschwan (China). GPIT/MA/04849 (**A**), GPIT/MA/4820 (**B**), and GPIT/MA/4818 (**C**) are juvenile mandibles in dorsal, ventral, lateral, anterior, and occlusal views. Scale bar: 10 cm (**A1–3**, **B1–3**, **C1**, and **C3–4**); 5 cm (**A4–5**, **B4–5**, **C2**, and **C5**).

bears a slight anterior and a strong posterior constriction, forming an antecrochet. The lingual cingulum is absent. At the entrance of the median valley, a small to prominent enamel pillar is present in all specimens. A crochet is always present, though its size may vary. A small crista is present in two specimens (GPIT/MA/04821 and GPIT/MA/04830). In GPIT/MA/04843, the crista is represented by a small enamel bump, whereas, in GPIT/MA/04842, it is completely missing. Strong anterior and posterior cingula are present, forming a short prefossette and a large postfossette. The parastyle and metastyle are well developed. The paracone fold is strong in the specimens where it is not broken off (GPIT/MA/04843 and GPIT/MA/04842), whereas the metacone fold is weak.

D4 is preserved in all partial skulls, and an isolated D4 (GPIT/MA/04821) is also present in the Kutschwan collection. The morphology of D4 resembles that of D3, but it is more hypsodont, and the antecrochet is more prominent and bends lingually. A large crochet is always present, but no crista is visible in any of the specimens. A strong anterior cingulum is present, and a strong posterior cingulum forms a wide postfossette. The parastyle is well developed, and the metastyle is large. The paracone fold is present in all specimens, along with a weak metacone fold. All D4s exhibit thin horizontal grooves in the lower part of the enamel on the lingual side of the tooth and "ω"-shaped grooves in the middle of the ectoloph, which are interpreted as hypoplasias (Mead 1999; Böhmer and Rössner 2018; Hullot and Antoine 2020). Below these enamel defects, the enamel becomes rougher and more irregular. The D4 of GPIT/MA/04842 also exhibits small pits in the enamel, slightly above the groove, which can also be interpreted as hypoplasias, whereas the D4 of GPIT/MA/04843 bears such small pits directly on the horizontal groove. Interestingly, in both specimens, the pits are present only on the protocone. Additionally, the D4 of GPIT/MA/04843 also features a second hypoplasia in the middle of the enamel, approximately 8 mm above the first one.

Four partially preserved mandibles (GPIT/MA/04849, GPIT/MA/04818, GPIT/MA/04820, and GPIT/MA/04821) are available in the Kutschwan collection of the GPIT (Fig. 8). Specimen GPIT/MA/04849 preserves an extremely small and short rudimentary d1 on its right hemimandible. It is single-rooted, and its crown is rounded, approximately 4 mm in diameter and only a few millimetres tall, without any morphological features. The d2 is well developed in all specimens. Its paralophid is anteriorly oriented and bears a buccal constriction, opposite to the anterior valley. The metalophid projects

lingually, as does the hypolophid, and is relatively wide, with a lingual constriction. Both the anterior and posterior valleys remain open until completely worn. A shallow ectolophid groove exists buccally. A relatively weak posterior cingulum is visible. No anterior, lingual, or buccal cingula exist in any d2 studied. In d3, the paralophid projects lingually, and its tip is slightly posteriorly curved. The paralophid is less developed than the metalophid and hypolophid. A slight constriction in the metalophid can be observed in all specimens except GPIT/MA/04818 due to its more advanced wear stage. The hypolophid also bears a slight anterior constriction. Both the anterior and posterior valleys remain open until completely worn. In only two specimens (GPIT/MA/04818 and GPIT/MA/04820), it is possible to observe an extremely small fossettid that might form immediately before being completely worn down. The ectolophid groove is relatively shallow but deeper than in d2. Anterior and posterior cingulids are visible, whereas lingual or buccal cingulids are absent. The d4 is preserved only in three specimens (GPIT/MA/04818, GPIT-PV115054, and GPIT/MA/04826); in GPIT/MA/04826, d4 is the only remaining deciduous tooth, next to permanent teeth. The paralophid is larger than in d3 but still smaller than the metalophid and hypolophid, which are similarly well developed. Both the metalophid and hypolophid exhibit a weak anterior constriction. At the base of the posterior valley, a small enamel pillar is present. The ectolophid groove is deep. Anterior and posterior cingulids are present, but they do not continue on the buccal or lingual sides. All d4s exhibit thin horizontal grooves in the enamel, best visible on the buccal side, which can be interpreted as hypoplasias (Mead 1999; Böhmer and Rössner 2018; Hullot and Antoine 2020).

Chilotherium schlosseri (Weber, 1905)

Figs 9–11

Neotype. A well-preserved skull (GPIH 3015) with an associated mandible (GPIH 3015a), designated by Kampouridis et al. (2023b).

Type locality. Upper Miocene deposits of Samos Island (Greece); exact locality unknown.

Material. An almost complete juvenile skull preserving D1–D4 and M1 on both sides (NHMW-GEO-2009z0088/0001); a partial juvenile skull preserving the maxillary with D1–D4 on both sides (SMNS 47913); a partial juvenile skull preserving only the maxillary, which bears D2–D4 on both sides (SMNS 47914); an isolated D1 (MGL 106691); two isolated D2s (GMM 570 and MGL 107103); a partial mandible preserving the right i2, p2, p3, d4, m1, and m2 and the left i2, p3, d4, m1, and m2 (NHMW-GEO-1911/0005/0033); a partial mandible preserving the right d1–d4, erupting m1, the left d2–d4, and erupting m1 (SMF M 6814); a partial mandible preserving the right p2, d3–d4, erupting m1, the left p2, d3–d4, and erupting m1 (SMF M 6815); and a partial juvenile mandible preserving d2–m1 on both sides, while the i2s are erupting (GMM 593).

Description. One almost complete (NHMW-GEO-2009z0088/0001) and one partial juvenile skull (SMNS 47913), along with some partial maxillae of *C. schlosseri*, exist in the studied material from the Upper Miocene of Samos in Greece (Fig. 9). The premaxillary bones are broken off in all specimens. In dorsal view, the suture between the nasals and the frontals is a relatively straight mediolateral line at the level of the anterior edge of the orbit. The suture between the two frontals is a straight line, when present, and the bones seem quite porous in comparison to the more massive nasals. In the youngest partial skull (SMNS 47913), no frontal-parietal crests are visible. In the ontogenetically older NHMW-GEO-2009z0088/0001, the frontal-parietal crests are well formed and already widely separated (minimum distance = 64 mm). The frontal-parietal suture forms a 50° angle to the frontal suture. Posteriorly, the frontal suture merges with the suture between the parietals.

In lateral view, the suture between the nasals and the maxillary is relatively straight, starting from the nasal notch and ending at the lacrimal. The position of the nasal notch slightly varies in the three available *C. schlosseri* specimens. In the youngest specimen (SMNS 47914), the nasal notch reaches the level of the contact between D2 and D3, whereas, in the slightly more mature SMNS 47913, it reaches the level of mid-D3. In the ontogenetically oldest specimen (NHMW-GEO-2009z0088/0001), the nasal notch reaches the level of the contact with D3 and D4. In lateral view, the nasal and lacrimal share a short suture, thus separating the maxillary from the frontal. Immediately behind the orbit, the beginning of the postorbital process on the frontal is visible in SMNS 47914. The maxillary and lacrimal are positioned below the nasals and frontals. The maxillary exhibits several infraorbital foramina, which can vary significantly, even in the same individual, from three to up to four foramina of variable size. Posteriorly, the maxillae extend into pockets, which house the unerupted molars. The lacrimal is relatively small, and it connects dorsally to the frontal and nasal, anteriorly to the maxillary, and ventrally to the jugal. The jugal shares a wide suture with the maxillary. The zygomatic arches are not preserved on any of the specimens. In lateral view, one of the most prominent parts is the orbital cavity, which is placed very high dorsally and has a thin dorsal margin. In ventral view, the maxillary constitutes the largest portion of the palatine. Posteriorly, the maxilla is sutured to the palatine. The palatine forms the anterior part of the choana, and two symmetrical foramina are placed near the maxillary-palatinal suture, at the posterior portion of D4.

The upper dental material of *C. schlosseri* can be studied based on a number of complete or partial deciduous tooth rows and some isolated teeth (Fig. 10). The D1s in SMNS 47913 are not fully erupted, as they are placed well below the occlusal level of the other teeth (Fig. 9B3, B4, 9C). Thus, D1 seems to finalise

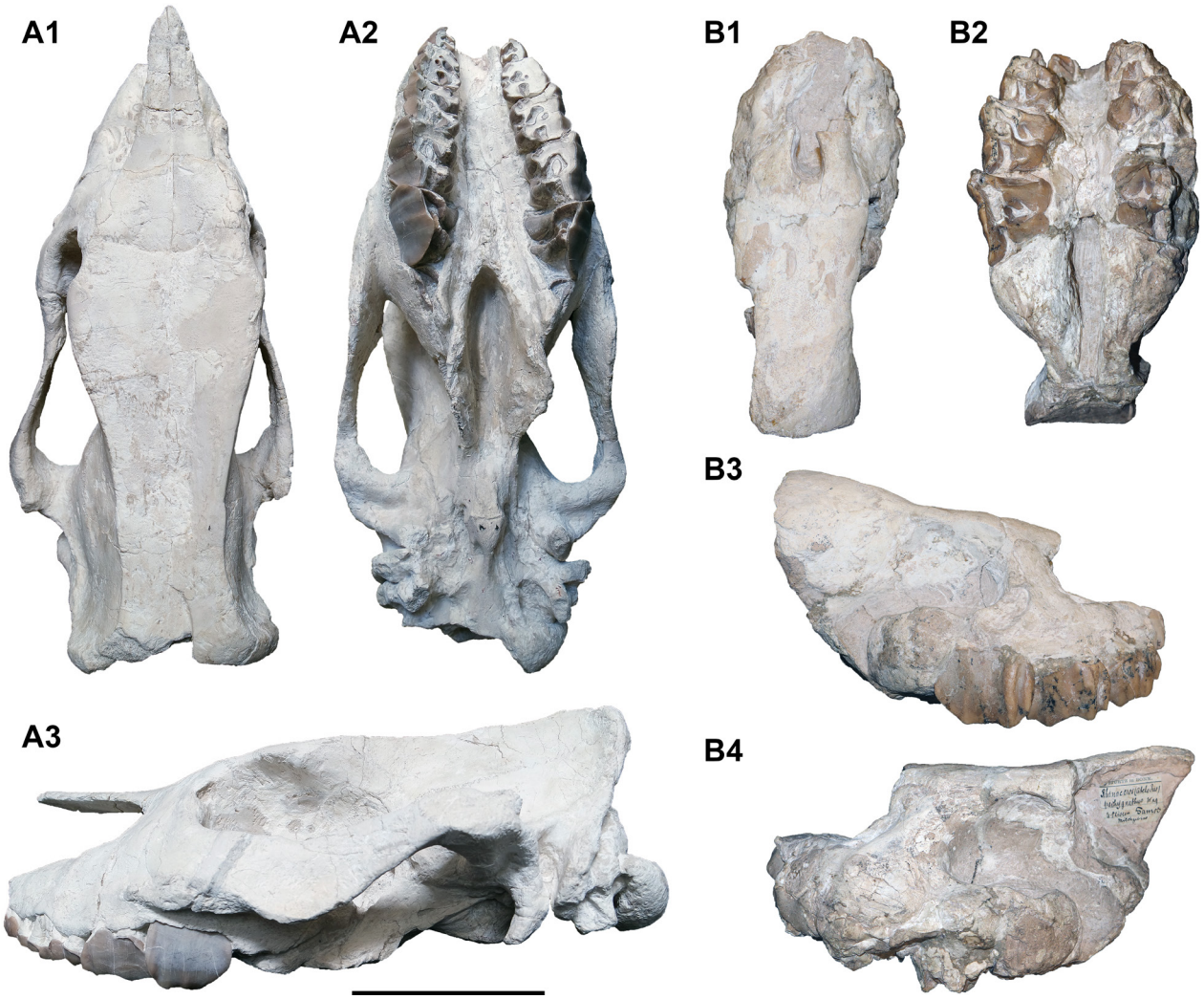

Figure 9. Juvenile skulls of *Chilotherium schlosseri* (Weber, 1905) from the Upper Miocene of Samos Island (Greece). NHMW-GEO-2009z0088/0001 (**A**) and SMNS 47913 (**B**) in dorsal (**A1** and **B1**), ventral (**A2** and **B2**), and lateral (**A3** and **B3–4**) views. Scale bar: 10 cm.

its eruption and start being worn after D4. The root of the tooth in this specimen is not yet formed, also demonstrating the early developmental stage of D1 in SMNS 47913. A continuous lingual cingulum is present, which continues on the posterior side of the tooth, becoming stronger and extremely high. The most prominent enamel fold is probably the metaloph, separating a large postfossette. Another weaker enamel fold in the middle of the tooth probably corresponds to the protoloph. The protocone and metacone seem to be connected to some degree lingually. The parastyle and metastyle are relatively well developed in comparison to the generally reduced D1.

Concerning the other deciduous premolars, D2 to D4 are hypsodont and highly molarised. In D2, the protocone is slightly smaller than the hypocone and bears a posterior and very weak anterior constriction, forming a short antecrochet. A small anterior constriction is present in the hypocone. An enamel pillar is present at the entrance of the median valley in all specimens. A very strong, continuous lingual cingulum is also present in all specimens except SMF M 6805 and NHMW-GEO-2009z0088/0001. The protoloph and metaloph are relatively thin, and a closed medifossette is always present. In all specimens that are adequately worn, a secondary fold splits off the crista and connects to the protoloph, creating a prominent fossette anterior to the medifossette. Very strong anterior and posterior cingula are present, forming large pre- and postfossettes. Both cingula continue slightly onto the ectoloph, even forming an extremely weak buccal cingulum in SMNS 47913. The parastyle and metastyle are very large. Weak paracone and metacone folds are present. All three specimens bear some enamel plications in the median valley. They are most prominent in the medifossette of the left D2 of SMNS 47913, where five small plications are visible.

In D3, the protocone and hypocone are of comparable size. The protocone bears strong anterior and posterior constrictions, forming an antecrochet. The hypocone is weakly constricted anteriorly. An almost continuous lingual cingulum is present in many specimens, although it is very weak in NHMW-GEO-2009z0088/0001 and

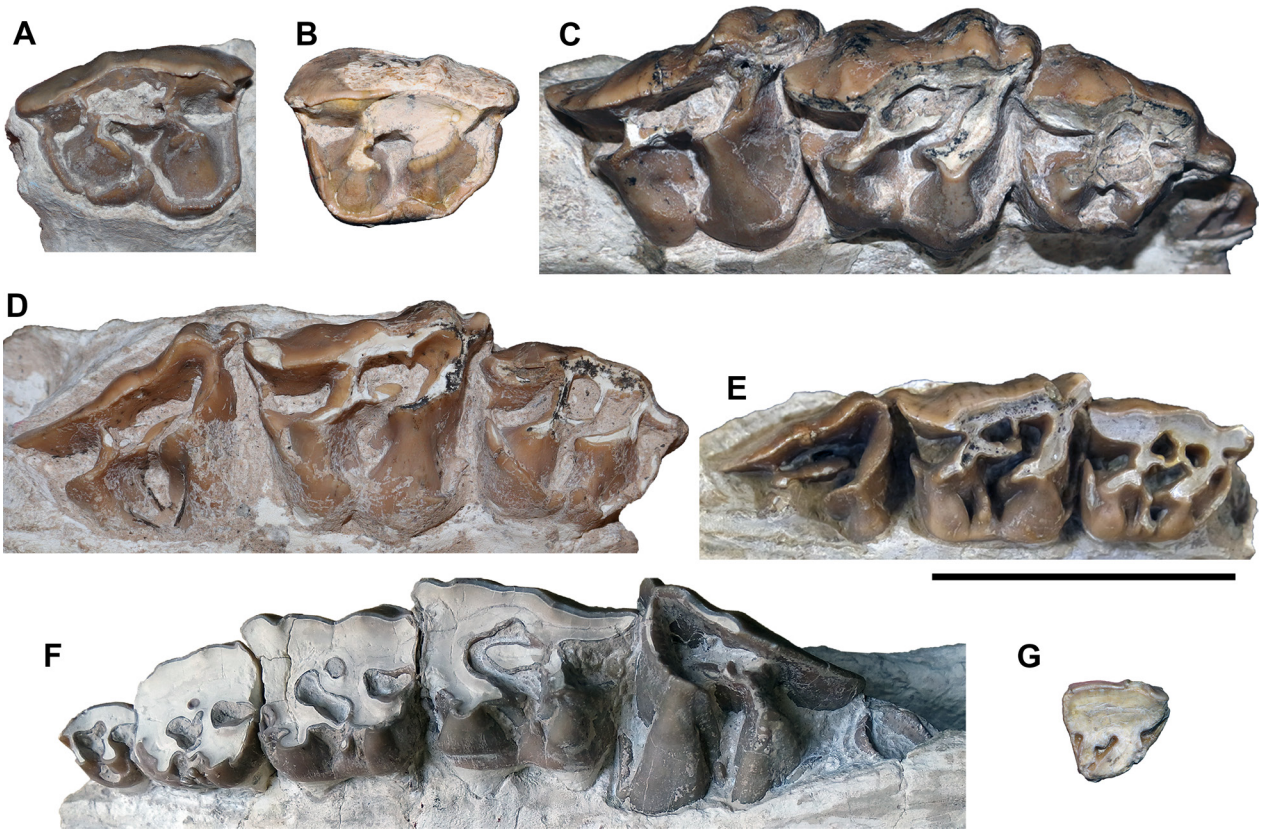

Figure 10. Upper deciduous dentition of *Chilotherium schlosseri* (Weber, 1905) from the Upper Miocene of Samos Island (Greece). **A.** GMM 570 (left D2); **B.** MGL 107103 (right D2); **C.** SMNS 47913 (right D1–D4); **D.** SMNS 47913 (right D1–D4); **E.** SMF M 6805 (right D2–D4); **F.** NHMW-GEO-2009z0088/0001 (left D1–D4, M1); and **G.** MGL 106691 (right D1) in occlusal view. Scale bar: 5 cm.

absent in SMF M 6805. At the entrance of the median valley, a small enamel pillar is present in all specimens. A well-developed crochet is always present. A small crista is present in all specimens, varying in size and shape. Strong anterior and posterior cingula are present, forming a large postfossette. The parastyle and metastyle are well developed. The paracone fold is strong, the mesostyle is extremely weak, and the metacone fold is faintly visible.

D4 has a similar morphology to D3, although the protocone is somewhat larger than the hypocone. The protocone bears strong anterior and posterior constrictions, forming a prominent antecrochet. The hypocone bears only an anterior constriction. A slight, discontinuous lingual cingulum is present in some D4 specimens. A large crochet is always present, but the crista is lacking in all specimens, although a very weak enamel bump might be present instead. A strong anterior cingulum is present, and a strong posterior cingulum forms a wide postfossette. The parastyle is well developed and the metastyle large. The paracone fold is well developed, a slight mesostyle is present, and a weak metacone fold is faintly visible. All D4s exhibit thin horizontal grooves at the base of the crown on the lingual and buccal sides of the enamel, which can be interpreted as hypoplasias (Mead 1999; Böhmer and Rössner 2018; Hullot and Antoine 2020).

Branching furrows are visible on the teeth of three specimens (MGL 107103, SMNS 47913, and SMNS 47914). The traces occur as a branched network of shallow, bleached furrows, covering large parts of the teeth of SMNS 47913 and SMNS 47914 (Fig. 10C, D) and almost the whole ectoloph of MGL 107103 (Fig. 10B). The concentration of these furrows varies significantly. Some areas are only sporadically covered with a few furrows, while in other areas, the furrows cover the surface of the enamel so densely that a continuous, bleached area is produced. These branching furrows represent root etching, which is commonly observed in extant and fossil bones and usually takes the form of irregular furrows, indicating that the bones were altered by plant growth (Behrensmeyer 1978; Andrews and Cook 1985; Fisher 1995; Montalvo 2002; Bader et al. 2009). Humic acids – produced by the plant roots to extract nutrients from the substrate – cause shallow depressions and bleaching of the bone (Behrensmeyer 1978; Morlan 1980), which can result in the pattern seen on the enamel of the studied teeth.

Four juvenile *C. schlosseri* mandibles from Samos in Greece (Fig. 11) were studied. One of them, GMM 593, was published by Andree (1921, pl. 2, figs 4, 5) and originally referred to as *Aceratherium wegneri*?, a junior synonym of *C. schlosseri* (Kampouridis et

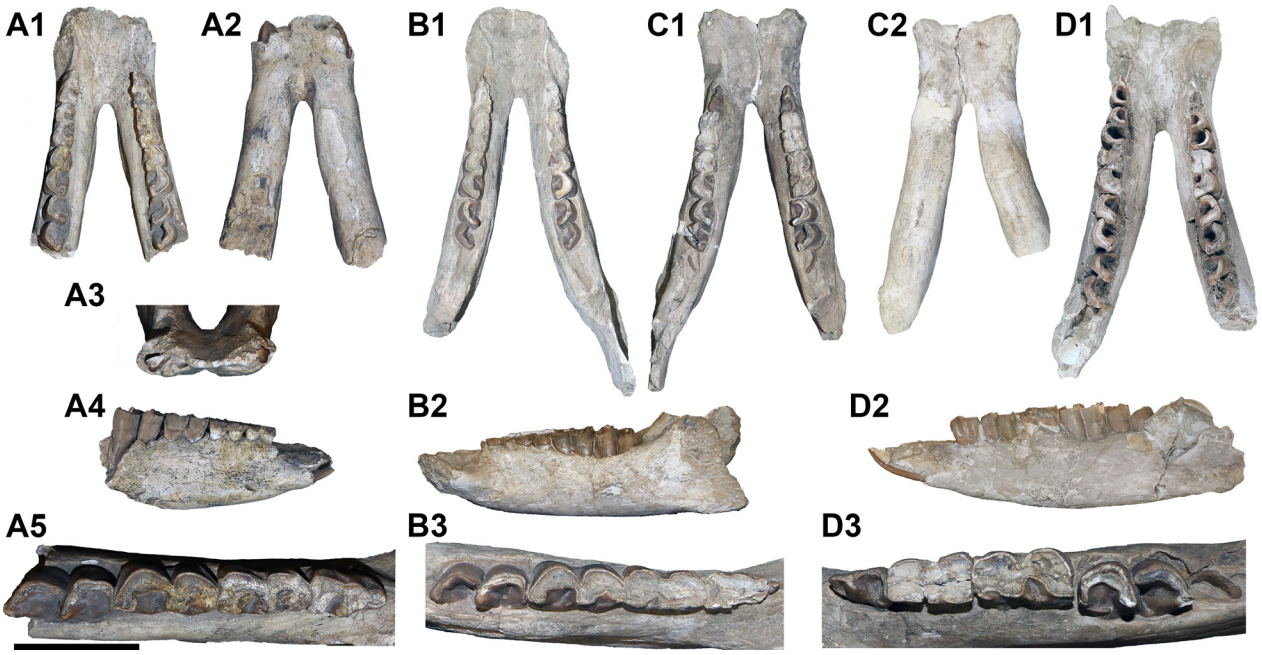

Figure 11. Juvenile mandibles of *Chilotherium schlosseri* (Weber, 1905) from the Upper Miocene of Samos Island (Greece). GMM 593 (**A**), SMF M 6814 (**B**), SMF M 6815 (**C**), and NHMW-GEO-1911/0005/0033 (**D**) in dorsal (**A1**, **B1**, **C1**, and **D1**), ventral (**A2** and **C2**), anterior (**A3**), lateral (**A4**, **B2**, and **D2**), and occlusal (**A5**, **B3**, and **D3**) views. Scale bar: 10 cm (**A1–4**, **B1–2**, **C1–2**, and **D1–2**); 5 cm (**A5**, **B3**, and **D3**).

al. 2022b; Svorligkou et al. 2025). Three additional mandibles are preserved in the studied collections (NHMW-GEO-1911/0005/0033, SMF M 6814, and SMF M 6815). Only one of these specimens, SMF M 6814, preserves the left d1. This tooth is extremely small and has a single, rounded tip that is approximately 6 mm in diameter and 10 mm in height. The d2 is preserved in only two specimens (GMM 593 and SMF M 6814) but is heavily worn in both, with the trigonid and talonid widely connected. The paralophid is constricted and anteriorly oriented. The metalophid projects lingually and slightly distally. The hypolophid projects lingually and is slightly wider than the metalophid. Both anterior and posterior valleys remain open until completely worn. A shallow ectolophid groove exists buccally. A slightly discontinuous buccal cingulum is visible, and it is probably connected to the anterior and posterior cingula, which are not preserved due to wear. The preserved d3s are quite worn down in all specimens, and a wide connection between the trigonid and talonid has been established. The paralophid is less developed than the metalophid and hypolophid. A weak constriction in the metalophid is visible in GMM 593, though only faintly, due to heavy wear. Both the anterior and posterior valleys remain open until completely worn in GMM 593; while in SMF M 6814, the anterior valley is already completely worn off, a small remnant of the posterior valley is still present. In SMF M 6815, both the anterior and posterior valleys are already worn off. The ectolophid groove is relatively shallow but deeper than in d2. A discontinuous cingulid is visible in buccal view, and a very small discontinuous cingulid is also visible lingually at the entrance of the anterior valley. The d4 is moderately to heavily worn in the studied specimens. A narrow connection between the trigonid and talonid is established in the ontogenetically youngest specimens, GMM 593 and SMF M 6814. In NHMW-GEO-1911/0005/0033 and SMF M 6815, the connection between the trigonid and talonid is somewhat wider. The paralophid is relatively short, whereas the metalophid and hypolophid are similarly well developed. In GMM 593, the paralophid of the right d4 exhibits a small distal projection, which is not visible on any other d4. The hypolophid exhibits an anterior constriction in GMM 593 and SMF M 6814. The anterior valley is quite small, whereas the posterior one was probably larger. The anterior valley probably would close shortly before being completely worn due to a small cingulid being present at its entrance in most d4s. The ectolophid groove is deep, and a small enamel pillar is located at its base in all four specimens. High anterior and posterior cingulids are present; they continue faintly on the buccal side and less so on the lingual side.

Chilotherium anderssoni Ringström, 1924

Fig. 12

Type material. The species was erected based on a number of cranial and postcranial elements, without the designation of a holotype (Ringström 1924). Therefore, all material referred by Ringström (1924) to *Chilotherium anderssoni* represents the syntype, including the specimens described herein.

Type locality. Upper Miocene deposits of Daijiagou in Shanxi Province (China), also referred to as “Lok. 30” (Ringström 1924) of the Lagrelius Collection.

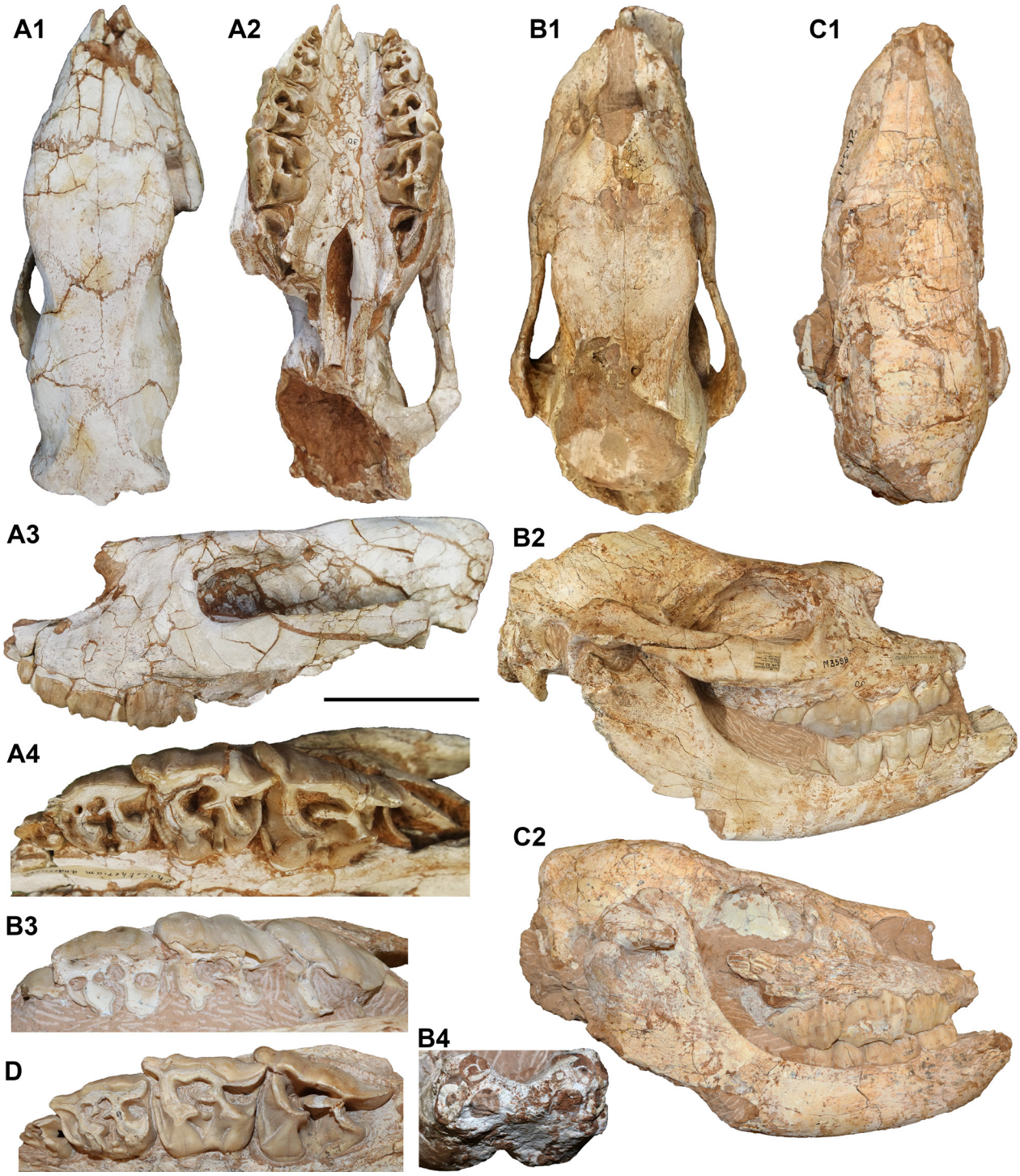

Figure 12. Juvenile skulls and upper dentition of *Chilotherium anderssoni* Ringström, 1924 from the Upper Miocene of Daijiagou (China). SMF M 3592 (**A**), SMF M 3598 (**B**), AMNH FM 26341 (**C**), and AMNH FM 26340 (**D**) in dorsal (**A1**, **B1**, and **C1**), ventral (**A2**), lateral (**A3**, **B2**, and **C2**), occlusal (**A4**, **B3**, and **D**), and anterior mandibular (**B4**) views. Scale bar: 10 cm (**A1–3**, **B1–2,** and **C1-2**); 5 cm (**A4**, **B3-4,** and **C**).

Material. Two almost complete juvenile skulls with their associated mandibles, both preserving all deciduous premolars (AMNH FM 26341 and SMF M 3598); an almost complete skull preserving D1–D4 on both sides (SMF M 3592); and a partial skull preserving D1–D4 on both sides (AMNH FM 26340).

Description. Four juvenile skulls of *C. anderssoni* from the Upper Miocene of Daijiagou or "Lok. 30" (China) are housed in the collections of the AMNH and SMF (Fig. 12) and were donated to these collections by the PMU, where they were originally housed. Specimens AMNH FM 26341 and SMF M 3598 are almost complete skulls with articulated mandibles. In both specimens, the skulls are slightly damaged, with parts of the nasals and zygomatic arches missing, and in SMF M 3598, the parietal and nuchal regions are heavily damaged.

The premaxillary bones are present only in AMNH FM 26340 and are broken off in all other specimens. In dorsal view, the suture between the nasals and the frontals is an almost straight transverse line. The frontals are flat, already slightly showing the frontal depression known in chilotheres. The parietal crests are already visible in all specimens except AMNH FM 26340 and are clearly separated in AMNH FM 26341 and SMF M 3592.

In lateral view, the suture between the nasals and the maxillary is relatively straight, starting from the nasal notch and ending at the lacrimal. The nasal notch is situated above D3 in all specimens, at slightly different levels. The nasal and lacrimal share a very short suture, separating the maxillary from the frontal. Immediately behind the orbit, a well-developed postorbital process is present in the frontal, at the widest part of the dorsal side of the cranium, which is especially well visible in SMF M 3592. From this point, the frontal-parietal crests extend towards the nuchal crest. The maxillary exhibits several infraorbital foramina; three on each side are visible in SMF M 3592. Posteriorly, the maxillary features long pockets, which include the unerupted molars. The lacrimal is relatively small; it connects dorsally to the frontal and nasal, anteriorly to the maxillary, and ventrally to the jugal. The jugal shares a wide suture with the maxillary. Immediately behind the orbit, it exhibits a less prominent postorbital process compared to the slightly more posteriorly positioned postorbital process on the frontals. The squamosal shares a suture with the jugal, starting at the postorbital process. The squamosal is posteriorly sutured to the parietal.

In lateral view, one of the most prominent parts is the orbital cavity, which is placed very high dorsally, creating a thin dorsal orbital rim. The anterior portion of the orbital cavity is formed by the frontal, lacrimal, and jugal. Two small lacrimal foramina are visible in SMF M 3598; they are placed next to each other within a cavity, while in the other specimens, only one foramen is visible. However, it is possible that this is due to remaining sediment covering the distinct foramina. No distinct lacrimal process is visible in either specimen, though it is not certain whether this is the normal morphology or a preservational bias. Within the orbital cavity, no more detailed observations can be made because of the presence of sediment and, in part, due to preservation.

Only AMNH FM 26340 and SMF M 3592 can be studied directly in ventral view, due to the still-attached mandible in the other two specimens. Additionally, Ringström (1924, pl. 3, fig. 1) provided illustrations of another juvenile skull, which is housed in the collections of the PMU, in ventral view. The maxillary constitutes the largest portion of the palate. Posteriorly, the maxillary is sutured to the palatine, which anteriorly reaches the level between D3 and D4. The palatine forms the largest part of the choana. In the palatine, close to the maxillary-palatinal suture, an asymmetrical number of foramina is present at the level of the unerupted M1; on the right side, three foramina are present, whereas on the left side, probably two are present, placed very close to each other.

In posterior view, three of the specimens are damaged. In AMNH FM 26340, the posterior portion is completely missing. In SMF M 3592, only the dorsal portion is preserved, including the nuchal crest, but the posterior side is almost completely covered by a layer of sediment. In SMF M 3598, only the ventral portion, including the foramen magnum, is preserved, while dorsally the brain cavity is exposed; the latter is filled with sediment. In AMNH FM 26341, most of the occipital region is preserved, with only slight damage and some parts partially covered by sediment. The outline of the skull is bell-shaped, and the central tubercle of the nuchal crest is rather weak. The occipital fossa seems fairly shallow, and the occipital crests are weak and fairly wide. The foramen magnum is large and shows a dorsal incision with a rounded end.

The upper deciduous dentition of *C. anderssoni* can be observed in all studied specimens, as well as in the specimen housed in the PMU illustrated by Ringström (1924, table 3, fig. 6). The occlusal surface of the upper dentition of SMF M 3598 is visible only for the left tooth row; however, even there, the lingual portion is still covered in sediment, and it is not possible to assess certain features, such as the lingual cingula and development of the proto- and hypocone constrictions, along with the antecrochet. D2 to D4 are hypsodont and highly molarised. D1 is present in all three specimens and has already been worn. In SMF M 3598, D4 has also just started being worn, based on the continuous wear facet from the parastyle to the protoloph. In AMNH FM 26340 and the specimen illustrated by Ringström (1924, table 3, fig. 6), D4 has barely started being worn, based on a tiny wear facet on the protoloph, while D1 exhibits a more extensive wear facet. Therefore, D1 erupts slightly before D4 in this species. A continuous lingual cingulum is present; it extends on the posterior side in both SMF M 3592 and the Ringström specimen. The hypocone is well formed in all specimens; in SMF M 3592, it is not directly connected to the metaloph, whereas, in the Ringström specimen, this connection is very weak. The metaloph separates a large postfossette. The protocone is smaller than the hypocone, and the protoloph is similar in size to the metaloph. The parastyle is well developed and anteriorly projecting. The metastyle is slightly shorter than the parastyle, but still relatively long.

On D2, the protocone is smaller than the hypocone and bears a posterior and weak anterior constriction, forming a short antecrochet. A weak anterior constriction is present in the hypocone. A moderate, discontinuous lingual cingulum is present, along with an enamel pillar at the entrance of the median valley. In SMF M 3592, there seems to be an enamel pillar next to the base of the antecrochet in the right D2. The protoloph is thinner than the metaloph. A strong crochet is present, along

with a crista; these folds are fused in the Ringström specimen and may also fuse in the other two specimens with further wear, forming a closed medifossette. In AMNH FM 26340 and SMF M 3592, a secondary fold splits off the crista and connects to the protoloph, closing off a prominent fossette anterior to the still-open medifossette. In SMF M 3598, a small secondary enamel fold branches off from the protoloph and nearly connects to the crista; with slightly more wear, it would likely fuse, creating the same fossette. In the Ringström specimen, the medifossette is already closed, and with further wear, it is possible that a similar fossette may form anterior to it. Very strong anterior and posterior cingula are present, forming large pre- and postfossettes. The posterior cingulum extends slightly onto the ectoloph. The parastyle and metastyle are very strong, whereas the paracone and metacone folds are weak.

In D3, the protocone and hypocone are of comparable size. The protocone bears strong anterior and posterior constrictions, forming an antecrochet, whereas the hypocone is only weakly constricted anteriorly. No lingual cingulum is present, but a small enamel pillar occurs in all specimens at the entrance of the median valley. A well-developed crochet is always present. A long crista is present in the Ringström specimen, while only a small enamel bump is visible in the other specimens. Strong anterior and posterior cingula are present, with the latter forming a large postfossette. The parastyle and metastyle are well developed. The paracone fold is strong, and an extremely weak mesostyle is present.

In D4, the protocone is somewhat larger than the hypocone. The protocone bears strong anterior and posterior constrictions that form a prominent antecrochet, and the hypocone bears an anterior constriction. An enamel pillar is present at the entrance of the median valley in SMF M 3592 but is absent in AMNH FM 26340. A large crochet is always present, and an enamel bump in place of a crista appears to be present. A strong anterior cingulum is present, and a strong posterior cingulum forms a wide postfossette. The parastyle is well developed, and the metastyle is wide. The paracone fold is well developed, the mesostyle is weak, and the metacone fold is faintly visible. D4 shows thin horizontal grooves at the base of the crown on the lingual side, as well as "ω"-shaped grooves in the middle of the ectoloph, which can be interpreted as enamel hypoplasias (Mead 1999; Böhmer and Rössner 2018; Hullot and Antoine 2020). In AMNH FM 26340, the hypoplasia is visible only on the lingual side because the D4s are not fully erupted. In AMNH FM 26341, the presence of hypoplasia cannot be assessed because the D4s are largely unerupted and the skull is still attached to the mandible, preventing evaluation of the lingual side.

Only one juvenile mandible of *C. anderssoni* from the Upper Miocene of Daijiagou (China) housed at the SMF and a specimen figured by Ringström (1924, table 3, figs 2, 5) can be studied. Specimen SMF M 3898 is articulated to the previously described skull (Fig. 12B2, B3), and the occlusal surfaces of the teeth are observable only on the right tooth row. Specimen AMNH FM 26341 also includes a skull and mandible that are attached, but the dentition cannot be observed in this specimen. In all three specimens, the anterior portion can be studied to some extent. In Ringström's specimen, two deciduous incisors, di1 and di2, are preserved, including the crowns of the teeth, which are very short, small, and rounded; di1 is less than half the size of di2. In SMF M 3898, only the roots of these teeth are visible, but both deciduous incisors are present (Fig. 12B4). The roots have a rounded cross-section and are small, with di1 being smaller than di2, though the size difference is less pronounced than in Ringström's specimen. In AMNH FM 26341, the anterior part is broken and covered by sediment, preventing observation of the incisor roots. SMF M 3898 preserves d1 on both tooth rows, whereas in Ringström's specimen, it is visible only on the right side. In AMNH FM 26341, d1 is not present on either side. Ringström (1924) noted that the presence of this tooth varies among specimens and may even differ between the right and left sides within the same individual, as in the specimen he illustrated (Ringström 1924, table 3, fig. 2). This tooth is extremely small and bears a single, rounded cusp. The d2 is moderately worn in both specimens, and the trigonid and talonid are connected. The paralophid is anteriorly oriented and constricted. The metalophid projects lingually and distally, and the hypolophid is slightly wider and also projects lingually. Both the anterior and posterior valleys seem to remain open until completely worn. An ectolophid groove exists buccally and appears deeper in Ringström's specimen than in SMF M 3898. No cingulids are visible. The d3 is likewise moderately worn in both specimens, with the trigonid and talonid already connected. The paralophid is less developed than the metalophid and hypolophid. A slight constriction of the metalophid is visible in Ringström's specimen. Both the anterior and posterior valleys probably remain open until completely worn, although, in Ringström's specimen, a weak lingual cingulid may be present in the anterior portion of the tooth. The ectolophid groove is relatively deep. No discontinuous cingulid is visible in buccal view in SMF M 3598. The morphology of d4 cannot be properly assessed, neither in SMF M 3598, because the tooth is embedded in sediment, nor in Ringström's specimen, because it is not fully erupted and properly worn. In Ringström's specimen, the paralophid is relatively short, whereas the metalophid and hypolophid are similarly well developed. A weak and most likely discontinuous cingulid seems to be present at the entrance of the anterior valley in d4 of Ringström's specimen. The ectolophid groove is deep, and a weak enamel bump is located at its base in SMF M 3598. In the latter specimen, an "ω"-shaped groove is visible approximately at the middle of the d4 crown in buccal view, which represents enamel hypoplasia (Mead 1999; Böhmer and Rössner 2018; Hullot and Antoine 2020).

Comparison

Late Miocene horned rhinoceroses

During the Late Miocene, several different Rhinocerotidae species occurred in Eurasia. Along with the hornless rhinocerotids or aceratheriines, horned rhinocerotines (e.g. Geraads and Koufos 1990; Antoine and Saraç 2005; Deng 2006b; Geraads and Spassov 2009; Antoine and Sen 2016; Hullot et al. 2023) and elasmotheriines were widespread on the continent (e.g. Chow 1958; Deng 2005b, 2006b, 2008; Kampouridis et al. 2022a; Antoine et al. 2025).

The differentiation of the studied material from elasmotheriines is very easy, as elasmotheriines are much larger in size, their teeth are highly hypsodont, and their enamel pattern is very complex, usually involving very long crochets, cristae, antecrochets, and, in the more derived elasmotheriines, enamel plications as a prominent feature (see Antoine 2002, 2003; Antoine et al. 2002; Deng 2007, 2008; Geraads and Zouhri 2021; Kampouridis et al. 2022a). For instance, the height of an almost unworn D4 of *C. habereri* (GPIT/MA/04830) from the Upper Miocene locality of Kutschwan (China) is 48 mm, whereas the height of a heavily worn D4, which is close to being shed, of *Parelasmotherium schansiense* (GPIT-PV-86051) from the same locality is 41 mm. Additionally, the teeth of elasmotheriines, including the deciduous ones, display more strongly developed cristae, crochets, antecrochets, and sometimes also strong enamel plications compared to chilotheres (e.g. Antoine 2002; Lu et al. 2023). In the case of *P. schansiense* (GPIT-PV-86051), D4 has a branched crochet and antecrochet (Kampouridis et al. 2022a, fig. 1A), along with multiple enamel plications, which are more pronounced when heavily worn (Kampouridis et al. 2022a, fig. 2A1).

The distinction of the studied material from rhinocerotines is more difficult and needs a more detailed comparison of the upper tooth morphology (Fig. 13; Table 1). For many species, the morphology of the deciduous teeth is not known at all or only poorly known, except for some well-sampled species. There are significant morphological differences in the deciduous dentition of horned rhinoceroses, such as *Dihoplus pikermiensis* and *Ceratotherium neumayri* (Fig. 13I, J) from the Upper Miocene of the Balkan-Iranian zoogeographical province (e.g. Geraads 1988; Giaourtsakis et al. 2006; Geraads and Spassov 2009; Giaourtsakis 2009); *Pliorhinus megarhinus* (de Christol, 1835) from the Upper Miocene to Early Pliocene of Europe (e.g. Dawkins 1865; Fukuchi et al. 2009; Pandolfi et al. 2021); *Pliorhinus ringstromi* (Arambourg, 1959) (Ringström 1924; Li et al. 2024) from the Upper Miocene of China; as well as *Lartetotherium sansaniense* (Lartet in Laurillard, 1848) from the Middle Miocene of Europe and *Lartetotherium cixianensis* (Chen & Wu, 1976) from the Middle Miocene of China (Cerdeño 1996; Heissig 2012; Li and Deng 2023), compared to the studied chilotheres (Fig. 13, Table 1).

For instance, D1 is generally smaller in chilotheres than in these horned species, and the morphology is not as well developed; it bears weaker and shorter proto- and metalophs, and the cusps are generally much smaller or even absent in chilotheres. In a sample of 35 studied *Chilotherium* D1s, the width is between 12.8 and 20.3 mm, whereas in *Ceratotherium neumayri*, it is at least 20.6 mm (Giaourtsakis et al. 2006, table 2; Geraads and Spassov 2009, table 5, $n = 8$; Alifieri 2019, table 2); in *D. pikermiensis*, it is at least 21.8 mm (Giaourtsakis et al. 2006, table 2; Geraads and Spassov 2009, table 5, $n = 15$; Alifieri 2019, table 2); in *Dihoplus schleiermacheri* (Kaup, 1832), D1 width is at least 24 mm ($n = 2$; Guérin 1980); and in *P. megarhinus*, it is at least 22 mm ($n = 2$; Guérin 1980). The only rhinocerotine species that bears a narrower D1 is *Lartetotherium*, where the width is between 16 mm and 23 mm (Guérin 1980; Cerdeño 1996; Heissig 2012; Li and Deng 2023), thereby somewhat overlapping with the value range of chilotheres. In D2, a prefossette is always present and relatively large, whereas in rhinocerotines, the prefossette is usually absent. The postfossette is larger and the paracone rib much weaker in chilotheres than in the mentioned horned rhinoceros species (Fig. 13). Additionally, the protocone constriction is more prominent in chilotheres than in any of the compared horned rhinoceroses; notably, the protocone is not at all constricted in *Ceratotherium neumayri* (Fig. 13) or *Lartetotherium* spp. Additionally, chilotheres have a much longer parastyle in D2 compared to the horned species (Fig. 13). In D3 and D4, the protocone bears strong mesial and distal constrictions, creating a strong antecrochet, whereas in *Ceratotherium neumayri*, the protocone is not constricted, and in *Lartetotherium sansaniense*, *D. pikermiensis*, *P. ringstromi*, and *P. megarhinus*, it is only slightly constricted, creating either no antecrochet or only a faint one (Fig. 13). Additionally, the hypocone is always constricted, moderately in D3 and strongly in D4 of chilotheres, whereas in *Ceratotherium neumayri*, it is not constricted at all, and in *Lartetotherium sansaniense*, *D. pikermiensis*, *P. ringstromi*, and *P. megarhinus*, it is only slightly constricted. Based on these features, a maxilla from Samos that was assigned to *Rhinoceros schleiermacheri* by Weber (1904, pl. 16, fig. 1) belongs to a chilothere, as previously suggested (Giaourtsakis et al. 2006). Based on the specific features that can be observed in this specimen, such as the protocone constriction, along with the strong and continuous lingual cingulum in D2 and a discontinuous lingual cingulum in D3, an assignment to *C. schlosseri* seems plausible. This specimen was housed in the collections of the SNSB-BSPG and was destroyed during the Second World War, along with a large part of the palaeontological collection (Nothdurft and Smith 2002; Kampouridis et al. 2023b). Concerning cranial morphology, when fairly complete skulls are available, it is very easy to distinguish chilotheres from any horned rhinoceros, including elasmotheriines, as the former are characterised by shorter and dorsally flattened crania that lack any nasal horn boss, which is documented in juvenile rhinocerotines (Figs 3A1,

Table 1. Morphological differences in the upper deciduous dentition of Late Miocene chilotheres and rhinocerotines. The latter are exemplified by *Ceratotherium neumayri* and *Dihoplus pikermiensis* (modified after Giaourtsakis et al. 2006, table 3).

	Feature	*Ceratotherium neumayri*	*Dihoplus pikermiensis*	Chilotheres
D1	Relative size	Slightly reduced	Normal	Very reduced
	Protoloph	Very long, bends posterolingually, blocking the entrance of medisinus	Normal, vertical, does not bend	Reduced, very short and narrow, if present
	Metaloph	Reduced, very short	Normal, long	Reduced, very short
D2	Lingual cingular pillar	Present in front of the entrance of medisinus	Absent	Usually present in front of the entrance of medisinus
	Protocone constriction	Unconstricted	Slightly constricted	Constricted
	Prefossette	Absent	Absent	Present, large
	Size of postfossete	Very small and narrow, if present	Large, wide	Very large, wide
	Hypostyle	Not developed or distinct from posterior cingulum	Present, distinct from posterior cingulum	Not developed or distinct from posterior cingulum
	Paracone rib	Very strong, usually double	Strong, always single	Weak
	Metacone rib	Absent or faint, only at the top of the crown	Present, clearly marked and continuous down to the base of the crown	Absent or faint only at the top of the crown
	Parastyle	Moderate	Moderate	Long
D3 and D4	Lingual cingular pillar	Present in front of the entrance of medisinus	Absent	Present in front of the entrance of medisinus (not always in D4)
	Protocone constriction	Unconstricted	Slightly constricted	Strongly constricted
	Hypocone constriction	Unconstricted	Slightly constricted	Moderately in D3, strongly in D4
	Antecrochet	Absent	Weak	Strong
	Crista	Always present	Always absent	Sometimes present but weak
	Medifossete	Usually present	Always absent	Sometimes present
	Metacone rib	Absent or faint, only at the top of the crown	Present, clearly marked and continuous down to the base of the crown	Weak, only at the top of the crown

2C1, 8A1, 11B). This morphology is well exemplified by the beautifully preserved juvenile *C. schlosseri* skull housed in the NHMW (NHMW-GEO-2009z0088/0001) and well-preserved skulls of *C. persiae* (MNHN.F.MAR3053 and MLU.GeoS.8030) and *C. anderssoni* (AMNH FM 26341 and SMF M 3598), in contrast to the morphology observed in *Ceratotherium neumayri* (Giaourtsakis et al. 2006, fig. 2a; Giaourtsakis 2009, pl. 2, fig. 2), *Lartetotherium* spp. (Cerdeño 1996, pl. 1, figs 1–2; Li and Deng 2023, fig. 1A–B), *P. ringstromi* (Li et al. 2024, fig. 5a), and *D. pikermiensis* (NHMW-GEO-1863/0001/0018).

In the mandible, there are also several features that can distinguish the studied chilothere material from horned rhinoceroses. For instance, chilotheres have a very wide mandibular symphysis, even in very young individuals, that fuses at a very early ontogenetic stage. In GPIT/MA/4820 of *C. habereri*, which is the ontogenetically youngest chilothere individual studied here, d2 and d3 are barely worn, and yet the symphysis is already fully fused. In GPIT/MA/04849, the anterior portion of the mandibular symphysis is broken off, but the root of the right di2 is visible, and its cross-section is round and approximately 10 mm in diameter. In MNHN.F.MAR3069 of *C. persiae*, all deciduous premolars have erupted and are moderately worn, and the symphysis is already rather wide and features a very long diastema between d2 and di2, with a crest running along it; this mandible also preserves a tiny di1. Two mandibles of *C. anderssoni* – SMF M 3598 and the specimen figured by Ringström (1924, pl. 3, figs 2, 5) – preserve both deciduous incisors, as also specifically mentioned by Ringström (1924). The condition concerning the incisors in horned rhinoceroses such as *Ceratotherium neumayri*, *Lartetotherium* spp., *D. pikermiensis*, *P. ringstromi*, and *P. megarhinus* differs from that observed in chilotheres. In the juvenile mandibles HLMD-Sam.77 and GPIH 3017 of *Ceratotherium neumayri*, there are no deciduous incisors, but it is possible that very small, diminutive incisors were present and are lacking in the specimens studied due to their state of preservation. In *D. pikermiensis*, *D. ringstromi*, and *D. megarhinus*, both deciduous incisors may be present (Ringström 1924, pl. 1, fig. 4; Giaourtsakis et al. 2006; Alifieri 2019, fig. 12; Pandolfi et al. 2021). However, the size and form of the symphysis differ significantly, as the symphysis in *Dihoplus* and *Pliorhinus* species is narrow compared to that in chilotheres and does not feature a prominent crest on the diastema (see Ringström 1924, pl. 1, fig. 4; Giaourtsakis et al. 2006). Another striking difference between chilotheres and rhinocerotines is the development of d1, which in chilotheres is either absent or, when present, extremely reduced and small, having a small, rounded tip with a diameter of 5 mm. In *Lartetotherium sansaniense*, *Ceratotherium neumayri*, *D. pikermiensis*, *D. ringstromi*, and *D. megarhinus*, d1 is always present and is not reduced; its length is usually more than 15 mm, and it has distinct morphological features (Dawkins 1865, figs 6, 7; Ringström 1924, pl. 1, fig. 4; Giaourtsakis 2009, pl. 7, figs 7–9; Heissig 2012),

Figure 13. Comparative figure with upper dentition (left D1-D4) of the studied Late Miocene chilothere species and rhinocerotines. **A, B.** *Chilotherium persiae* from Maragheh in Iran (**A.** MNHN.F.MAR3820 and **B.** MNHN.F.MAR3053, mirrored); **C, D.** *Chilotherium habereri* from Kutschwan in China (**C.** GPIT/MA/04842 and **D.** GPIT/MA/04843); **E, F.** *Chilotherium schlosseri* from Samos in Greece (**E.** SMNS 47914, mirrored, and **F.** NHMW-GEO-2009z0088/0001); **G, H.** *Chilotherium anderssoni* from Daijiagou in China (**G.** AMNH FM 26341 and **H.** SMF M 3598); **I.** *Ceratotherium neumayri* (HLMD-Sam.231); and **J.** *Dihoplus pikermiensis* (NHMW-GEO-1911/0005/0030) from Samos (Greece). Scale bar: 5 cm.

unlike in chilotheres. Additionally, the morphology of the other deciduous lower premolars differs between chilotheres and rhinocerotines. In d2 of the rhinocerotines *Lartetotherium sansaniense*, *Ceratotherium neumayri*, *D. pikermiensis*, *P. ringstromi*, and *P. megarhinus*, after moderate wear, a closed-off fossettid forms in the talonid (Dawkins 1865; Ringström 1924, pl. 1, fig. 4; Lehmann 1984, pl. 1, fig. 4; Giaourtsakis 2009, pl. 4, figs 8, 9; Heissig 2012, figs 59, 60; Alifieri 2019, fig. 12). Lastly, in d2, and in some cases in d3 as well, the paralophid splits into two lobes in these species, which may connect to form a small fossettid, as observed in some d3s of *Ceratotherium neumayri*, such as in GPIH 3017 and Giaourtsakis (2009, pl. 4, fig. 8).

Late Miocene aceratheriines

The distinction of the chilothere material studied herein from other hornless rhinocerotids that lived during the Late Miocene in Eurasia is even more difficult than their separation from horned rhinoceroses. One of the issues that makes their distinction so difficult is that, for many species, no deciduous dentition has been described so far. Juvenile specimens are available for some species: a juvenile skull of *Acerorhinus yuanmouensis* Zong, 1998 was recently described from the Yuanmou Basin (China) (Lu 2013); the species *Persiatherium rodleri* is based on a subadult skull from Maragheh (Iran) that still bears D4 (Pandolfi 2016); a juvenile skull with its

associated mandible of *Acerorhinus neleus* Athanassiou et al., 2014 was recently reported from the Upper Miocene locality of Pikermi (Greece) (Giaourtsakis et al. 2018); and *Alicornops complanatum* (Heissig, 1972), *sensu* Antoine et al. (2003), was reported from Upper Miocene beds of the Siwaliks (Heissig 1972, table 7, fig. 13). Additionally, a few characters on the deciduous dentition of *Aceratherium incisivum* Kaup, 1832 can be partially extrapolated from Guérin (1980). The comparison with these specimens shows that *A. neleus* has a much narrower mandibular symphysis, even in juvenile specimens. This is especially evident when the mandible of *A. neleus* and the mandible GMM 593 of *C. schlosseri* from Samos are compared, which are of similar ontogenetic age – the d4s are moderately worn, representing wear stage 6 or 7 (Hillman-Smith et al. 1986; Hullot and Antoine 2020). In GMM 593 of *C. schlosseri*, the symphysis is already very wide and massive, showing a long diastema between d2 and the (d)i2 alveolus, with a crest running along the diastema, whereas the symphysis of *A. neleus* is much narrower. Also, in all four of these non-chilothere aceratheriines, as well as in *Aceratherium incisivum*, the protocone in D3 and D4 is not as strongly constricted as in chilotheres, which also display a prominent and lingually projecting antecrochet. In *Alicornops complanatum*, the paracone fold is much stronger than in chilotheres; this difference is especially evident in D2, which in chilotheres bears a very weak paracone fold, whereas in *Alicornops*, it is very strong (Heissig 1972, table 7, fig. 13). In contrast to the other aceratheriines, some of the studied chilothere specimens preserve a thin layer of cement coating on the ectoloph – although this feature can vary significantly, and the cement layer can often be removed during the preparation of the specimens.

Chilotheriina

The material of the different studied *Chilotherium* species is rather similar, and any specific identification is very difficult (Fig. 13). There are several characters that show some degree of variation; however, it is often very difficult to assess whether this represents intraspecific variation or interspecific variation of taxonomic significance. For instance, the distance between the orbit and the nasal notch (nasal-orbital bar) and the relative position of the nasal notch seem to vary between the considered species. The length of the nasal-orbital bar depends significantly on the ontogenetic age of the individual but exhibits an approximately linear increase with age (Fig. 14). The comparison of the studied chilothere species shows that the values of *C. persiae*, *C. habereri*, and *C. anderssoni* are close and overlap to some degree. Especially *C. persiae* and *C. habereri* present incredibly similar values with almost perfectly overlapping trendlines (Fig. 14). In contrast to these three species, the values of *C. schlosseri* are consistently lower (Fig. 14). It must be noted here that, in adult skulls, the nasal-orbital bar seems to be of similar size at least in *C. persiae* (79 mm, $n = 1$), *C. habereri* (79–85 mm, $n = 2$), and *C. schlosseri* (72–80 mm, $n = 2$). This would suggest different ontogenetic development in *C. schlosseri*, corresponding either to a somewhat longer period of development or accelerated development towards the later juvenile/subadult life of the individual.

The size of D1 varies amongst chilotheres, with *C. habereri* exhibiting the lowest values within the group, separating this species from all other chilotheres (Fig. 15), whereas *C. persiae* exhibits the greatest length values and *Shansirhinus ringstromi* Kretzoi, 1942 from the Upper Miocene of China the greatest width values in D1 (Fig. 15). In the same diagram (Fig. 15), *C. schlosseri* overlaps with *C. persiae*, *Shansirhinus ringstromi*, and *C. anderssoni*, while *Shansirhinus ringstromi* and *C. persiae* only marginally overlap. More specifically, in *C. habereri*, both the length and width of D1 are lower than those of *C. persiae* and *C. schlosseri*. The few values of *C. anderssoni* overlap with *Shansirhinus ringstromi* and *C. schlosseri*; Ringström (1924) provided value ranges for D1 of the *C. anderssoni* specimens that he studied ($L = 18–21$ and $W = 15–17$), which do not fully agree with the measured values. Nonetheless, they show that *C. anderssoni* overlapped little with the other species and mainly filled the gap between the small D1 of *C. habereri* and the larger D1s of *C. persiae* and *C. schlosseri*. This suggests that the size of D1 can be used to some extent for taxonomic purposes within the genus *Chilotherium* and Chilotheriina in general, with *C. habereri* exhibiting the lowest values in general and *Shansirhinus ringstromi* the greatest width. When other chilotheres are also compared, the picture becomes even more complicated and diverse, with D1 of *E. samium* having almost the same dimensions ($L = 20$ mm and $W = 18.2$ mm, based on the adult neotype SMF M 3601) as *C. anderssoni*, the type species of the genus (Ringström 1924). The dimensions for D1 of '*Chilotherium*' *wimani* from the Upper Miocene of Beihougou in China, based on measurements of the type material provided by Ringström (1924, pp. 50–51), are also rather close to those values, with one specimen having exactly the same dimensions as two *C. anderssoni* D1s, while another specimen has slightly smaller dimensions ($L = 18$ mm and $W = 18$ mm). Deng (2001, table 3) provided measurements of a D1 of '*C.*' *wimani* ($L = 15$ mm and $W = 18$ mm) with a significantly lower length value; it is possible that the intraspecific variation in the size of D1 is relatively broad in this species, possibly similar to the value range provided by Ringström (1924) for *C. anderssoni*. Deng (2005a) and Lu et al. (2015) described cranial and dental material of *Shansirhinus ringstromi*, providing measurements for six D1s, in addition to a D1 of the same species that was measured on a skull housed at the SNSB-BSPG (SNSB-BSPG-2002-I-1). The value range is very broad and seems to vary more significantly than in the studied *Chilotherium* species ($L = 17.7–22.4$ mm and $W = 14.9–21.9$), but D1 is generally larger than in most chilotheres that were measured, with the greatest overlap with *C. schlosseri* (Fig. 15), which is one of the largest *Chilotherium* species (Kampouridis et al. 2025).

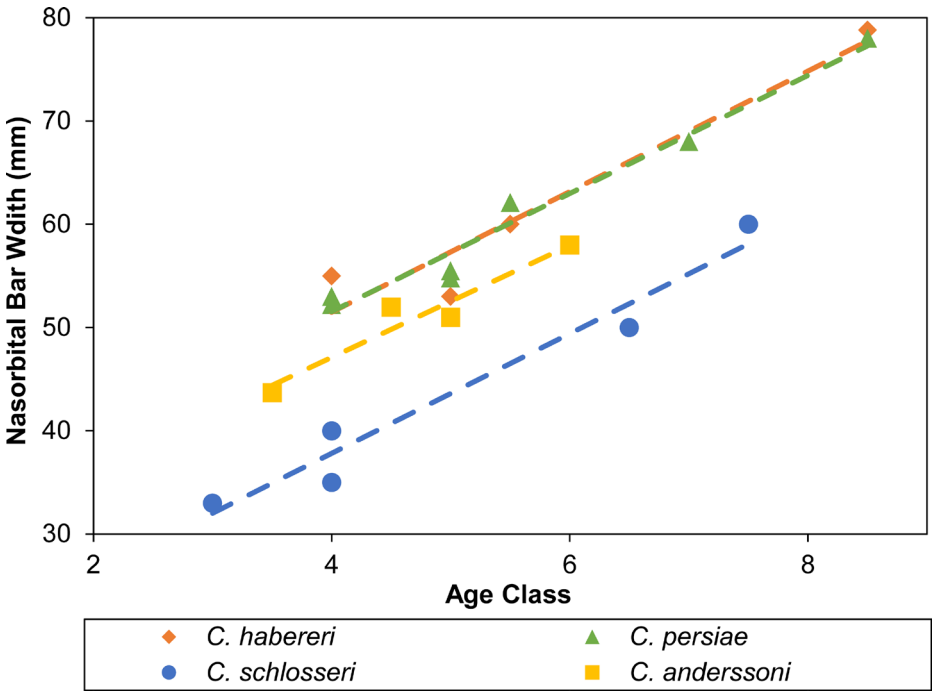

Figure 14. Ontogenetic development of the nasal-orbital bar. Scatter diagram of the distance between the orbit and nasal notch (nasal-orbital bar) and the age class of the respective specimen, along with the trendline showing the ontogenetic development of the length of the nasal-orbital bar in each of the studied Late Miocene chilotheres: *Chilotherium persiae* from Maragheh (Iran), *Chilotherium habereri* from Kutschwan (China), *Chilotherium schlosseri* from Samos (Greece), and *Chilotherium anderssoni* from Daijiagou (China). For detailed data, see Suppl. material 1: table S1.

The morphology of D1 is extremely uniform throughout aceratheriines and shows some degree of intraspecific variability, as also reported by Ringström (1924, p. 31) for *C. anderssoni*. Within chilotheres, it seems that a few characters differ between the considered species (Fig. 13). For instance, while all species exhibit a lingual cingulum, it is discontinuous in *C. persiae* and *C. habereri*, whereas it is continuous in *C. schlosseri* and *C. anderssoni*. In *C. schlosseri*, this cingulum continues into a strong and very high distal cingulum that closes off a postfossette at an early wear stage. In *C. persiae* and *C. habereri*, the postfossette is similarly large but closes off at a later wear stage, whereas in *C. anderssoni*, the metaloph is either absent or very thin, with a weak distal cingulum – possibly leaving an open postfossette. The protoloph and protocone are represented by a small enamel fold in most specimens. In *C. persiae* and *C. anderssoni*, this fold is more pronounced and reaches higher up; in *C. habereri*, this fold is very small and is found almost at the base of the crown, whereas in *C. schlosseri*, this fold is quite strong and closes off the median valley after moderate wear.

In D2, *C. schlosseri* seems to have a consistently closed medifossette, and at least in some specimens, some enamel plications are present in the median valley and medifossette (Fig. 13E, F). The D2 described by Weber (1905, pl. 8, fig. 4) as *C. schlosseri* and D2 of the maxilla described by Weber (1904, pl. 16, fig. 1) as *Rhinoceros schleiermacheri* (assigned herein to *C. schlosseri*) also feature a closed medifossette, though no enamel plications are visible in the published drawings. In other *Chilotherium* species, the closure of the medifossette seems variable. Ringström (1924) figured a D2 of *C. anderssoni* (Ringström 1924, pl. 3, fig. 6) and a D2 of '*C.*' *wimani* (Ringström 1924, pl. 7, fig. 4), both with a closed medifossette, but mentioned the variability of this feature (Ringström 1924, p. 32). In *C. habereri* from Kutschwan, none of the D2s feature a closed medifossette (Fig. 13C, D). Similarly, in D2 of *C. persiae* (MNHN.F.MAR3053), the medifossette remains open, though the crista is well developed and almost reaches the crochet (Fig. 13A, B). The D2 of *C.* '*habereri* var. *laticeps*' Ringström, 1924 (synonymised with *C. anderssoni* by Heissig 1975, table 6), illustrated by Ringström (1924, table 5, fig. 2), also exhibits an open medifossette, despite its advanced wear stage. Also, none of these three species features any enamel plications. In *C. kowalevskii*, the medifossette seems to, at least occasionally, close, and enamel plications also seem to be present at least in some cases (Pavlow 1913, pl. 17, figs 2, 3). The D2 of *E. samium* (Weber 1905, pl. 9, fig. 4) also features a completely closed medifossette and a small enamel plication below the lingual wall of the medifossette. Additionally, the lingual cingulum differs among the studied chilotheres. In *C. schlosseri*, it is usually more pronounced than in *C. anderssoni*, *C. habereri*, *C. wimani*, *C. persiae*, and *C. kowalevskii* (Fig. 13). A very strong lingual cingulum is also clearly visible in D2 of *C. schlosseri,* described by Weber (1905, pl. 8, fig. 4), whereas that of *E. samium* (Weber 1905, pl. 9, fig. 4) features a discontinuous

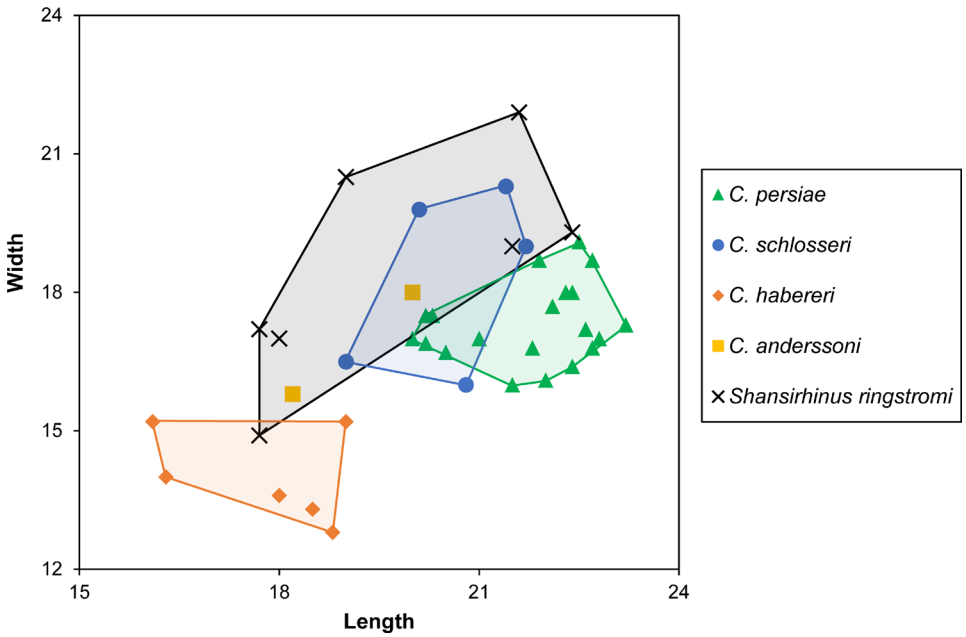

Figure 15. Size differences in D1 of chilotheres. Scatter diagram of the length and width of D1 in the Late Miocene chilotheres *Chilotherium persiae* from Maragheh (Iran), *Chilotherium habereri* from Kutschwan (China), *Chilotherium schlosseri* from Samos (Greece), *Chilotherium anderssoni* from Daijiagou (China), and *Shansirhinus ringstromi* from China. For detailed data, see Suppl. material 1: table S1.

cingulum. While in most studied chilothere specimens D2 features both closed-off pre- and postfossettes, in *C. persiae*, the prefossette is not always closed. In D2 of '*C.*' *wimani* (Ringström 1924, pl. 7, fig. 4), the parastyle is shorter compared to the other chilotheres.

D3 seems to have a very conservative morphology throughout chilotheres. Ringström (1924) described D3 of *C. anderssoni* as usually lacking an enamel pillar at the entrance of the median valley and a lingual cingulum and having an 'insignificant' crista, but he illustrated a D3 (Ringström 1924, table 3, fig. 6) with both an enamel pillar and a long crista that closes the medifossette when slightly more worn. In one *C. anderssoni* specimen (SMF M 3592), an enamel pillar is present at the entrance of the median valley, whereas the other studied specimens do not exhibit an enamel pillar. Instead of a crista, the three *C. anderssoni* specimens only exhibit a weak enamel bump in D3 (Fig. 13G, H). In *C.* '*habereri* var. *laticeps*' (Ringström 1924, table 5, fig. 2) and '*C.*' *wimani* (Ringström 1924, table 7, fig. 4), neither a crista nor a continuous lingual cingulum is visible, though an enamel pillar exists at the entrance of the median valley. Similarly, in *C. habereri* from Kutschwan, the size of the crochet and crista vary within the three studied specimens (Fig. 13C, D). In GPIT/MA/04843, D3 has a very small crochet and a small enamel bump in place of the crista, whereas the other two specimens have longer crochets, and in GPIT/MA/04830, a small but distinct crista is also present. In *C. persiae* from Maragheh, all studied specimens feature a well-developed crochet, whereas a crista is present only in some specimens, closing off the medifossette (i.e. NHMW-GEO-2020/0014/0093). In *C. kowalevskii*, the crista seems to be small or absent and the crochet large (Pavlow 1913, table 17, figs 1–3). In *C. schlosseri*, a crista is present in all D3s studied herein and may close off the medifossette after moderate wear. In the illustration of a D3 of *C. schlosseri* by Weber (1905, table 8, fig. 4), a crista is not visible. Another feature in *C. schlosseri* that seems to differ from other chilotheres is the existence of a continuous or slightly discontinuous lingual cingulum on D3, which is present in all three specimens studied herein and in the *C. schlosseri* D3 depicted by Weber (1905, table 8, fig. 4). Moreover, the *C. schlosseri* specimens also feature some small enamel plications, as seen in SMNS 47913 and SMNS 47914. Overall, the presence and development of the crista and enamel plications also seem to vary within *C. schlosseri* but might be most commonly present.

D4 is morphologically very similar to D3 but is the most molarised tooth among the deciduous premolars, often being confused with M1 or M2. A long crochet, a strongly constricted protocone, and a well-developed antecrochet are present in all the considered species (Fig. 13). Also, no crista is present in any of the studied specimens, although a small enamel bump might at least be present. The only features that seem to be somewhat common in *C. schlosseri* but lacking or less developed in the other species are the presence of enamel plications and a discontinuous lingual cingulum. Neither *C. persiae*, *C. habereri*, nor *C. anderssoni* exhibits any lingual cingulum in D4. Interestingly, in both deciduous dentitions for *C. schlosseri* and *E. samium* illustrated by Weber (1905), a lingual cingulum seems to be present in D4. The D4 that was assigned to *E. samium* (Weber 1905, table 9, fig. 4) even features several enamel plications on the crochet. The deciduous tooth row assigned

to *E. samium* by Weber (1905, table 9, fig. 4) exhibits several features that are otherwise characteristic of *C. schlosseri*, such as the closed medifossette in D2 and D3 and the multiple enamel plications in D4, suggesting that this specimen belongs to *C. schlosseri*.

Discussion

Taxonomy

The taxonomy of chilotheres is a complicated and often debated topic. There are many controversies about the validity of species and their potential synonymy (e.g. Kiernik 1913; Krokos 1917; Heissig 1975; Deng 2006a; Țibuleac 2014; Kampouridis et al. 2022b, 2023b). Originally, Ringström (1924) suggested that the cranial morphology of most species is too similar to be used for their distinction, and he used dental morphology, including that of deciduous teeth, to separate the different species. However, it is now known that dental morphology is often interspecifically very uniform and can vary greatly depending on the wear stage (see Țibuleac 2014; Antoine and Sen 2016). Cranial morphology, instead, is more diagnostic than initially expected (Kampouridis et al. 2023b), and many species can be distinguished based on the morphology of their skulls. For instance, *C. sarmaticum* differs from *C. kowalevskii* in having shorter nasal bones and more widely separated parietal crests. *Chilotherium schlosseri* has more widely separated parietal crests than any other chilothere (Svorligkou et al. 2025). These three species, along with *C. persiae*, *C. habereri*, *C. anderssoni*, *C. orlovi*, *C. xijangensis*, and *C. licenti*, represent *Chilotherium sensu stricto* and bear a prominent depression in the frontal region, which is lacking in *Shansirhinus* spp., *E. samium*, '*C.*' *wimani*, and '*C.*' *primigenium*. For this reason, the latter three species have been proposed to be removed from the genus *Chilotherium* (Kampouridis et al. 2023b). Few studies have also attempted to use postcranial morphology for the taxonomic identification of chilotheres (Korotkevich 1970; Deng 2002; Kampouridis et al. 2025), which showed that at least some features in the postcranium present diagnostic characters. For instance, a recent study suggested that the morphology of the articular facets of the astragalus for the calcaneum can be used to separate some species, and the patella and tibia are helpful for species identification, though more material is needed to confirm these hypotheses and refine these diagnostic characters (Kampouridis et al. 2025).

The deciduous dentition of chilotheres is often overlooked, and little is known about its potential taxonomic value. It is known that, in some rhinoceros groups, deciduous teeth can be used to identify the genus or even the species (e.g. Guérin 1980; Heissig 1984; Giaourtsakis et al. 2006; Becker et al. 2009; Böhme et al. 2021a; Kampouridis et al. 2022a). Nonetheless, Ringström (1924, p. 41) suggested that the deciduous dentition of *C. habereri* and *C. anderssoni* varies intraspecifically to a degree that does not allow their specific separation. The results of the comparisons suggest that, although the morphology of the deciduous dentition is rather uniform, some characters can be used to help with the identification of the abovementioned species (Fig. 13). The size and morphology of D1 vary between the species, with *C. habereri* from Kutschwan (China) exhibiting the smallest dimensions for D1 (Fig. 15) and also featuring a shorter protoloph and weaker protocone than the other species. *Chilotherium schlosseri* from Samos (Greece) often includes some enamel plications in the deciduous premolars, which are much rarer in the other studied chilothere species, *C. persiae*, *C. habereri*, and *C. anderssoni*. This has also been observed in the permanent dentition of the species (Kampouridis et al. 2023b). Additionally, *C. schlosseri* exhibits more pronounced enamel folds in the deciduous teeth than other chilotheres, such as a mesial and distal protocone constriction in D2, a crista in D3, a closed-off medifossette in both D2 and D3, and commonly strong lingual cingula. Lastly, the prefossette in D2 is always present in *C. habereri* and *C. schlosseri*, whereas it is absent in some specimens of *C. persiae* (Fig. 13).

Tooth eruption in *Chilotherium*

Tooth eruption in rhinoceroses is usually conservative, without much variation between different species (Koenigswald et al. 2007). For this reason, it has been studied in only a few taxa (e.g. Goddard 1970; Hillman-Smith et al. 1986; Koenigswald et al. 2007; Böhmer et al. 2016), and consequently, it has never been described for chilotheres. Herein, the eruption sequence of the deciduous and permanent dentition of the four studied species of chilotheres is evaluated, also taking into account the literature for other chilothere species (Pavlow 1913; Ringström 1924; Deng 2005a). In all chilothere species, d/D2 and d/D3 are the first teeth to erupt, which must start immediately after birth, since there is no single specimen where these teeth are still unerupted. The ontogenetically youngest specimen is the mandible GPIT/MA/04820 of *C. habereri* from Kutschwan, in which d2 and d3 have erupted but exhibit only very weak wear, with very small wear facets in the posterior part of the talonid of d2 and the trigonid of d3 (Fig. 8B). In this specimen, there are no signs of a distal wear facet on d3 for d4; therefore, d4 had not erupted yet. The d1 is not always present, and it is not possible to assess its eruption compared to the other lower teeth. D1 and d/D4 erupt later, and some disparity is observed. In most studied specimens of chilotheres, such as *C. habereri*, *C. persiae*, and *C. kowalevskii* (Pavlow 1913, pl. 17, figs 1, 2; Ringström 1924, pl. 3, figs 1, 6), D1 erupts before or simultaneously with D4. In *C. schlosseri*, only one specimen preserves both teeth, allowing assessment of the relative eruption time (SMNS 47913): D4 is already fully erupted, though unworn, whereas D1 is

only beginning to erupt, with its tip barely reaching the level of the tooth crown base of the D2 crown, thereby deviating from the pattern observed in other chilotheres. In a specimen of *C. persiae* (MNHN.F.MAR3820), a similar condition can be observed: D4 is at the same eruption stage as in SMNS 47913 of *C. schlosseri*, and D1 is not fully erupted yet, though the tip of D1 reaches the middle of D2, thereby being at a more advanced eruption stage than in SMNS 47913. It is difficult to determine the exact eruption sequence of these two teeth with certainty because they erupt at approximately the same time, and their relative eruption timing appears to vary at least in *C. persiae*. D1 is the only deciduous tooth that is not replaced and is retained into adulthood, being retained even in ontogenetically very old specimens such as NHMW-GEO-1911/0005/0128 (see Svorligkou et al. 2025, fig. 6a).

Enamel hypoplasia in *Chilotherium*

Enamel hypoplasia is a deficiency in enamel thickness resulting from stress when a certain threshold is met (Goodman and Rose 1990, fig. 14) during the secretory phase of amelogenesis (Goodman and Rose 1990). Linear enamel hypoplasia (LEH) is the most common form of these defects (Goodman and Rose 1990). Though well studied in some mammalian groups such as humans, enamel hypoplasia is a topic that, until recently, had received little attention in rhinoceroses (e.g. Bratlund 1999; Mead 1999; Roohi et al. 2015; Böhmer and Rössner 2018). However, in recent years, several studies have dealt with the topic, trying to standardise the study of hypoplasias in rhinoceroses based on work in other groups (e.g. Hullot et al. 2021, 2023, 2024a, 2024b, 2024c; Hullot and Antoine 2022).

The aetiology of enamel hypoplasias in general is a very complex and controversial topic, but it has been extensively discussed in primates (Skinner 1986; Eckhardt and Protsch von Zieten 1993; Hillson and Bond 1997; Guatelli-Steinberg and Lukacs 1998; Guatelli-Steinberg and Skinner 2000; Guatelli-Steinberg 2001; Hannibal and Guatelli-Steinberg 2005; Chollet and Teaford 2009; Skinner et al. 2014). Their taxonomic distribution in primates seems to be somewhat dichotomous because they are very rare in monkeys (Guatelli-Steinberg and Lukacs 1998; Guatelli-Steinberg 2000, 2001; Chollet and Teaford 2009) but very common in great apes, often having multiple defects in one tooth (Skinner 1986; Eckhardt and Protsch von Zieten 1993; Hannibal and Guatelli-Steinberg 2005). The reason for this taxonomic discrepancy in the distribution of linear enamel hypoplasias has been discussed by many authors and includes the length of tooth maturation (Guatelli-Steinberg 2000; Newell et al. 2006; Chollet and Teaford 2009), crown morphology (Guatelli-Steinberg 2000), differences in the spacing of perikymata (Hannibal and Guatelli-Steinberg 2005), and differences in enamel thickness (Lukacs 1999), though it seems to overlap in some taxa (Shellis et al. 1998) and probably does not relate to the occurrence of hypoplasias (Hannibal and Guatelli-Steinberg 2005; Chollet and Teaford 2009). However, Hannibal and Guatelli-Steinberg (2005) demonstrated that, within the great apes, gorillas exhibit a low frequency of enamel hypoplasias compared to chimpanzees and orangutans, which they correlate with their somewhat different diet and the perikymata spacing. They also observed that, within the same taxon group, chimpanzees and gorillas, the hypoplasia frequency varies by location but were unable to correlate it with any kind of food availability or pathogens that differ between the two regions (Hannibal and Guatelli-Steinberg 2005). Chollet and Teaford (2009) investigated the presence of enamel hypoplasias in *Cebus* canines from Brazil in relation to some environmental factors. They found that hypoplasias were more prevalent in semi-deciduous forests and lower average temperatures than in coastal regions or tropical rainforests and high temperatures and were unable to trace any correlation with precipitation (Chollet and Teaford 2009).

Concerning the presently studied material, numerous deciduous teeth were found featuring hypoplasia (Fig. 16). More specifically, hypoplasias in d/D2 and d/D3 are rather rare, whereas hypoplasia in d/D4 was observed in all available specimens in all four studied species (Figs 16–18, Table 2). In the studied sample of *C. persiae* from Maragheh (Iran), only two teeth of the 33 d/D3s show hypoplasia, whereas none of the 29 d/D2s exhibit hypoplasia. In contrast, in the 34 d/D4 specimens, every single one exhibits hypoplasia, always in the same position. In the studied sample of *C. habereri* from Kutschwan (China), of the six d/D2s and eight d/D3s, only one specimen (GPIT/MA/04849) shows hypoplasias. In this specimen, both d2 and d3 present multiple weakly developed hypoplasias in the lower part of the respective teeth on both sides. The hypoplasias in d2–3 are almost at the same level in the tooth crowns in both teeth and were most probably caused by the same event(s), which further indicates that these teeth developed at the same time. Another specimen (GPIT/MA/04820) exhibits more subtle hypoplasias in d2 and d3 that are represented by small pits (Fig. 17A, B), as described by Hullot et al. (2021), in the lower half of the tooth crown. Concerning the d/D4s of *C. habereri*, all seven specimens feature hypoplasia, all located in the middle of the tooth crown. In the mandible GPIT/MA/04849, the d4s have not erupted yet, with only the tip of the tooth crown visible. The CT scan of the specimen revealed the d4 hypoplasia, which was well pronounced (Fig. 17C, D). In the studied sample of *C. schlosseri* from Samos (Greece), not a single hypoplasia was found among the 17 d/D2s and d/D3s, whereas among the nine examined d/D4s (Table 2), all exhibit hypoplasia (see Fig. 17I–O). This hypoplasia differs from the hypoplasias found in d/D4 in the other three studied species.

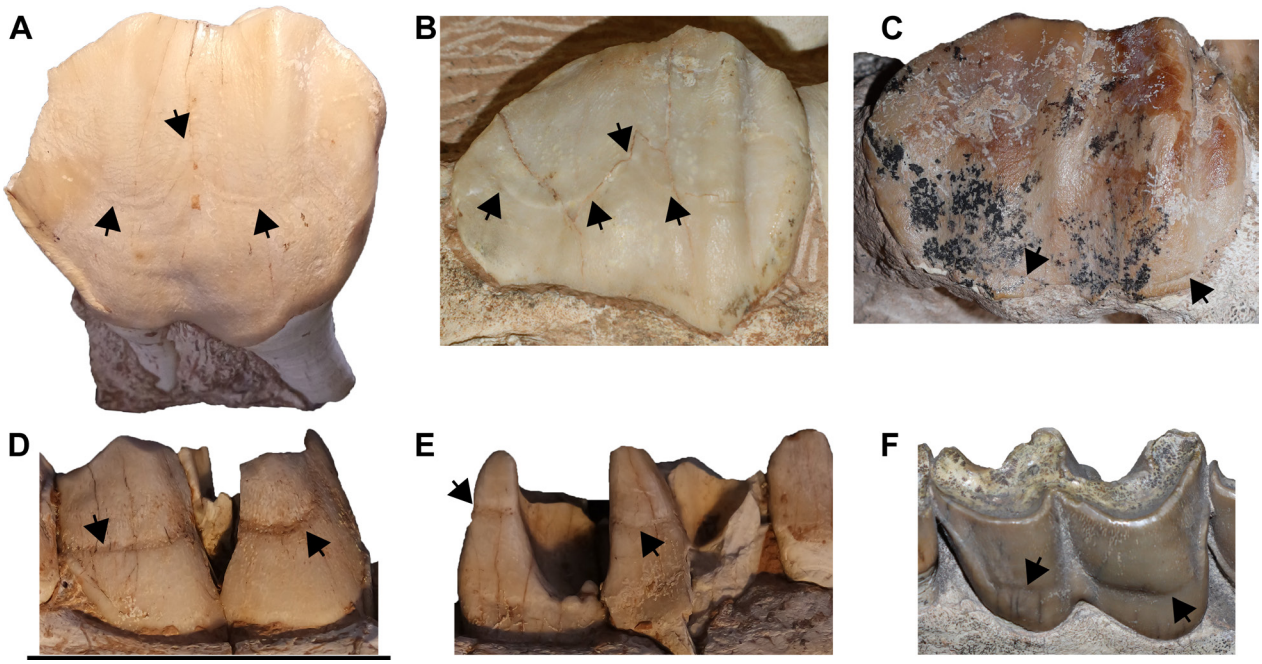

Figure 16. Hypoplasias in d4 and D4 of the studied Late Miocene chilotheres. *Chilotherium habereri* from Kutschwan in China (**A.** GPIT/MA/04817, D4; and **D–E.** GPIT/MA/04818, d4 in buccal and lingual views), *Chilotherium anderssoni* from Daijiagou in China (**B.** SMF M 3598, D4), and *Chilotherium schlosseri* from Samos in Greece (**C.** SMNS 47914, D4 and **E.** GMM 593, d4). Black arrows indicate enamel hypoplasias. Scale bar: 5 cm.

In the upper D4 of *C. persiae*, *C. habereri*, and *C. anderssoni*, the hypoplasia is represented by a horizontal groove close to the base of the crown on the lingual side of the tooth and an "ω"-shaped groove in the middle of the ectoloph (Figs 16A, B, 17G, H). In D4 of *C. schlosseri*, it has a different form and is found at a different position (Figs 16C, 17I–O) in all specimens. The hypoplasia is found at the base of the crown on both the lingual and buccal sides, and on the ectoloph (Fig. 17J, N), it takes the shape of an almost straight horizontal line (Fig. 16C) instead of an "ω", which is seen in the other chilotheres. The position and "ω"-shaped form of the enamel defect on the buccal side of d/D4 are consistent with what has been observed in other rhinoceroses. It is comparable to the hypoplasia reported in *Prosantorhinus germanicus* (Wang, 1928) from the Miocene of Sandelzhausen (Germany) (Böhmer and Rössner 2018) and *Teleoceras* from the Miocene of North America (Mead 1999; Gajewski 2026). Bratlund (1999) studied a large collection of *Stephanorhinus kirchbergensis* (Jäger, 1839) specimens (368 teeth), of which only nine featured some kind of enamel hypoplasia. Hullot et al. (2021) investigated the ecology of different Miocene rhinoceros species from France with a multiproxy approach consisting of micro- and mesowear and an investigation of enamel hypoplasias. Hullot et al. (2023) studied the ecology of the rhinoceros assemblage that inhabited the Balkan-Iranian zoogeographical province during the Late Miocene, also investigating hypoplasias in these animals, including some chilothere species such as *C. persiae* from Maragheh (Iran), *C. schlosseri* from Samos, and *E. samium* from Pentalophos (Greece).

Table 2. Prevalence of hypoplasia in the deciduous teeth of the studied chilotheres by species and tooth.

Species	Hypoplasia	d/D2	d/D3	d/D4
C. persiae - Maragheh (Iran)	present	0	2	33
	absent	28	30	0
	Prevalence (%)	0	6	100
C. habereri - Kutschwan (China)	present	2	2	7
	absent	4	6	0
	Prevalence (%)	33	25	100
C. schlosseri - Samos (Greece)	present	0	0	9
	absent	8	9	0
	Prevalence (%)	0	0	100
C. anderssoni - Daijiagou (China)	present	0	0	4
	absent	4	4	0
	Prevalence (%)	0	0	100
***Chilotherium* spp.**	present	2	4	53
	absent	44	49	0
	Prevalence (%)	4	8	100

Although in the d/D4s of chilotheres, hypoplasia is always present, when the other deciduous teeth are concerned, hypoplasias are rather rare, with only 4% and 8% of d/D2s and d/D3s, respectively, exhibiting hypoplasia (Fig. 18, Table 2). The presence of hypoplasias on deciduous teeth can vary from species to species and from locality to locality but is usually not very frequent (Hullot et al. 2023, 2024a, 2024c). In a comparative sample of *D. pikermiensis* specimens from Pikermi and Samos (Greece), one of eight studied d/D2s (12.5%) and two of eight d/D3s (25%) have hypoplasia. Hullot et al. (2023) studied hypoplasias in the same species, mainly based on material from Bulgarian Late Miocene localities, and

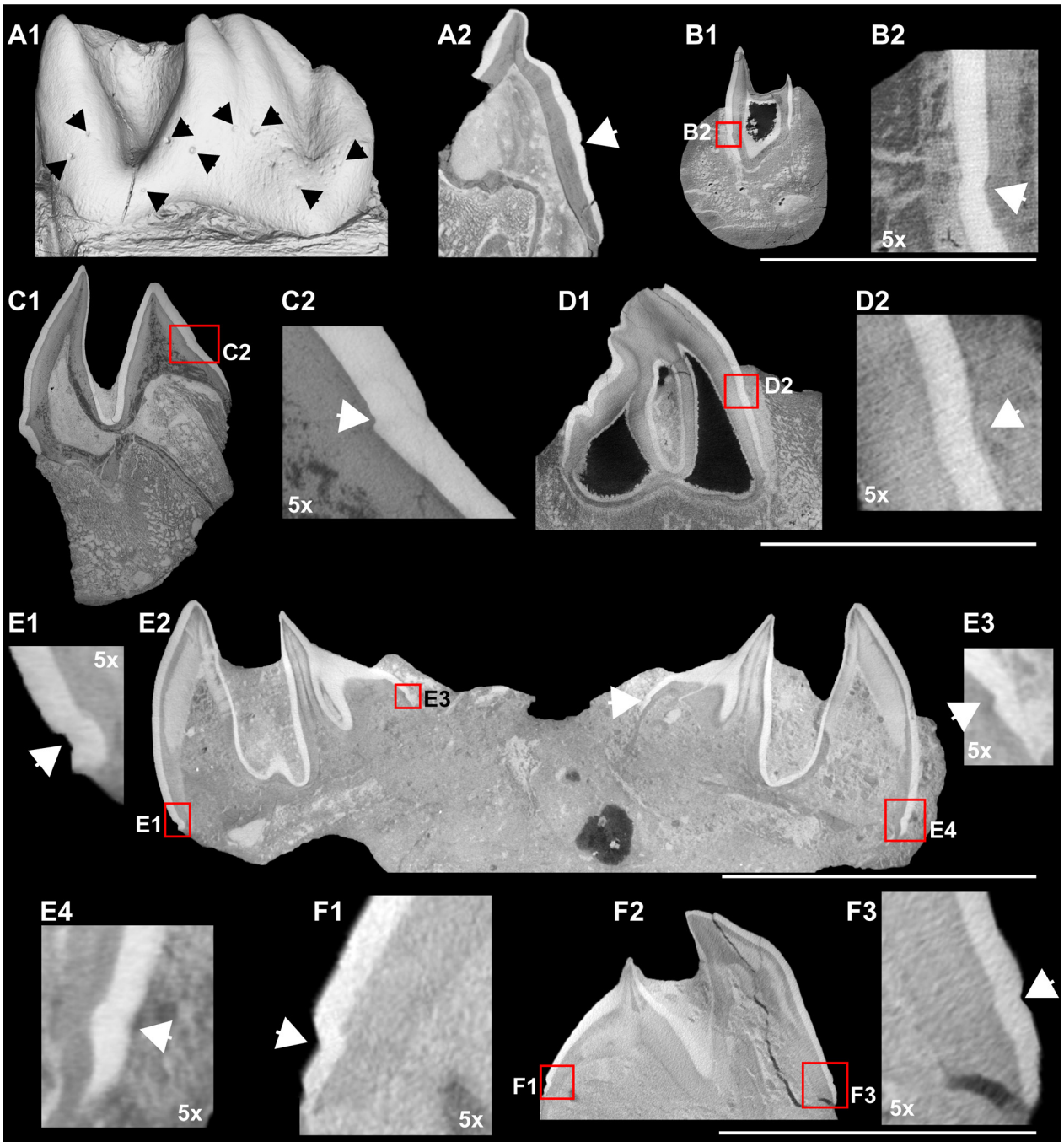

Figure 17. Hypoplasias in the deciduous dentition of the studied Late Miocene chilotheres through µCT scans. Virtual cross-sections of µCT scans of: **A–D.** *Chilotherium habereri* from Kutschwan in China (**A.** GPIT/MA/04820, d2; **B.** GPIT/MA/04849, d4; **C.** GPIT/MA/044817, D4; and **D.** GPIT/MA/04820, D4); and **E–F.** *Chilotherium schlosseri* from Samos in Greece (**E.** SMNS 47914, D4s; and **F.** SMNS 47913, D4). Black arrows indicate pit-shaped hypoplasias in d2, and white arrows indicate linear enamel hypoplasias in d/D4. Scale bar: 5 cm for **A1**, **B1**, **C1**, **D1**, **E2**, and **F2**, and 1 cm for the magnified images **A2**, **B2**, **C2**, **D2**, **E1**, **E3–4**, **F1**, and **F3**, indicated with "5x".

found a similar prevalence in these tooth positions. This defect in chilotheres shows a lower frequency in these deciduous premolars, though it also varies between localities and species, as seen in the relatively high prevalence in the rather limited sample of *C. habereri* from Kutschwan (33% for d/D2 and 25% for d/D3, Table 2).

As already mentioned, hypoplasia in d/D4 is constantly present in all chilothere specimens studied here, contrary to the contemporaneous horned rhinoceros *D. pikermiensis* from Pikermi and Samos (Greece), for which only two (22.2%) of the nine studied d/D4s exhibited hypoplasia. In a sample of 14 d/D4s of another horned rhinoceros, *Ceratotherium neumayri*, seven (50%) specimens exhibit hypoplasia, demonstrating a much higher prevalence. In a relatively small sample of five juvenile crania of the extant black rhinoceros from the Kunene

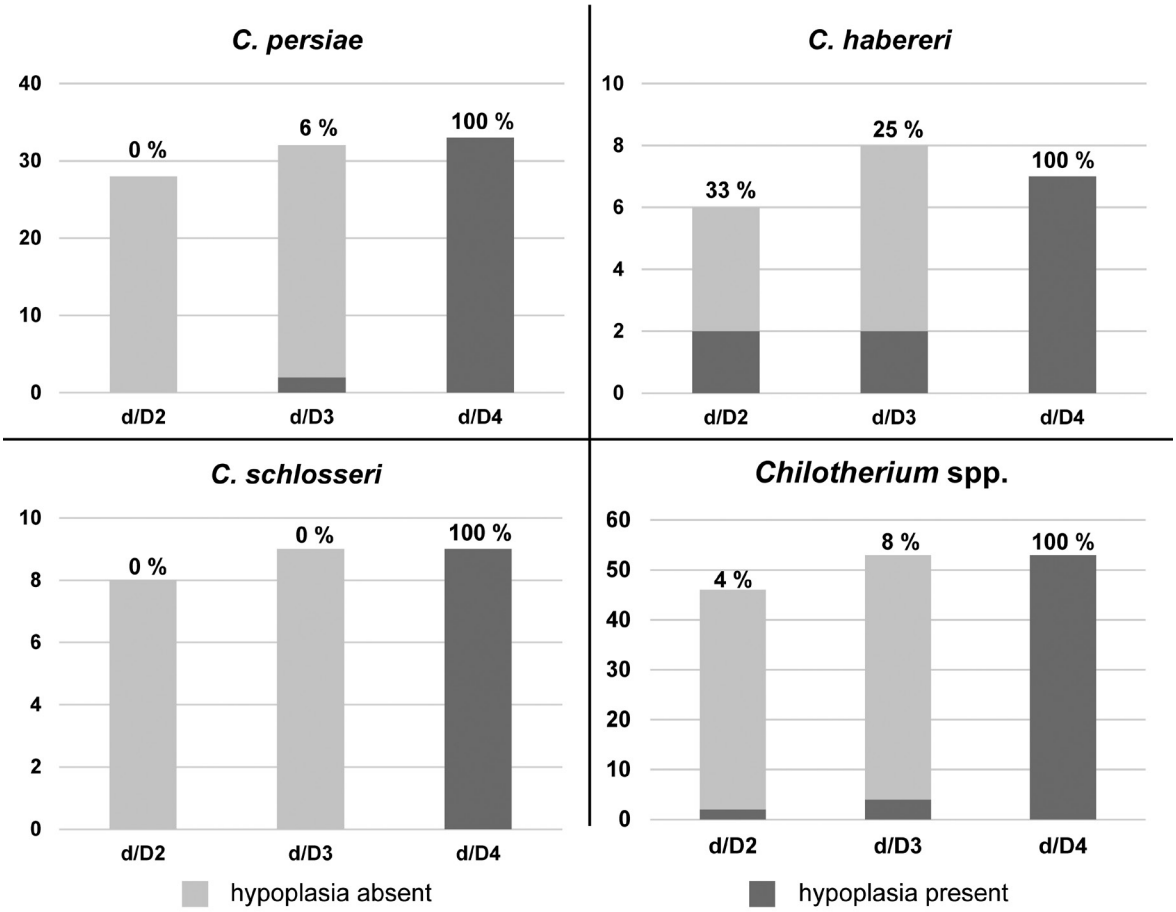

Figure 18. Prevalence of hypoplasias in the deciduous teeth of the studied Late Miocene chilotheres. Detailed diagrams for *Chilotherium persiae* from Maragheh (Iran), *Chilotherium habereri* from Kutschwan (China), *Chilotherium schlosseri* from Samos (Greece), and data from all three species, along with *Chilotherium anderssoni* from Daijiagou (China), merged. For detailed data, see Table 2.

Region (Namibia) studied at the facilities of the Save the Rhino Trust, all specimens exhibit hypoplasia in d/D4. It is not known how the presence of this defect may vary in these species or to what degree its presence is affected by environmental conditions or other external pressures.

The main causes of enamel hypoplasias include: 1. localised trauma, 2. genetic defects, and 3. physiological and systemic stress (nutritional). Enamel hypoplasia as a result of localised trauma appears only in a few teeth on the side of injury (Goodman and Rose 1990). This contrasts with the hypoplasias present in the studied material of *Chilotherium*, where the defects are present on both sides of the same maxilla or mandible and, in the case of d/D2 and d/D3, can affect multiple teeth if they were formed at the same time. Enamel hypoplasia as a result of a genetic defect typically occurs in all teeth and often occurs with other congenital anomalies (Goodman and Rose 1990). On the contrary, in the *Chilotherium* material, no other anomalies can be observed in the studied material, and hypoplasia is usually present only in one single tooth position, as in the case of d/D4. Lastly, enamel hypoplasia resulting from systemic stress, whether nutritional or disease-related, appears in all teeth that were developing at the time of the stress (Goodman and Rose 1990), thereby presenting the only fitting explanation.

The fact that enamel hypoplasias in the studied sample are primarily found in d/D4 in both the mandible and maxilla requires further clarification. In the extant white rhinoceros, d4 can start erupting as early as the second month (Hillman-Smith et al. 1986). Based on a radiographical image provided by Goddard (1970, pl. 2a), in the extant black rhinoceros, d4, which starts erupting a few months after birth, is already fully formed in a 5.5-month-old calf. Thus, Mead (1999) correlated the hypoplasias in d/D4 of *Teleoceras* with the timing of birth of the individuals. Enamel hypoplasias in different mammalian groups have been linked to high-stress situations, such as birth (e.g. Goodman and Rose 1990; Upex and Dobney 2012), and a study concerning hypoplasias in extant white-tailed deer correlated linear enamel hypoplasias in d4 with the timing of birth or the first week following birth (Davis and Mead 2013).

The hypoplasias reported herein in d/D4 of *Chilotherium* are consistent throughout several individuals of three distinct species, being situated in the same portion of the tooth crown, and while, in *C. schlosseri*, the position of the d/D4 hypoplasia differs, it is intraspecifically extremely consistent being always at the base of the crown, without any variation. Other enamel defects were extremely rare or absent. Consequently, a random

event that caused hypoplasia at the same exact position in all d/D4s can be excluded. An event that could cause such a defect in amelogenesis and is normal and undeviating in the life of all individuals and at a common ontogenetic stage, during the formation of d/D4, must be looked for as a cause. The only such event that could cause a stressful situation during the formation of d/D4 is the birth of the animal. Therefore, Mead (1999) and Hullot et al. (2021) are followed in supporting that this enamel hypoplasia is the result of birth-related stress.

In the present case, the prevalence of hypoplasias in d/D2 and d/D3 is rather similar and remarkably low in *C. schlosseri*, *C. anderssoni*, and *C. persiae*, with only d/D3 of *C. persiae* exhibiting any hypoplasias (6%, *n* = 32, Fig. 18, Table 2). Hullot et al. (2023) provided the first results on hypoplasias in chilothere teeth, with none found in 12 d/D2s and d/D3s of *E. samium* (referred to as *C. kiliasi* in their study) from Pentalophos-1 in Greece. This is the only other chilothere present during the Late Miocene in Greece, and even though Pentalophos-1 is of Vallesian age (late MN9) and Samos is Turolian (MN11–13, depending on the horizon), it does not present any hypoplasia in these teeth, as in *C. schlosseri* from Samos. On the contrary, *C. habereri* from Kutschwan (China) exhibits a comparably very high prevalence of hypoplasias in d/D2 (33%, *n* = 6) and d/D3 (25%, *n* = 8) in a rather limited specimen sample (Fig. 18, Table 2).

Regarding d/D4, the results of the present study show that there is no taxonomic disparity in the prevalence of hypoplasias because hypoplasia is found in all specimens. However, there is an important discrepancy between the present results and those of Hullot et al. (2023) in the prevalence of hypoplasias in the studied chilotheres. Most importantly, Hullot et al. (2023) studied the *C. persiae* material housed in the NHMW, which is also the subject of the current study, and listed several d/D4s that do not exhibit hypoplasia. They mentioned that, in 22 d/D4s, only 15 (68.2%) feature hypoplasia. However, the deviating results seem to stem from the exclusion in our study of worn-down and damaged specimens, in which the portion of the tooth where the hypoplasia would be visible is not preserved, along with teeth that are at least partially covered by cement, which complicates the observation of potential hypoplasia.

While hypoplasia was found to always be present in d/D4 of chilotheres, a significant disparity was observed in the position of the hypoplasia in *C. schlosseri* from Samos. As mentioned above, in this species, the hypoplasia is an almost straight line and is placed at the base of the tooth crown, whereas, in *C. persiae*, *C. habereri*, and *C. anderssoni*, the hypoplasia is placed in the middle of the tooth and has an "ω" shape on the buccal side of D4. In both cases, the creation of hypoplasia can be correlated with the birth of the individual, as the only constant event that could cause that much stress in so many individuals, as also discussed above. The observed deviation of the position of the hypoplasia might be related to some external environmental factor or interspecific differences, or a combination of both may affect the timing of birth to some degree.

The four studied chilothere species come from different localities across Eurasia, with *C. schlosseri* representing the westernmost species, found in Samos in Greece, *C. anderssoni* and *C. habereri* representing the easternmost species, both coming from Shanxi Province, China, and *C. persiae* having an intermediate position in Maragheh in Iran (Fig. 1). While all four localities are placed in the Upper Miocene, they differ in age, with Maragheh preserving the oldest record, spanning from 9 to 7.4 Ma (Mirzaie Ataabadi et al. 2013, 2016), and Daijiagou, the type locality of *C. anderssoni*, being the youngest locality, having been dated to 5.7 Ma (Kaakinen et al. 2013). The fossiliferous horizons on Samos Island stratigraphically overlap to a large degree with the Maragheh levels, having been dated to 8–6.7 Ma (Kostopoulos et al. 2003; Koufos et al. 2011), whereas Kutschwan is the only fossil site for which no information about the exact location and age is available (Kampouridis et al. 2022a; Kargopoulos et al. 2023). Overall, the Late Miocene was a time of changing environments, with the expansion of more open habitats and grasslands (Böhme et al. 2017, 2021b; Denk et al. 2018; Kaya et al. 2018; Fortelius et al. 2019; Li et al. 2020). In northeastern China, the palaeoenvironment was a C3 steppe with mild seasonality that was most probably affected by summer monsoons during the Late Miocene (Ciner et al. 2015; Li et al. 2020) but was subject to significant environmental changes, with the expansion of C4 plants and climatic changes resulting from the uplift of the Tibetan Plateau (Li et al. 2014; Liu et al. 2016). In western Asia, the climate was mainly characterised by winter rainfall and differed significantly from the climatic conditions in Europe (Böhme et al. 2021b). This could have led to different environmental conditions to which each chilothere was adapted, depending on the area in which it lived, thus resulting in subtle or more pronounced changes in their ecology, especially between the European (*C. schlosseri*) and eastern Asian (*C. anderssoni* and *C. habereri*) species. Nonetheless, even with these potential environmental differences, it is unlikely that, by themselves, they would have led to a significant change in the position of d/D4 hypoplasia. Nevertheless, in combination with additional factors, they may have contributed to the observed displacement of the hypoplasia.

Interspecific differences may have affected this divergence of the hypoplasia placement in d/D4 of *C. schlosseri* from Samos. They could reflect some change in the physiology of this species, such as a deviating tooth height, earlier development of d/D4 or all deciduous teeth, a longer pregnancy length, or a different breeding season. Comparing the complete heights of D4 is very difficult because only few isolated, complete, and unworn specimens were investigated. In the few specimens that were studied, *C. schlosseri* did, in fact, exhibit the shortest tooth crown (39–41 mm, *n* = 2), though only marginally shorter than *C. anderssoni* (42 mm, *n* = 1). Most importantly, while *C. persiae* (45–47 mm, *n* = 2) and *C. habereri* (49 mm, *n* = 1) did exhibit higher tooth

crowns, the hypoplasias were found closer to the crown tip, which is the starting point during tooth development. In *C. schlosseri*, the hypoplasia exhibits the greatest distance from the crown tip (~36 mm, $n = 2$), compared to the other three studied chilothere species (22–26 mm). Therefore, tooth height by itself does not explain the observed differences in the position of the hypoplasia. Earlier development of d/D4 would probably also result in earlier eruption of this tooth, which would mean that the already erupted deciduous teeth, d/D2 and d/D3, would be comparably less worn in *C. schlosseri*. However, the comparison of the wear stages of D2 and D3 in SMNS 47913 of *C. schlosseri* (Fig. 10C) and GPIT/MA/04842 of *C. habereri* (Fig. 7B) suggests that D4 erupts almost at the exact same time in these two species, based on the extremely similar wear stages, with the teeth of *C. habereri* being even slightly less worn than those of *C. schlosseri*. Therefore, a hypothesis about earlier development of d/D4 in *C. schlosseri* cannot be supported. Differences in breeding season or gestation period cannot be tested for the studied extinct taxa, but it is known that extant rhinoceroses present some variability. For instance, it is generally accepted that rhinoceroses today are non-seasonal breeders, but African rhinoceroses have preferred breeding seasons, in contrast to Asian rhinoceroses, which do not (Kretzschmar et al. 2004; Schwarzenberger and Hermes 2023). Further, a slight intraspecific variation in gestation length has also been observed that is associated with the season of breeding and climatic conditions (Schwarzenberger and Hermes 2023).

Therefore, a combination of different climatic conditions that may affect breeding and gestation time and some interspecific differences, such as slight differences in crown height, would be a plausible explanation for the lower placement of hypoplasia in d/D4 of *C. schlosseri*. Nonetheless, proving the existence of such differences in fossil taxa is very difficult. A potential difference in the gestation of the animal could only be investigated using Ca isotopes that may expose differences in the isotope composition before and after birth (e.g. Hassler et al. 2021). Based solely on external morphology, it is impossible to confirm such differences. However, the morphology and position of the D4 hypoplasia differ significantly from those of the other chilotheres, and it is possible that this could even represent a distinguishing feature for the species.

Concluding remarks

Deciduous dentition is commonly overlooked in many groups, including rhinoceroses. This is particularly true for chilotheres, which have long been affected by taxonomic uncertainty. A careful examination of the deciduous dentition of four chilothere species – *Chilotherium persiae* from Maragheh (Iran), *Chilotherium habereri* from Kutschwan (China), *Chilotherium schlosseri* from Samos (Greece), and *Chilotherium anderssoni* from Daijiagou (China) – shows that deciduous teeth can be a unique source of taxonomic information. Chilotheres have generally rather molarised deciduous premolars. In particular, the presence and development of the lingual cingulum and enamel plications can be used for the identification of *C. schlosseri*, whereas the dimensions and morphology of D1 seem to differ in *C. habereri*. Additionally, the ontogenetic development of the nasal-orbital bar varies among the studied species, with *C. persiae* and *C. habereri* showing broadly similar trends, slightly differing from *C. anderssoni*, and *C. schlosseri* exhibiting the greatest deviation. It was possible to determine the eruption sequence of the deciduous dentition and the order in which the teeth are shed and replaced. The d/D2 and d/D3 erupt first, very early in ontogeny, followed by D1 and d/D4. The relative eruption timing of D1 and D4 seems to vary. Replacement of the deciduous teeth by the permanent dentition begins with d/D2, followed by d/D3 and lastly d/D4, whereas D1 is retained into adulthood. Finally, it was detected that d/D2 and d/D3 rarely exhibit enamel hypoplasia (4% and 8%, respectively), whereas d/D4 consistently shows hypoplasia at nearly the same position on the crown in *C. persiae*, *C. habereri*, and *C. anderssoni*. In these three species, the defect shows an "ω" shape near the middle of the tooth crown, whereas in *C. schlosseri*, it is a straight line near the base of the crown. The constant presence of hypoplasia in d/D4 suggests that its aetiology is linked to birth. Overall, these results show that chilothere deciduous dentition potentially preserves consistent, taxonomically and phylogenetically informative characters and should be incorporated into future systematic and developmental studies.

Acknowledgements

The authors thank M. Hullot (Jurassica Museum, Porrentruy, Switzerland), who generously provided comparative information and photos of rhinoceros teeth with hypoplasias that she studied. The authors thank A. Gishlick, J. Meng (AMNH), S. Roussiakis, G. Svorligkou, G. Theodorou (AMPG), S. Trümper (GMM), U. Kotthoff (GPIH), I. Werneburg (GPIT), M. Blume, O. Sandrock (HLMD), A. Pictet (MGL), R. Rozzi, M. Albrecht (MLU), C. Argot (MNHN), S. Pappa (NHMUK), U. Göhlich (NHMW), R. Brocke, L. Kraus (SMF), E. Amson (SMNS), G. Rössner (SNSB-BSPG), and the Save the Rhino Trust for access to and photographs of material under their care. The authors thank G. Ferreira (University of São Paulo) and the 3D Imaging Lab of the SHEP at the Eberhard Karls University of Tübingen, Germany, for the acquisition of µCT scans of part of the material. PK acknowledges support from the Joachim Herz Stiftung (Add-on Fellowship for Interdisciplinary Life Science 2024) and the AMNH's Richard Gilder Graduate School (Collection Study Grant) for visiting collections. The authors thank the Editor-in-Chief F. Witzmann, J. Tissier, and an anonymous reviewer for their helpful comments on the manuscript.

References

Alifieri E (2019) Morphological study of cranial material from the rhinocerotids (Mammalia, Perissodactyla) from the old excavations of Pikermi, Attica. Undergraduate Thesis. National and Kapodistrian University of Athens.

Andree J (1921) Rhinocerotiden aus dem Unterpliocän von Samos. Paläontologische Zeitschrift 3: 189–212. https://doi.org/10.1007/bf03190415

Andrews P, Cook J (1985) Natural Modifications to Bones in a Temperate Setting. Man 20: 675–691. https://doi.org/10.2307/2802756

Antoine P-O (2002) Phylogénie et évolution des Elasmotheriina (Mammalia, Rhinocerotidae). Mémoires du Muséum National d'Histoire Naturelle 188: 1–359.

Antoine P-O (2003) Middle Miocene elasmotheriine Rhinocerotidae from China and Mongolia: taxonomic revision and phylogenetic relationships. Zoologica Scripta 32: 95–118. https://doi.org/10.1046/j.1463-6409.2003.00106.x

Antoine P-O, Saraç G (2005) Rhinocerotidae (Mammalia, Perissodactyla) from the late Miocene of Akkaşdağı, Turkey. Geodiversitas 27: 601–632.

Antoine P-O, Sen S (2016) Rhinocerotidae and Chalicotheriidae (Perissodactyla, Tapiromorpha). Geodiversitas 38: 245–259. https://doi.org/10.5252/g2016n2a6

Antoine P-O, Alférez F, Iñigo C (2002) A new elasmotheriine (Mammalia, Rhinocerotidae) from the Early Miocene of Spain. Comptes Rendus Palevol 1: 19–26. https://doi.org/10.1016/S1631-0683(02)00005-2

Antoine P-O, Duranthon F, Welcomme J-L (2003) *Alicornops* (Mammalia, Rhinocerotidae) dans le Miocène supérieur des Collines Bugti (Balouchistan, Pakistan) : implications phylogénétiques. Geodiversitas 25: 575–603.

Antoine P-O, Becker D, Pandolfi L, Geraads D (2025) Evolution and Fossil Record of Old World Rhinocerotidae. In: Melletti M, Talukdar B, Balfour D (Eds), Rhinos of the World. Fascinating Life Sciences. Springer Nature Switzerland, Cham, 31–48. https://doi.org/10.1007/978-3-031-67169-2_2

Arambourg C (1959) Vertébrés continentaux da Miocène supérieur de l'Afrique du Nord. Publications du Service de la Carte Géologique de l'Algérie (Nouvelle Série) Paléontologie, Mémoires 4: 1–159.

Athanassiou A, Roussiakis SJ, Giaourtsakis IX, Theodorou GE, Iliopoulos G (2014) A new hornless rhinoceros of the genus *Acerorhinus* (Perissodactyla: Rhinocerotidae) from the Upper Miocene of Kerassiá (Euboea, Greece), with a revision of related forms. Palaeontographica Abteilung A 303: 23–59. https://doi.org/10.1127/pala/303/2014/23

Bader KS, Hasiotis ST, Martin LD (2009) Application of forensic science techniques to trace fossils on dinosaur bones from a quarry in the Upper Jurassic Morrison Formation, northeastern Wyoming. Palaios 24: 140–158. https://doi.org/10.2110/palo.2008.p08-058r

Bayshashov BU (1982) A new rhinoceros species of the genus *Chilotherium* from Pavlodar. In: Mesozoic and Cenozoic vertebrate fauna and flora of North-Eastern and southern Kazakhstan. Academy of Sciences of Kazakhstan, Almaty, 72–83.

Becker D, Bürgin T, Oberli U, Scherler L (2009) *Diaceratherium lemanense* (Rhinocerotidae) from Eschenbach (eastern Switzerland): systematics, palaeoecology, palaeobiogeography. Neues Jahrbuch für Geologie und Paläontologie - Abhandlungen 254: 5–39. https://doi.org/10.1127/0077-7749/2009/0002

Behrensmeyer AK (1978) Taphonomic and ecologic information from bone weathering. Paleobiology 4: 150–162. https://doi.org/10.1017/S0094837300005820

Bernor RL (1986) Mammalian biostratigraphy, geochronology, and zoogeographic relationships of the Late Miocene Maragheh fauna, Iran. Journal of Vertebrate Paleontology 6: 76–95. https://doi.org/10.1080/02724634.1986.10011600

Bohlin B (1926) Die Famillie Giraffidae. Palaeontologia Sinica, Series C 4: 1–178.

Bohlin B (1935) Cavicornier der *Hipparion*-Fauna Nord-Chinas. Palaeontologia Sinica, Series C 9: 1–166.

Böhme M, Kampouridis P, Markov GN, Hristova L, Spassov N (2021a) Large mammals (Proboscidea, Perissodactyla) from the late Miocene Burel Basin in West Bulgaria. Neues Jahrbuch für Geologie und Paläontologie - Abhandlungen 302: 117–129. https://doi.org/10.1127/njgpa/2021/1022

Böhme M, Spassov N, Majidifard MR, Gärtner A, Kirscher U, Marks M, Dietzel C, Uhlig G, El Atfy H, Begun DR, Winklhofer M (2021b) Neogene hyperaridity in Arabia drove the directions of mammalian dispersal between Africa and Eurasia. Communications Earth & Environment 2: 85. https://doi.org/10.1038/s43247-021-00158-y

Böhme M, Spassov N, Ebner M, Geraads D, Hristova L, Kirscher U, Kötter S, Linnemann U, Prieto J, Roussiakis S, Theodorou G, Uhlig G, Winklhofer M (2017) Messinian age and savannah environment of the possible hominin Graecopithecus from Europe. Macchiarelli R (Ed.). PLoS ONE 12: e0177347. https://doi.org/10.1371/journal.pone.0177347

Böhmer C, Rössner GE (2018) Dental paleopathology in fossil rhinoceroses: etiology and implications. Journal of Zoology 304: 3–12. https://doi.org/10.1111/jzo.12518

Böhmer C, Heissig K, Rössner GE (2016) Dental Eruption Series and Replacement Pattern in Miocene *Prosantorhinus* (Rhinocerotidae) as Revealed by Macroscopy and X-ray: Implications for Ontogeny and Mortality Profile. Journal of Mammalian Evolution 23: 265–279. https://doi.org/10.1007/s10914-015-9313-x

Bratlund B (1999) Taubach revisited. Jahrbuch des Römisch-Germanischen Zentralmuseums Mainz 46: 61–174.

Cabreira SF, Schultz CL, da Silva LR, Lora LHP, Pakulski C, do Rêgo RCB, Soares MB, Smith MM, Richter M (2022) Diphyodont tooth replacement of *Brasilodon*—A Late Triassic eucynodont that challenges the time of origin of mammals. Journal of Anatomy 241: 1424–1440. https://doi.org/10.1111/joa.13756

Campbell BG, Aminit MH, Bernor RL, Dickinsont W, Drake R (1980) Maragheh: a classical late Miocene vertebrate locality in northwestern Iran. Nature 287: 837–841. https://doi.org/10.1038/287837a0

Cerdeño E (1995) Cladistic Analysis of the Family Rhinocerotidae (Perissodactyla). American Museum Novitates 3143: 1–25.

Cerdeño E (1996) *Lartetotherium* (Rhinocerotidae) en la fauna con *Hispanotherium* de! Mioceno Medio de La Retama, Cuenca, Espana. Revista Española de Paleontología 11: 193–197.

Chen GF, Wu WY (1976) Mammalian fossils from the Miocene Jiulongkou locality, Cixian County, Heibei Province. Vertebrata PalAsiatica 14: 6–15.

Chollet MB, Teaford MF (2009) Ecological stress and linear enamel hypoplasia in *Cebus*. American Journal of Physical Anthropology: NA-NA. https://doi.org/10.1002/ajpa.21182

Chow M (1958) New elasmotherine rhinoceros from Shansi. Vertebrata PalAsiatica 2: 131–142.

de Christol M (1835) Recherches sur les caractères des grandes espèces de Rhinocèros fossiles. Annales des Sciences Naturelles 2: 44–112. https://doi.org/10.5962/bhl.title.16189

Ciner B, Wang Y, Deng T, Flynn L, Hou S, Wu W (2015) Stable carbon and oxygen isotopic evidence for Late Cenozoic environmental change in Northern China. Palaeogeography, Palaeoclimatology, Palaeoecology 440: 750–762. https://doi.org/10.1016/j.palaeo.2015.10.009

Davis H, Mead AJ (2013) Enamel Hypoplasia as an Indicator of Nutritional Stress in Juvenile White-Tailed Deer. Georgia Journal of Science 71: 95–101. https://doi.org/10.1515/9780820367521-032

Dawkins WB (1865) On the dentition of *Rhinoceros megarhinus*. The Natural History Review 5: 399–414. https://doi.org/10.1144/gsl.jgs.1867.023.01-02.36

Deng T (2001) New material of *Chilotherium wimani* (Perissodactyla, RHinoceritdae) from the Late Miocene of Fugu, Shaanxi 39: 129–138.

Deng T (2002) Limb bones of *Chilotherium wimani* (Perissodactyla, Rhinocerotidae) from the Late Miocene of the Linxia Basin in Gansu, China. Vertebrata PalAsiatica 40: 305–316.

Deng T (2005a) New cranial material of *Shansirhinus* (Rhinocerotidae, Perissodactyla) from the Lower Pliocene of the Linxia Basin in Gansu, China. Geobios 38: 301–313. https://doi.org/10.1016/j.geobios.2003.12.003

Deng T (2005b) New discovery of *Iranotherium morgani* (Perissodactyla, Rhinocerotidae) from the late Miocene of the Linxia Basin in Gansu, China, and its sexual dimorphism. Journal of Vertebrate Paleontology 25: 442–450. https://doi.org/10.1671/0272-4634(2005)025[0442:ndoimp]2.0.co;2]2.0.CO;2

Deng T (2006a) A primitive species of *Chilotherium* (Perissodactyla, Rhinocerotidae) from the Late Miocene of Linxia Basin (Gansu, China). Cainozoic Research 5: 93–102. https://doi.org/10.1016/j.geobios.2008.01.006

Deng T (2006b) Neogene Rhinoceroses of the Linxia Basin (Gansu, China). Courier des Forschungsinstituts Senckenberg 256: 43–56.

Deng T (2007) Skull of *Parelasmotherium* (Perissodactyla, Rhinocerotidae) from the Upper Miocene in the Linxia Basin (Gansu, China). Journal of Vertebrate Paleontology 27: 467–475. https://doi.org/10.1671/0272-4634(2007)27[467:sopprf]2.0.co;2]2.0.CO;2

Deng T (2008) A new elasmothere (Perissodactyla, Rhinocerotidae) from the late Miocene of the Linxia Basin in Gansu, China. Geobios 41: 719–728. https://doi.org/10.1016/j.geobios.2008.01.006

Deng T, Downs WR (2002) Evolution of Chinese Neogene Rhinocerotidae and Its Response to Climatic Variations. Acta Geologica Sinica 76: 139–145. https://doi.org/10.1111/j.1755-6724.2002.tb00080.x

Denk T, Zohner CM, Grimm GW, Renner SS (2018) Plant fossils reveal major biomes occupied by the late Miocene Old-World Pikermian fauna. Nature Ecology & Evolution 2: 1864–1870. https://doi.org/10.1038/s41559-018-0695-z

Dollo L (1885) Rhinocéros vivants et fossiles. Revue de Questions Scientifiques 17: 293–299.

Eckhardt RB, Protsch von Zieten R (1993) Enamel hypoplasias as indicators of developmental stress in pongids and hominids. Human Evolution 8: 93–99. https://doi.org/10.1007/BF02436608

Edinger T (1937) Ein Steinkern der Gehirn-, Nasen- und Nebenhöhlen von *Chilotherium*. Bulletin of the Geological Institution of the University of Uppsala 27: 32–41.

Fernández M, Fernicola JC, Cerdeño E (2021) Deciduous dentition and dental eruption sequence in Interatheriinae (Notoungulata, Interatheriidae): implications in the systematics of the group. Journal of Paleontology 95: 861–885. https://doi.org/10.1017/jpa.2021.7

Fisher JW (1995) Bone Surface Modifications in Zooarchaeology. Journal of Archaeological Method and Theory 2: 7–68. https://doi.org/10.1007/bf02228434

Fortelius M, Heissig K (1989) The phylogenetic relationships of the Elasmotherini. Mitteilungen der Bayerischen Staatssammlung für Paläontologie und historische Geologie 29: 227–233.

Fortelius M, Bibi F, Tang H, Žliobaitė I, Eronen JT, Kaya F (2019) The nature of the Old World savannah palaeobiome. Nature Ecology & Evolution 3: 504–504. https://doi.org/10.1038/s41559-019-0857-7

Fukuchi A, Nakaya H, Takai M, Ogino S (2009) A preliminary report on the Pliocene rhinoceros from Udunga, Transbaikalia, Russia. Asian Paleoprimatology 5: 61–98.

Gajewski JA (2026) Ontogeny and the Effects of Perinatal Stress in the First Immature Skeleton of *Teleoceras aepysoma* (Perissodactyla, Rhinocerotidae). Master's Thesis. East Tennessee State University

Geraads D (1988) Révision des Rhinocerotinae (Mammalia) du Turolien de Pikermi. Comparaison avec les formes voisines. Annales de Paléontologie 74: 13–41.

Geraads D, Koufos G (1990) Upper Miocene Rhinocerotidae (Mammalia) from Pentalophos-1, Macedonia, Greece. Palaeontographica Abteilung A 210: 151–168.

Geraads D, Spassov N (2009) Rhinocerotidae (Mammalia) from the Late Miocene of Bulgaria. Palaeontographica Abteilung A 287: 99–122. https://doi.org/10.1127/pala/287/2009/99

Geraads D, Zouhri S (2021) A new late Miocene elasmotheriine rhinoceros from Morocco. Acta Palaeontologica Polonica 66. https://doi.org/10.4202/app.00904.2021

Giaourtsakis IX (2003) Late Neogene Rhinocerotidae of Greece: distribution, diversity and stratigraphical range. Deinsea 10: 235–253. https://doi.org/10.1525/9780520942509-018

Giaourtsakis IX (2009) The Late Miocene Mammal Faunas of the Mytilinii Basin, Samos Island, Greece: New Collection 9. Rhinocerotidae. Beiträge zur Paläontologie 31: 157–187. https://doi.org/10.1525/9780520942509-018

Giaourtsakis IX (2022) The Fossil Record of Rhinocerotids (Mammalia: Perissodactyla: Rhinocerotidae) in Greece. In: Vlachos E (Ed.), Fossil Vertebrates of Greece Vol. 2. Springer International Publishing, Cham, 409–500. https://doi.org/10.1007/978-3-030-68442-6_14

Giaourtsakis IX, Svorligkou G, Roussiakis S (2018) A juvenile skull of the hornless rhinocerotid *Acerorhinus neleus* (Rhinocerotidae, Mammalia) from the Late Miocene locality of Pikermi (Attica, Greece). In: Bristol, UK, 81. https://doi.org/10.13140/rg.2.2.14335.46244/1

Giaourtsakis IX, Theodorou G, Roussiakis S, Athanassiou A, Iliopoulos G (2006) Late Miocene horned rhinoceroses (Rhinocerotinae, Mammalia) from Kerassia (Euboea, Greece). Neues Jahrbuch für Geologie und Paläontologie - Abhandlungen 239: 367–398. https://doi.org/10.1127/njgpa/239/2006/367

Goddard J (1970) Age criteria and vital statistics of a black rhinoceros population. East African Wildlife Journal 8: 105–121. https://doi.org/10.1111/j.1365-2028.1970.tb00834.x

Gomes Rodrigues H, Lihoreau F, Orliac M, Boisserie J-R (2021) Characters from the deciduous dentition and its interest for phylogenetic reconstruction in Hippopotamoidea (Cetartiodactyla: Mammalia).

Zoological Journal of the Linnean Society 193: 413–431. https://doi.org/10.1093/zoolinnean/zlaa147

Goodman AH, Rose JC (1990) Assessment of systemic physiological perturbations from dental enamel hypoplasias and associated histological structures. American Journal of Physical Anthropology 33: 59–110. https://doi.org/10.1002/ajpa.1330330506

Gray JE (1821) On the natural arrangemenet of vertebrose animals. London Medical Repository 15: 297–310.

Guatelli-Steinberg D (2000) Linear enamel hypoplasia in gibbons (*Hylobates lar carpenteri*). American Journal of Physical Anthropology 112: 395–410. https://doi.org/10.1002/1096-8644(200007)112:3<395::aid-ajpa9>3.0.co;2-h

Guatelli-Steinberg D (2001) What can developmental defects of enamel reveal about physiological stress in nonhuman primates? Evolutionary Anthropology: Issues, News, and Reviews 10: 138–151. https://doi.org/10.1002/evan.1027

Guatelli-Steinberg D, Lukacs JR (1998) Preferential expression of linear enamel hypoplasia on the sectorial premolars of rhesus monkeys (*Macaca mulatta*). American Journal of Physical Anthropology 107: 179–186. https://doi.org/10.1002/(sici)1096-8644(199810)107:2<179::aid-ajpa4>3.3.co;2-q

Guatelli-Steinberg D, Skinner M (2000) Prevalence and Etiology of Linear Enamel Hypoplasia in Monkeys and Apes from Asia and Africa. Folia Primatologica 71: 115–132. https://doi.org/10.1159/000021740

Guérin C (1980) Les Rhinocéros (Mammalia, Perissodactyla) du Miocène terminal au Pleistocène supérieur en Europe occidentale: comparaison avec les espèces actuelles. Documents des Laboratoires de Géologie de la Faculté des Sciences de Lyon 79: 1–1185. https://doi.org/10.1016/s0016-6995(06)80220-2

Hannibal DL, Guatelli-Steinberg D (2005) Linear enamel hypoplasia in the great apes: Analysis by genus and locality. American Journal of Physical Anthropology 127: 13–25. https://doi.org/10.1002/ajpa.20141

Hassler A, Martin JE, Ferchaud S, Grivault D, Le Goff S, Albalat E, Hernandez J-A, Tacail T, Balter V (2021) Lactation and gestation controls on calcium isotopic compositions in a mammalian model. Metallomics 13: mfab019. https://doi.org/10.1093/mtomcs/mfab019

Heissig K (1972) Paläontologische und geologische Untersuchungen im Tertiär von Pakistan 5. Rhinocerotidae (Mamm.) aus den unteren und mittleren Siwalik-Schichten. Bayerische Akademie der Wissenschaften Mathematisch-Naturwissenschaftliche Klasse Abhandlungen - Neue Folge 152: 1–112.

Heissig K (1975) Rhinocerotidae aus dem Jungtertiär Anatoliens. Geologisches Jahrbuch (B) 15: 145–151.

Heissig K (1981) Probleme bei der cladistischen Analyse einer Gruppe mit wenigen eindeutigen Apomorphien: Rhinocerotidae. Paläontologische Zeitschrift 55: 117–123. https://doi.org/10.1007/BF02986041

Heissig K (1984) Nashornverwandte (Rhinocerotidae) aus der Oberen Süsswassermolasse und ihre Bedeutung für deren Lokalstratigraphie. Heimatliche Schriftenreihe des Landkreises Günzburg 2: 62–74.

Heissig K (2012) Les Rhinocerotidae (Perissodactyla) de Sansan. In: Mammifères de Sansan. Muséum national d'Histoire naturelle, Paris, 317–485.

Hillman-Smith AKK, Owen-Smith RN, Anderson JL, Hall-Martin AJ, Selaladi JP (1986) Age estimation of the White rhinoceros (*Ceratotherium simum*). Journal of Zoology 210: 355–379. https://doi.org/10.1111/j.1469-7998.1986.tb03639.x

Hillson S, Bond S (1997) Relationship of enamel hypoplasia to the pattern of tooth crown growth: A discussion. American Journal of Physical Anthropology 104: 89–103. https://doi.org/10.1002/(sici)1096-8644(199709)104:1<89::aid-ajpa6>3.0.co;2-8

Hullot M, Antoine P-O (2020) Mortality curves and population structures of late early Miocene Rhinocerotidae (Mammalia, Perissodactyla) remains from the Béon 1 locality of Montréal-du-Gers, France. Palaeogeography, Palaeoclimatology, Palaeoecology 558: 109938. https://doi.org/10.1016/j.palaeo.2020.109938

Hullot M, Antoine P-O (2022) Enamel hypoplasia on rhinocerotoid teeth: Does CT-scan imaging detect the defects better than the naked eye? Palaeovertebrata 45: e2. https://doi.org/10.18563/pv.45.1.e2

Hullot M, Laurent Y, Merceron G, Antoine P-O (2021) Paleoecology of the Rhinocerotidae (Mammalia, Perissodactyla) from Béon 1, Montréal-du-Gers (late early Miocene, SW France): Insights from dental microwear texture analysis, mesowear, and enamel hypoplasia. Palaeontologia Electronica 24: a27. https://doi.org/10.26879/1163

Hullot M, Martin C, Blondel C, Rössner GE (2024a) Life in a Central European warm-temperate to subtropical open forest: Paleoecology of the rhinocerotids from Ulm-Westtangente (Aquitanian, Early Miocene, Germany). The Science of Nature 111: 10. https://doi.org/10.1007/s00114-024-01893-w

Hullot M, Antoine P-O, Spassov N, Koufos GD, Merceron G (2023) Late Miocene rhinocerotids from the Balkan-Iranian province: ecological insights from dental microwear textures and enamel hypoplasia. Historical Biology 35: 1417–1434. https://doi.org/10.1080/08912963.2022.2095910

Hullot M, Martin C, Blondel C, Becker D, Rössner GE (2024b) Evolutionary palaeoecology of European rhinocerotids across the Oligocene–Miocene transition. Royal Society Open Science 11: 240987. https://doi.org/10.1098/rsos.240987

Hullot M, Martin C, Blondel C, Becker D, Rössner GE (2024c) Paleobiology and paleoecology of the woolly rhinoceros (*Coelodonta antiquitatis*) in Northern and Central Europe: New insights from multi-proxy data. Quaternary International 713: 109573. https://doi.org/10.1016/j.quaint.2024.10.005

Jäger GF (1839) Über die fossilen Säugetiere welche in Würtemberg in verschiedenen Formationen aufgefunden worden sind, nebst geognotischen Bemerkungen über diese Formationen. Carl Erhard Verlag, Stuttgart, 139 pp.

Jäger KRK, Gill PG, Corfe I, Martin T (2019) Occlusion and dental function of *Morganucodon* and *Megazostrodon*. Journal of Vertebrate Paleontology 39: e1635135. https://doi.org/10.1080/02724634.2019.1635135

Ji HX, Xu QQ, Huang WB (1980) The *Hipparion* fauna from Guizhong Basin, Xizang. In: Palaeontology of Xizang, Book 1. The Comprehensive Scientific Expedition to the Qinghai-Xizang Plateau of the Chinese Academy of Sciences. Science Press, Beijing, 18–32.

Kaakinen A, Passey BH, Zhang Z-Q, Liu L-P, Pesonen Z, Fortelius M (2013) Stratigraphy and Paleoecology of the Classical Dragon Bone Localities of Baode County, Shanxi Province. In: Fortelius M, Wang X, Flynn L (Eds) Fossil Mammals of Asia. Columbia University Press, 203–217. https://doi.org/10.7312/columbia/9780231150125.003.0007

Kampouridis P, Hartung J, Ferreira GS, Böhme M (2022a) Reappraisal of the late Miocene elasmotheriine *Parelasmotherium schansiense*

from Kutschwan (Shanxi Province, China) and its phylogenetic relationships. Journal of Vertebrate Paleontology 41: e2080556. https://doi.org/10.1080/02724634.2021.2080556

Kampouridis P, Svorligkou G, Kargopoulos N, Augustin FJ (2022b) Reassessment of '*Chilotherium wegneri*' (Mammalia, Rhinocerotidae) from the late Miocene of Samos (Greece) and the European record of *Chilotherium*. Historical Biology 34: 412–420. https://doi.org/10.1080/08912963.2021.1920939

Kampouridis P, Mirzaie Ataabadi M, Hartung J, Augustin FJ (2024) The easternmost occurrence of the Late Miocene schizotheriine chalicothere *Ancylotherium pentelicum* at the classical locality of Maragheh (Iran). Journal of Mammalian Evolution 31: 36. https://doi.org/10.1007/s10914-024-09730-7

Kampouridis P, Svorligkou G, Spassov N, Böhme M (2025) Postcranial anatomy of the Late Miocene Eurasian hornless rhinocerotid *Chilotherium*. PLoS ONE 20: e0336590. https://doi.org/10.1371/journal.pone.0336590

Kampouridis P, Hartung J, Augustin FJ, El Atfy H, Ferreira GS (2023a) Dental eruption and adult dentition of the enigmatic ptolemaiid *Qarunavus meyeri* from the Oligocene of the Fayum Depression (Egypt) revealed by micro-computed tomography clarifies its phylogenetic position. Zoological Journal of the Linnean Society: zlad065. https://doi.org/10.1093/zoolinnean/zlad065

Kampouridis P, Svorligkou G, Kargopoulos N, Spassov N, Böhme M (2023b) Revision of the Late Miocene hornless rhinocerotids from Samos Island (Greece) with the designation of neotypes and implications for the European chilotheres. Journal of Vertebrate Paleontology. https://doi.org/10.1080/02724634.2023.2254360

Kargopoulos N, Kampouridis P, Hartung J, Böhme M (2023) Hyaenid remains from the Late Miocene of Kutschwan (Shanxi Province, China). PalZ. https://doi.org/10.1007/s12542-023-00658-6

Kaup J (1832) Über *Rhinoceros incisivus* Cuv., und eine neue Art, *Rhinoceros schleiermacheri*. Isis von Oken: 898–904.

Kaya F, Bibi F, Žliobaitė I, Eronen JT, Hui T, Fortelius M (2018) The rise and fall of the Old World savannah fauna and the origins of the African savannah biome. Nature Ecology & Evolution 2: 241–246. https://doi.org/10.1038/s41559-017-0414-1

Kiernik E (1913) Über einen *Aceratherium* schädel aus der Umgebung von Odessa. Bulletin international de l'Académie des sciences de Cracovie 1913: 808–864.

Killgus H (1922) Die Unterpliocaenen Chinesischen Säugetierreste der Tafelschen Sammlung zu Tübingen. Ph.D. Dissertation. Eberhard-Karls University of Tübingen

Killgus H (1923) Unterpliozäne Säuger aus China. Paläontologische Zeitschrift 5: 251–257. https://doi.org/10.1007/bf03160375

Koenigswald W, Smith BH, Arbor A, Keller T (2007) Supernumerary teeth in a subadult rhino mandible (*Stephanorhinus hundsheimensis*) from the middle Pleistocene of Mosbach in Wiesbaden (Germany). Paläontologische Zeitschrift 81: 416–428. https://doi.org/10.1007/bf02990253

Korotkevich OL (1958) A new *Chilotherium* species from the Sarmatian deposits of the Ukraine. Dopovidi Akad. Nauk Ukrainskoi RSR 12: 1372–1376.

Korotkevich OL (1970) The mammals of the Berislav late Sarmatian *Hipparion*-fauna. In: The Natural Environment and the fauna of the past. Naukova Dumka, 121.

Kostopoulos DS, Sen S, Koufos GD (2003) Magnetostratigraphy and revised chronology of the late Miocene mammal localities of Samos, Greece. International Journal of Earth Sciences 92: 779–794. https://doi.org/10.1007/s00531-003-0353-8

Kostopoulos DS, Koufos GD, Sylvestrou IA, Syrides GE, Tsombachidou E (2009) The Late Miocene Mammal Faunas of the Mytilinii Basin, Samos Island, Greece: New Collection: 2. Lithostratigraphy and Fossiliferous Sites. Beiträge zur Paläontologie 31: 13–26. https://doi.org/10.1016/j.geobios.2010.08.004

Koufos GD (2009) The Late Miocene Mammal Faunas of the Mytilinii Basin, Samos Island, Greece: New Collection: 1. History of the Samos Fossil Mammals. Beiträge zur Paläontologie 31: 1–12. https://doi.org/10.1016/j.geobios.2010.08.004

Koufos GD, Kostopoulos DS, Vlachou TD (2009) The Late Miocene Mammal Faunas of the Mytilinii Basin, Samos Island, Greece: New Collection 16. Biochronology. Beiträge zur Paläontologie 31: 397–408. https://doi.org/10.1016/j.geobios.2010.08.004

Koufos GD, Kostopoulos DS, Vlachou TD, Konidaris GE (2011) A synopsis of the late Miocene Mammal Fauna of Samos Island, Aegean Sea, Greece. Geobios 44: 237–251. https://doi.org/10.1016/j.geobios.2010.08.004

Kretzschmar P, Ganslo\u00dfer U, Dehnhard M (2004) Relationship between androgens, environmental factors and reproductive behavior in male white rhinoceros (*Ceratotherium simum simum*). Hormones and Behavior 45: 1–9. https://doi.org/10.1016/j.yhbeh.2003.08.001

Krokos WI (1917) *Aceratherium schlosseri* Web. du village de Grebeniki du gouvernement de Kherson. Memoires of the Agricultural Society of Southern Russia 82: 1–96.

Laurillard F (1848) Rhinoceros fossiles. In: Dictionnaire universel d'Histoire naturelle, volume 11. Renard Martinet & Cie édit, Paris, 99–102.

Lehmann U (1984) Notiz für Säugerreste von der Insel Samos in der Sammlung des Geologisch-Paläontologischen Instituts und Museums Hamburg. Mitteilungen des Geologisch-Paläontologischen Instituts der Universität Hamburg 57: 147–156.

Li J, Fang X, Song C, Pan B, Ma Y, Yan M (2014) Late Miocene–Quaternary rapid stepwise uplift of the NE Tibetan Plateau and its effects on climatic and environmental changes. Quaternary Research 81: 400–423. https://doi.org/10.1016/j.yqres.2014.01.002

Li S, Sanisidro O, Wang S, Yang R, Deng T (2024) New materials of *Pliorhinus ringstromi* from the Linxia Basin (Late Miocene, eastern Asia) and their taxonomical and evolutionary implications. Journal of Mammalian Evolution 31: 6. https://doi.org/10.1007/s10914-023-09698-w

Li S-J, Deng T (2023) Restudy of Rhinocerotini fossils from the Miocene Jiulongkou Fauna of China. Vertebrata PalAsiatica 61: 198–211.

Li Y, Deng T, Hua H, Zhang Y, Wang J (2020) Isotopic record of palaeodiet of a 7.4 Ma Hipparionine fauna from the central Loess Plateau, northern China: Palaeo-ecological and palaeo-climatic implications. Chemical Geology 532: 119353. https://doi.org/10.1016/j.chemgeo.2019.119353

Linnaeus C (1758) Systema naturæ per regna tria naturæ, secundum classes, ordines, genera, species, cum characteribus, differentiis, synonymis, locis. Editio decima, reformata, Holmiae, Laurentii Salvii, 824 pp.

Liu J, Li JJ, Song CH, Yu H, Peng TJ, Hui ZC, Ye XY (2016) Palynological evidence for late Miocene stepwise aridification on the northeastern Tibetan Plateau. Climate of the Past 12: 1473–1484. https://doi.org/10.5194/cp-12-1473-2016

Lu X (2013) A juvenile skull of *Acerorhinus yuanmouensis* (Mammalia: Rhinocerotidae) from the Late Miocene hominoid fauna of the Yuanmou Basin (Yunnan, China). Geobios 46: 539–548. https://doi.org/10.1016/j.geobios.2013.10.001

Lu X, Chen S, He W (2015) New skulls of *Shansirhinus ringstromi* from the upper Neogene of the Linxia Basin, and their paleoenvironmental context. Quaternary Research 35: 539–549. https://doi.org/10.11928/j.issn.1001-7410.2015.03.06

Lu X-K, Deng T, Pandolfi L (2023) Reconstructing the phylogeny of the hornless rhinoceros Aceratheriinae. Frontiers in Ecology and Evolution 11: 1005126. https://doi.org/10.3389/fevo.2023.1005126

Lukacs JR (1999) Enamel hypoplasia in deciduous teeth of great apes: Do differences in defect prevalence imply differential levels of physiological stress? American Journal of Physical Anthropology 110: 351–363. https://doi.org/10.1002/(sici)1096-8644(199911)110:3<351::aid-ajpa7>3.0.co;2-2

Mateer NJ, Lucas SG (1985) Swedish vertebrate palaeontology in China: A history of the Lagrelius Collection. Bulletin of the Geological Institutions of the University of Uppsala, New Series 11: 1–24.

Mead AJ (1999) Enamel hypoplasia in Miocene rhinoceroses (*Teleoceras*) from Nebraska: evidence of severe physiological stress. Journal of Vertebrate Paleontology 19: 391–397. https://doi.org/10.1080/02724634.1999.10011150

Mecquenem R de (1908a) Contribution à l'étude du gisement des vertébrés de Maragha et de ses environs. Annales d'histoire naturelle 1: 27–98.

Mecquenem R de (1908b) Le lac D'ourmiah. Annales de Géographie 17: 128–144. https://doi.org/10.3406/geo.1908.18216

Mecquenem R de (1924) Contribution à l'étude des fossiles de Maragha. Annales de Paléontologie 13–14: 135–160, 1–36.

Mirzaie Ataabadi M, Bernor RL, Kostopoulos DS, Wolf D, Orak Z, Zare G, Nakaya H, Watabe M, Fortelius M (2013) Recent Advances in Paleobiological Research of the Late Miocene Maragheh Fauna, Northwest Iran. In: Fortelius M, Wang X, Flynn L (Eds) Fossil Mammals of Asia. Columbia University Press, 546–565. https://doi.org/10.7312/columbia/9780231150125.003.0025

Mirzaie Ataabadi M, Kaakinen A, Kunimatsu Y, Nakaya H, Orak Z, Paknia M, Sakai T, Salminen J, Sawada Y, Sen S, Suwa G, Watabe M, Zaree G, Zhaoqun Z, Fortelius M (2016) The late Miocene hominoid-bearing site in the Maragheh Formation, Northwest Iran. Palaeobiodiversity and Palaeoenvironments 96: 349–371. https://doi.org/10.1007/s12549-016-0241-4

Montalvo CI (2002) Root traces in fossil bones from the Huayquerian (Late Miocene) faunal assemblage of Telén, La Pampa, Argentina. Acta geologica hispanica 37: 37–42.

Morlan RE (1980) Taphonomy and Archaeology in the Upper Pleistocene of the Northern Yukon Territory: A Glimpse of the Peopling of the New World. University of Ottawa Press, Ottawa, 428 pp. https://doi.org/10.2307/j.ctv16tq6

Newell EA, Guatelli-Steinberg D, Field M, Cooke C, Feeney RNM (2006) Life history, enamel formation, and linear enamel hypoplasia in the Ceboidea. American Journal of Physical Anthropology 131: 252–260. https://doi.org/10.1002/ajpa.20436

Nothdurft W, Smith JB (2002) The lost dinosaurs of Egypt. Random House, New York, 256 pp.

Osborn HF (1900) Phylogeny of the rhinoceroses of Europe. Bulletin of the American Museum of Natural History 12: 229–267.

Owen R (1848) Description of teeth and portions of jaws of two extinct anthracotherioid quadrupeds (*Hyopotamus vectianus* and *Hyop. bovinus*) discovered by the Marchioness of Hastings in the Eocene deposits on the N.W. coast of the Isle of Wight; with an attempt to develop Cuvier's idea of the classification of pachyderms by the number of their toes. Quarterly Journal of the Geological Society of London 4: 103–141. https://doi.org/10.1144/gsl.jgs.1848.004.01-02.21

Pandolfi L (2016) *Persiatherium rodleri* , gen. et sp. nov. (Mammalia, Rhinocerotidae) from the upper Miocene of Maragheh (northwestern iran). Journal of Vertebrate Paleontology 36: e1040118. https://doi.org/10.1080/02724634.2015.1040118

Pandolfi L, Pierre-Olivier A, Bukhsianidze M, Lordkipanidze D, Rook L (2021) Northern Eurasian rhinocerotines (Mammalia, Perissodactyla) by the Pliocene–Pleistocene transition: phylogeny and historical biogeography. Journal of Systematic Palaeontology 19: 1031–1057. https://doi.org/10.1080/14772019.2021.1995907

Pavlow M (1913) Mammifères tertiaires de la Nouvelle Russie, 1. Partie: Artiodactyla, Perissodactyla (*Aceratherium kowalevskii* n.s.). Nouveaux Mémoires de la Société Impériale des Naturalistes de Moscou 17: 1–68.

Peter K (2002) Odontologie der Nashornverwandten (Rhinocerotidae) aus dem Miozän (MN5) von Sandelzhausen (Bayern). Zitteliana 22: 3–168.

Pohlig H (1884a) Geologische Untersuchungen in Persien. Verhandlungen der kaiserlich-königlichen geologischen Reichsanstalt 14: 281–284.

Pohlig H (1884b) Ueber weitere Reiseergebnisse des Herrn Dr. Pohlig in Persien. Sitzungsberichte der naturforschenden Gesellschaft in Bonn: 173–175.

Pohlig H (1885) Ueber eine Hipparionen-Fauna von Maragha in Nordpersien, über fossile Elephantenreste Kaukasiens und Persiens und über die Resultate einer Monographie der fossilen Elephanten Deutschalnds und Italiens. Zeitschrift der Deutschen Geologischen Gesellschaft 37: 1022–1027.

Pohlig H (1886) On the Pliocene of Maragha, Persia, and its resemblance to that of Pikermi in Greece. Quaterly Journal of the Geological Society of London 42: 177–179. https://doi.org/10.1144/gsl.jgs.1886.042.01-04.20

Qiu ZX, Xie JY, Yan DF (1987) A new chilothere skull from Hezheng, Gansu, China, with special reference to the Chinese "*Diceratherium*". Scientia Sinica B: 545–552.

Ringström T (1923) *Sinotherium lagrelii*. Ringström. A new fossil rhinocerotid from Shansi, China. Bulletin of the Geological Survey of China 5: 91–93.

Ringström T (1924) Nashörner der Hipparion-Fauna Nord-Chinas. Palaeontologia Sinica 1: 1–156.

Ringström T (1927) Über quartäre und jungtertiäre Rhinocerotiden aus China und der Mongolei. Palaeontologia Sinica, Series C 4: 1–21.

Rodler A (1885) Das Knochenlager und die Fauna von Maragha. Verhandlungen der kaiserlich-königlichen geologischen Reichsanstalt 14: 333–337.

Roohi G, Raza SM, Khan AM, Ahmad RM, Akhtar M (2015) Enamel Hypoplasia in Siwalik Rhinocerotids and its Correlation with Neogene Climate. Pakistan Journal of Zoology 47: 1433–1443.

Schlosser M (1903) Die fossilen Säugethiere Chinas nebst einer Odontographie der recenten Antilopen. Abhandlungen der Königlichen Bayerischen Akademie der Wissenschaften 22: 1–221.

Schwarzenberger F, Hermes R (2023) Comparative analysis of gestation in three rhinoceros species (*Diceros bicornis*; *Ceratotherium simum*; *Rhinoceros unicornis*). General and Comparative Endocrinology 334: 114214. https://doi.org/10.1016/j.ygcen.2023.114214

Sefve I (1927) Die Hipparionen Nord-Chinas. Palaeontologia SInica, Series C 4: 1–91.

Shellis RP, Beynon AD, Reid DJ, Hiiemae KM (1998) Variations in molar enamel thickness among primates. Journal of Human Evolution 35: 507–522. https://doi.org/10.1006/jhev.1998.0238

Skinner MF (1986) Enamel hypoplasia in sympatric chimpanzee and gorilla. Human Evolution 1: 289–312. https://doi.org/10.1007/BF02436704

Skinner MF, Rodrigues AT, Byra C (2014) Developing a pig model for crypt fenestration-induced localized hypoplastic enamel defects in humans: Localized Enamel Hypoplasia In Pigs. American Journal of Physical Anthropology 154: 239–250. https://doi.org/10.1002/ajpa.22497

Spassov N, Geraads D, Hristova L, Markov GN, Garevska B, Garevski R (2018) The late Miocene mammal faunas of the Republic of Macedonia (FYROM). Palaeontographica Abteilung A 311: 1–85. https://doi.org/10.1127/pala/2018/0073

Sun D-H, Li Y, Deng T (2018) A new species of *Chilotherium* (Perissodactyla, Rhinocerotidae) from the Late Miocene of Qingyang, Gansu, China. Vertebrata PalAsiatica 56: 216–228. https://doi.org/10.26879/838

Svorligkou G, Kampouridis P, Kargopoulos N, Pandolfi L (2025) Craniodental anatomy of the hornless rhinocerotid *Chilotherium schlosseri* (Mammalia, Perissodactyla) from the Late Miocene of Samos Island, Greece. Journal of Mammalian Evolution 32: 36. https://doi.org/10.1007/s10914-025-09777-0

Țibuleac P (2014) Presence of the genus *Choerolophodon* (Proboscidea: Mammalia) within the Moldavian Platform framework (Eastern Carpathians Foreland, Romania). Comptes Rendus Palevol.

Țibuleac P, Tissier J, Petculescu A, Becker D (2023) *Chilotherium schlosseri* (Weber, 1905) (Rhinocerotidae, M ammalia) from the late Miocene of the foreland of the Eastern Carpathians in Romania. Comptes Rendus Palevol 22: 729–752. https://doi.org/10.5852/cr-palevol2023v22a36

Toula F (1906) Das Gebiss und Reste der Nsenbeine von *Rhinoceros* (*Ceratorhinus* Osborn) *hundsheimensis*. Abhandlungen der k.k. Geologischen Reichsanstalt, Wien 20: 1–38.

Ungar PS (2010) Mammal Teeth: Origin, Evolution, and Diversity. JHU Press, 316 pp. https://doi.org/10.1353/book.485

Upex B, Dobney K (2012) Dental enamel hypoplasia as indicators of seasonal environmental and physiological impacts in modern sheep populations: a model for interpreting the zooarchaeological record. Kitchener A (Ed.). Journal of Zoology 287: 259–268. https://doi.org/10.1111/j.1469-7998.2012.00912.x

Wang K-M (1928) Die obermiozänen Rhinocerotiden von Bayern. Paläontologische Zeitschrift 10: 184–212. https://doi.org/10.1007/BF03041571

Weber M (1904) Ueber Tertiäre Rhinocerotiden von der Insel Samos. Bulletin de la Société Impériale des Naturalistes de Moscou 17: 477–501.

Weber M (1905) Über Tertiäre Rhinocerotiden von der Insel Samos. II. Bulletin de la Société Imperériale des Naturalistes de Moscou 18: 344–363.

Wessel P, Luis JF, Uieda L, Scharroo R, Wobbe F, Smith WHF, Tian D (2019) The Generic Mapping Tools Version 6. Geochemistry, Geophysics, Geosystems 20: 5556–5564. https://doi.org/10.1029/2019GC008515

Zdansky O (1924) Jungtertiäre Carnivoren Chinas. Palaeontologia Sinica, Series C 2: 1–149.

Zdansky O (1925a) Fossile Hirsche Chinas. Palaeontologia Sinica, Series C 2: 1–94.

Zdansky O (1925b) Quartäre Carnivoren aus Nord-Chiina. Palaeontologia Sinica, Series C 2: 1–25.

Zdansky O (1927a) Weitere Bermerkungen über fossile Carnivoren aus China. Palaeontologia Sinica, Series C 4: 1–30.

Zdansky O (1927b) Weitere Bermerkungen über fossile Cerviden aus China. Palaeontologia Sinica, Series C 5: 1–21.

Zong GF (1998) A new evidence of dividing in the Neogene stratigraphy of Yuanmou Basin. Memories of Beijing Natural History Museum 56: 159–178.

Supplementary material 1

Measurements of D1 and nasal-orbital bar

Authors: Panagiotis Kampouridis, Luca Pandolfi, Christina Kyriakouli, Nikolai Spassov, Madelaine Böhme

Data type: xlsx

Link: https://doi.org/10.3897/fr.29.192018.suppl1